



UNIVERSIDADE FEDERAL DO PARÁ
INSTITUTO DE GEOCIÊNCIAS
CURSO DE PÓS-GRADUAÇÃO EM GEOFÍSICA

MASTER DEGREE DISSERTATION

Rock Physics Attributes Analysis for Identification and
Characterization of Fluid Content at Hydrocarbon
Reservoirs - Revisiting the Viking Graben Basin dataset

JORGE ANTONIO TERUYA MONROE

Belém
April, 2015

JORGE ANTONIO TERUYA MONROE

**Rock Physics Attributes Analysis for Identification and
Characterization of Fluid Content at Hydrocarbon
Reservoirs - Revisiting the Viking Graben Basin
dataset**

Dissertation submitted to the Graduate Program
in Geophysics of the Univerdade Federal do
Pará for obtaining a Master's Degree in
Geophysics.

Concentration area: Seismic Methods

Supervisor: Dr. José Jadsom Sampaio de
Figueiredo

Belém
2015

Dados Internacionais de Catalogação na Publicação
(CIP) Sistemas de Bibliotecas da UFPA

Jorge Antonio Teruya Monroe
Rock Physics Attributes Analysis for Identification
and Characterization of Fluid Content at Hydrocarbon
Reservoirs - Revisiting the Viking Graben Basin dataset/
Jorge Antonio Teruya Monroe; Adviser: Dr. José Jadsom
Sampaio de Figueiredo; - April, 2015
89 f.: il.

Dissertação (mestrado em Geofísica) - Universidade
Federal do Pará, Instituto de Geociências, Programa de
Graduação em Geofísica, Belém, April, 2015.

I. Jorge Antonio Teruya Monroe, *orient.* II.
Universidade Federal do Pará. III. Título.

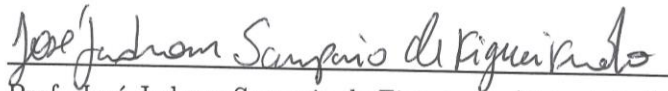
JORGE ANTONIO TERUTA MONROE

**Rock Physics Attributes Analysis for Identification and Characterization
of Fluid Content at Hydrocarbon Reservoirs - Revisiting the Viking
Graben Basin dataset**

Dissertation submitted to the Graduate
Program in Geophysics of the Universidade
Federal do Pará for obtaining a Master's
Degree in Geophysics.

Approval Date: 17/04/2015

Examining Committee: *Excelente*



Prof. José Jadsom Sampaio de Figueiredo (Orientador)

Doutor em Geofísica

Universidade Federal do Pará



Prof^a. Dra. Carolina Barros da Silva. (CPGf-UFPa)

Doutora em Geofísica

Universidade Federal do Pará



Prof. Dr. Fabio Henrique Garcia Domingos (UFPa).

Doutor em Geologia

Universidade Federal do Pará

In memory of my father Jorge Teruya Teruya
who always instilled in me the wisdom to tire
my goals, I know he still cares for me...

ACKNOWLEDGEMENTS

To God for the health and perseverance to complete another stage of my professional life, overcoming the difficulties presented by the way, to the professor Ellen Gomes, by the confidence in our work and effort, to my advisor professor José Jadsom Sampaio de Figueiredo since their guidance and dedication was essential to the completion of this professional stage.

I give special thanks to my wife Iris Judith Roncalla de Teruya, without her support, I could not have overcome the difficulties of this stage, to my mother Rosa Maria Monroe de Teruya and all my family Ana Lucía Teruya Monroe and José Luis Fernandez Teruya, for all encouragement and support provided, as well as the trust placed in my plans. My friends, who were always supporting me, directly or indirectly, during this challenge, I thank in a special way to my friends Ana Alzira, Francisco Oliveira, Leo Kirchhof and Manuel Espejo who contributed to this work.

To the members of the examining committee, Prof. Dr. Fabio Henrique Garcia Domingos and Prof. Dra. Carolina Barros da Silva, by the attention and patience provided in reading and corrections of this work. To the CPGf by confidence in the success of this project, providing facilities and resources for the development of this project.

To CNPq and INCT-Gp, whose financial support was instrumental in this work, through the stock incentive, I would like to thank to the company Exxon-Mobil by the data provided for the development of this work. The dear secretaries of the graduate program in geophysics, Benildes and Lucibela, competent professionals, always ready to solve any problem with a patient service, polite and affectionate.

ABSTRACT

In the characterization of hydrocarbon reservoir, most of methodologies used in rock physics or seismic reflection are based on the physical properties analysis of rocks which are associated to anomalous effects in seismic sections. These anomalies are, many often, associated to indicators of fluids (oil, gas and/or water) in the hydrocarbon reservoir. In this work, we perform a study in order to characterize a hydrocarbon reservoir at north Viking Graben region, in the North Sea. In addition to the seismic data, well-logs from two locations (wells A e B) were also used in our analysis. However, in our data set analysis, beyond to perform AVO analysis, V_p/V_s versus impedance (I_p) and $V_p/V_s - \Phi$ we applied the trend angle methodology and well-logs data set analysis as well as Gassmann fluid substitution. Through AVO analysis in the re-processing of Viking Graben seismic data set, where found three anomalous zones with a high potential for the presence of fluids (gas/oil). Thus using templates of rock-physics and the analysis by attributes (trend angle) to classifying the fluids and determinate the possibility of gas-sand that are present at wells A and B.

Keywords: Rock-physics templates. Impedance. Petro-physics. AVO analysis, Seismic Velocities.

RESUMO

Na caracterização de reservatórios de hidrocarbonetos, grande parte das metodologias usadas em física de rochas ou sísmica de reflexão são baseados na análise das propriedades físicas de rochas, que no caso da sísmica, estão associados a efeitos anômalos em seções sísmicas. Essas anomalias são, a maior parte do tempo, associadas aos indicadores de fluidos (petróleo, gás e água) no reservatório de hidrocarboneto. Neste trabalho, realizamos um estudo sistemático de caracterização de reservatório de hidrocarboneto no campo Viking Graben do Mar do Norte. Além do dado sísmico, dados de dois poços (poços A e B) também foram utilizados na nossa análise. No entanto, em nossa análise, além de realizarmos análises de AVO, V_p/V_s versus impedância (I_p) e $V_p/V_s - \Phi$ foi aplicada a metodologia do ângulo de tendência e uma análise de substituição de fluidos usando o modelo Gassmann também foi realizada nos dois poços. Através da análise de AVO no dado sísmico 2D do campo Viking Graben, foram encontrados três zonas de anomalias cujo os aspectos indicam possíveis locais com a presença de fluidos (gás/óleo) (isto é confirmado pelo dado de poço). Além disso, usando modelos de física de rochas e análise do ângulo de tendência, em alguma região ao longo do poços A e B, mostraram-se a possibilidade da presença de gás de areia.

Palavras-Chave: Templates de física de rochas. Impedância acústica. Petrofísica. Análises AVO. Velocidades sísmicas.

LIST OF FIGURES

2.1 Illustration of the convolutional model of seismic trace.	22
2.2 Graph relating the variation of Poisson's ratio and the change in acoustic impedance, in which the orders of the type of fluid contained in relation to the variation of porosity, density and depth are in milliseconds.	29
2.3 Graphic interpretation of the example of Figure 2.2 where the type of possible fluids contained is different regions from log depends of the degree of porosity, density and depth.	30
2.4 Illustration of trend angle's definition applied to the elastic parameters, wherein the fluid content variation is shown relative to the porosity and physical parameters variation.	31
2.5 Example of trend angle applied to the crossplot of the acoustic impedance versus the change of velocity P and S, where we can determine variations in the anomalous data presented (colored dots), inserted in the base data.	32
2.6 Graphic example of trend angle applied to real data, where the target areas were determined. These areas have a high probability of containing hydrocarbon. (a) Acoustic Impedance plot versus Depth (b) Ratio of P and S velocities and (c) Trend Angle depending on the depth.	34
2.7 Gamma ray log showing the geological events and variations in the clay content, which can be inferred as target areas.	35
2.8 Example of the theory of AVO applied to synthetic data. This illustration shows the change in amplitude with the variation of the incidence angle of the wave in the reflector, (a) synthetic seismogram and (b) plot of magnitude of amplitudes as function of incidence angle.	38
2.9 Graphical definition of AVO classification in AVO analysis chart. In a general words, this graphics are showing the classification of the fluids by varying physical properties: (a) plane-wave reflection coefficients at the top from Rutherford & Williams (1989) classification of gas sand. Class IV sands have a negative normal-incidence reflection coefficient, but decrease in amplitude magnitude with offset (from Castagna et al. (1998)) and (b) AVO classification scheme for identifying the magnitude and class of a seismic reflection. The polarity convention in this display denotes a decrease in acoustic impedance by a peak.	40
3.1 Workflow chart applied to the seismic and well-logs data set processing.	43
3.2 Basic seismic processing step performed in our seismic data.	44
3.3 This workflow chart shows all stages performed in the well-log data	45

processing.	
3.4 This workflow chart shows the point in our analysis that information from seismic section and well-logs are combined to provide an interpretation about this reservoir.	46
4.1 Map of the Viking Graben field area.	47
4.2 Time migrated and interpreted seismic section of the study area, where the main geological structures, faults, anomalies and geological facies are shown.	48
4.3 (a) P-wave velocity model, used to reach the migrated seismic section. As it can be seen the lateral and vertical anisotropy are present in the area.	50
4.4 Time migrated section and seismic traces related to the well locations (CMP 808 and CMP 1572), where the structural variations present on the sub-surface are shown:(a) time migrated seismic section, (b) seismic trace from well A and (c) seismic trace from well B.	51
4.5 Comparison between S-wave velocity logs measured and estimated by the Castagna et al. (1985)'s equations: (a) well A and (b) well B.	52
4.6 From well A: (a) P-wave velocity log. (b) S-wave velocities measured (med) and calculated by the Castagna et al. (1985)'s equation 2.5. (c) Poisson ratio estimated from Vs using the Castagna et al. (1985)'s equation.	53
4.7 From well B: (a) P-wave velocity log. (b) S-wave velocities measured (med) and calculated by the Castagna et al. (1985)'s equation 2.5. (c) Poisson ratio estimated from Vs using the Castagna et al. (1985)'s equation.	54
4.8 Well logs from well A. (a) gamma ray log, (b) estimated porosity log and (c) P-wave and S-wave velocities, where the mainly geological events are shown and the areas with better porosity rate.	56
4.9 Well logs from well B. (a) estimated porosity log and (b) P-wave and S-wave velocities, where mainly the porosity events are shown and the areas with better velocity ratio.	57
4.10 From (a) density log and P-wave log shown in Figure 4.6, the (b) acoustic impedance log was calculated and (c) the coefficient reflection log were estimated for Well A.	58
4.11 From (a) density log and P-wave log shown in Figure 4.6, the (b) acoustic impedance log was calculated and (c) the coefficient reflection log were estimated for Well B.	59
4.12 S-wave velocity obtained by P-wave velocity model. This velocity model will be used to application of the trend angle technique and the	60

templates of rock-physics for characterizing the reservoir.

- 4.13 Logs, from well A, showing the three main anomalous zones found by the trend angle technique, which are compared with the logs of acoustic impedance and Poisson's ratio, (a) acoustic impedance plot versus depth (b) ratio of P and S velocities and (c) trend angle depending on the depth. 62
- 4.14 Logs, from well B, showing the three main anomalous zones found by the trend angle technique, which are compared with the logs of acoustic impedance and Poisson's ratio, (a) acoustic impedance plot versus depth (b) ratio of P and S velocities and (c) trend angle depending on the depth. 63
- 4.15 The application of angle trend technique in the anomalous zone present in approximately 2000 ms and CMP 600, the log presented was performed by creating a pseudo-well, where were found the physical parameters necessary for the application of the technical trend angle: (a) impedance map and (b) trend angle log applied between CMP 500 to CMP 700. 64
- 4.16 Chart showing the comparison between different velocities calculated and measured velocities (in situ), showing three anomalous areas with a high probability of containing gas sand: (a) for well A and (b) for well B. 66
- 4.17 From well A: (a) template that shows the behavior of the physical properties compared to the elastic properties, where the type of fluid present is classified and (b) template relating the acoustic impedance with the content of porosity, where we can determine the type of environment present related to each depth level. 67
- 4.18 From well B: (a) template that shows the behavior of the physical properties, into the well B, with the elastic properties and (b) template, showing relating between the acoustic impedance with the porosity. 68
- 4.19 Gassmann methodology applied to anomalous zone A (Figure 4.13) shown in the trend angle, where we can see the variation of modulus K at different percentages of saturation: (a) log showing the variation of the bulk modulus, (b) record, where we can see the variation in the P-wave velocity with the saturation change and (c) record showing that there is not variation in the S-wave velocity, generated by the saturation changes. 70

4.20 Gassmann theory applied to anomalous zone B in the target section shown in the Figure 4.13, where we can see interbedded areas containing high porosity zones and low porosity zones: (a) bulk modulus K, (b) record showing the change of the P-wave velocity with the saturation change and (c) record of the S-wave velocity without change by saturation.	71
4.21 Example of trend angle for well A, in case of saturated medium estimated by Gassmann methodology.	72
4.22 Plot showing the variation of V_P/V_S ratio versus porosity for different Depth intervals: (a) information is for well A and (b) information from well B.	73
4.23 Empirical relationship V_p/V_s versus ϕ . This relationship of porosity and V_P/V_S ratio and type of fluid content are showed for different depth interval: (a) Well A and (b) Well B.	74
4.24 (a) AVO analysis from the seismic section, where we can confirm the presence of a fluid with a high potential for gas due to variations position in their physical properties, (b) map of seismic AVO attribute related to seismic section depicted in Figure 4.4. It can be note that anomalous zones are related to areas with high rate of fracturing, (c) reflectivity map showing the anomalous zones present in the CMP 600 as well as anomalous areas close to the well A. We also can see the fractured zones. Both data were obtained by PROMAX software.	76
4.25 (a) seismic gradient map we can see the anomalous zones is present in the CMP 600 and in the area near the well A. (b) intercept seismic map derived from the application of the AVO technique to seismic section, (c) map of gradient x intercept attribute related to seismic section depicted in Figure 4.4. It can be noted that anomalous zones are related to areas with high rate of fracturing.	77
4.26 AVO analysis from well A, showing the trend of the data, which can Infer the presence of gas sand classification of the fluids contained in the well A.	78
4.28 AVO analysis applied to the well data B, where the presence of the fluids is mostly water formation, such analysis is inferred from the trend of the data.	79
4.29 Comparisons between the synthetic seismogram and the seismogram from seismic section for well B. (a) real seismogram, (b) synthetic seismogram and (c) acoustic impedance log. Although there are some	79

polarity inversion between the synthetic and real seismic data, most of section are well correlated.	
4.30 CMP 808 in variable density color -graph that displays the anomalies found with the technique of trend angle: (A) anomaly-1, (B) anomaly-2 - seal and (C) anomaly-3.	80
4.31 (CMP 1572 in variable density color - graph that displays the anomalies found with the technique of trend angle (A) anomaly-1, (B) anomaly - 2 - seal and (C) anomaly-3.	81
4.32 Graph that displays the amplitude behavior and their tendency present in the anomaly A - well A.	82
4.33 Graph showing the trend in amplitude behavior and the presence of a type of seal at the anomaly B - well A.	82
4.34 Graph showing the trend in amplitude behavior in the anomaly C well A.	83
4.35 Graph that displays the amplitude behavior and their tendency present in the anomaly A - well B.	83
4.36 Graph showing the trend in amplitude behavior and the presence of a type of seal at the anomaly B - well B.	84
4.37 Graph showing the trend in amplitude behavior in the anomaly C well B.	84
A.1 Map of the Viking Graben area (modified from Brown, 1990).	88
A.2 Schematic representation of a horst and grabens succession.	89
A.3 Stratigraphic column for northern North Sea reservoir rocks (after Parsley, 1990).	90

LIST OF ABBREVIATIONS

ABBREVIATIONS	DESCRIPTION
AI	From english Acoustic Impedance.
API	From english American Petroleum Institute.
AVO	From english Amplitude Versus Offset.
BCU	From english Base cretaceous unconformity.
Cs	From english Castagna Relationship.
CMP	From english Common Midpoint.
CDP	From english Common depth point.
DTC	From english Sonic log reading in zone of interest ($\mu\text{sec}/\text{ft.}$ or $\mu\text{sec}/\text{m}$).
DTCMA	From english Sonic log reading 100% matrix rock ($\mu\text{sec}/\text{ft.}$ or $\mu\text{sec}/\text{m}$).
DTCW	From english Sonic log reading in 100% water ($\mu\text{sec}/\text{ft.}$ or $\mu\text{sec}/\text{m}$).
GR	From english Gamma ray.
KCP	From english Compaction factor (fractional).
Med	From english Contraction of Measured.
NMO	From english Contraction of Measured From english Normal moveout.
PHIS	From english Porosity from sonic log (fractional).
RMS	From english Root Mean Square.
RPT	From english Rock Physics Template
s/n	From english Signal noise relation
TOC	From english Total Organic Carbon

LIST OF SYMBOLS

SYMBOLS	DESCRIPTION
S_w	Saturation
α	Attribute value of trend angle
V_p	P-wave velocity
V_s	S-wave velocity
μ	Shear modulus
ρ	Density
*	Convolution operator
V_p/V_s	Poisson's ratio ν
ΔA_I	Density contrast
Δ	Contrast or variation of the physical property
R_p	Reflection with zero offset
θ	Angle variation in AVO techniques
ϕ	Porosity
K	Bulk modulus
K_{fl}	Bulk modulus of fluid
K_{dry}	Bulk modulus of dry sample
K_w	Bulk modulus of water
K_{gas}	Bulk modulus of gas
K_{sat}	Bulk modulus of saturated sample
K_{min}	Bulk modulus of matrix of sample
G	Shear modulus
ρ_b	Initial Density

CONTENTS

1	INTRODUCTION	16
1.1	Motivation.....	17
1.2	Objectives and disposition of the chapters of the dissertation	18
2	THEORETICAL FRAMEWORK	20
2.1	Standard seismic processing.....	20
2.1.1	Usual seismic processing workflow.....	22
2.2	Well Log Data.....	23
2.3	Rock Physics Attributes.....	26
2.3.1	Rock-physics template.....	27
2.3.2	Trend angle.....	28
2.3.3	AVO theory.....	32
2.3.3.1	AVO classification.....	36
3	METHODOLOGY	40
3.1	Processing sequence of the seismic data.....	40
3.2	Processing sequence of the well-log data.....	41
4	RESULTS	46
4.1	Location.....	46
4.2	Seismic data preparation.....	48
4.3	V_s and porosity predictions.....	49
4.4	Data interpretation.....	52
4.4.1	Trend angle analysis.....	53
4.4.2	Gassmann fluid substitution analysis.....	60
4.4.3	$V_p/v_s - \phi$ relationship.....	63
4.4.4	AVO analysis.....	64
5	CONCLUSIONS	84
	BIBLIOGRAPHY	86
	ANNEX	
ANNEX A	GEOLOGY	91
ANNEX B	GASSMANN'S THEORY	96
ANNEX B.1	Gassmann's equations.....	97
ANNEX B.2	Gassmann's procedure.....	98

1 INTRODUCTION

Recently, estimates show that around 60% of oil and gas reservoirs in the Earth's sub-surface are contained in unconventional reservoirs like carbonate and/or shales rocks (WEIWEI, 2011). However, it is important to note that the increase in efficiency in the exploitation of oil reservoirs (for any type of rock) is a direct consequence of better knowledge of the physical and petrophysical properties that favor or disfavor the fluid flow, distribution of oil saturation and the type of medium (isotropic or anisotropic), or which is present in this fluid. It is known that seismic velocities and elastic parameters (shear moduli and bulk modulus) depends on the overburden, confining and pore pressures and petrophysical parameters of the medium (micro/macro porosity, permeability etc.). Understanding these dependencies is important step for reliable interpretation and inversion of a seismic data with (CIZ; SHAPIRO, 2007).

There are several methods for the study of static and dynamic properties of fluids in reservoirs and most of these studies focused on the integration of information originating from plug-ins data, well, seismic and knowledge of the depositional related to the reservoir system. However, the biggest challenge is the characterization of fluid presence in reservoirs are variables such as oil or water saturation which the response of fluid saturations can shows different values from scales of laboratory data, well-logs and seismic data. In the oil industry, many situations requires the detailed behavior of fluids in the reservoir (KHAN; JACOBSON, 2008). For this reason the use of indirect methods such as seismic reflection and rock physics are preponderant to characterize rock fluids in a reservoir (KHAN; JACOBSON, 2008). Both seismic and rock physics are most commonly used to investigate the influence of rock properties in the elastic wave propagation.

The seismic reflection through subsurface imaging can detect geological structures favorable for hydrocarbon deposits, as this technique (seismic reflection) is based on mechanical waves that travels through the subsurface (Kallivokas et al., 2013). This method is related directly to the variations in physical properties present in the reservoir of hydrocarbon (contrast difference between layers). Using analysis such as AVO technique (Amplitude Versus Offset) it is possible to detect possible candidates to hydrocarbon reservoir from seismic section. This detectability is

verified after the well drilling. This stage of hydrocarbon prospecting, allows us to find reservoirs in other scales and with higher resolution. In this case, the integration of different geophysical data (well-logs, seismic data and plugs) provides the information from micro to reservoir scales. Analysis petrophysical of well logs data as well laboratory samples characterization provide information with more details of spatial distribution of fluids in the reservoir.

A hydrocarbon reservoir can have different type fluids in different levels and in different depth. A manner to characterize the fluids contained in a reservoir is through (i) ultrasonic and petrophysical measurements of plugs, (ii) using different types of well-log data and from (iii) seismic data. In practice, the characterization is complex and requires the development and analysis of multidisciplinary areas. The selection of techniques and procedures depends mainly on the type and quality of the information to be handled (TYSON, 2007).

1.1 Motivation

The rock-physics establishes a link between the elastic properties and the reservoir properties such as porosity, water saturation and clay content (DVORKIN; MAVKO, 2013). Due to the feature of seismic signals and his behavior are directly governed by these elastic parameters, rock physics template and the seismic attributes provides a methodology to infer the geology and the structure of the reservoir, as well as the anomalous zones, both qualitatively and quantitatively. In this way, the rock-physics workflows which are related with the elastic properties of the reservoir is necessary to provide with accurate data to infer a feasible lithology. For this goal, it is necessary to perform a mathematical treatment of the empirical formulas, which are closely related to the work of rock physics analysis (BORUAH, 2010).

Rock physics and the seismic attributes analysis and interpretation have emerged as tools for help geophysicists to characterize reservoir properties related to seismic elastic parameters. In addition, rock-physics models have been presented as a ratio of sedimentology and matrix rock for changes in elastic properties (MADIBA; MCMECHAN, 2003). Through the application of this technique in seismic data, rock physics templates (AVSETH; VEGGELAND, 2014) can be used to determine geological tendencies (in the reservoir) as well as the influence of different elastic

parameters in seismic sections or in well-logs data. The importance to relate the reservoir parameters with seismic parameters, is the main interest for the purpose of assessing reservoir quality and economic viability of oil exploitation (BORUAH, 2010).

1.2 Objectives and Disposition of the Chapters in the Dissertation

The main goal of this work is to revisit and extend reservoir characterization analysis performed by Madiba and McMechan (2003) in the 2D North Viking Graben seismic data set provided by ExxonMobil.

For this study we used the same seismic section and some well-logs used by Madiba and McMechan (2003) in their analysis. As it made in Madiba and McMechan (2003), information from seismic sections and interval velocity models was used to create numeric models in order to identify anomalous zones which could contain hydrocarbon, the processing and interpretation of the well logs was realized previously, after was made a reservoir characterization by seismic attributes, for which it was necessary the seismic section calibrated with well logs.

Here, in this work, beyond to perform AVO analysis, V_P / V_s versus impedance (I_P), $V_P / V_s - \phi$ we used the trend angle methodology developed by Avseth and Veggeland (2014) to delineate top and base of reservoir as well as identify regions with different types of pore fluid. The application of the trend angle method in the present data set is the main remark of this work. In summary, this method evaluates the basic elastic properties of the medium (rock matrix) and their interaction with external elements (liquids of different properties), which identifies the method used in the distribution patterns of external elements through response together.

The numerical modeling of well data is one of the most accurate methods for calibrating seismic data, in addition to facilitating the classification of fluids present using different methods and techniques. Due to problems like bad calibration and mishandling of the tool, that can be present in the acquisition of well data, usually what is done is a filtering and reconstruction of logs, by empirical formulation, for the improvement or replacement of one or more logs. Having understood the need to know the distribution of the fluid in the reservoir characterization, we consider necessary to model the response of the seismic attributes in a media with different fluids in the rock theories. Gassmann classical model was used in order to relate the

elastic properties of partially saturated rocks with fluid properties of rock matrix and the fluid was used (GASSMANN, 1951).

This dissertation, includes the introductory chapter, three main chapters and two appendix. Chapter 2 presents a review of some concepts of the theory of seismic processing emphasizing the velocity analysis in the creation of a velocity model and seismic migration (depth and time). This chapter also describes the methods and methodologies used in this work. In other words, we discuss about the types of some seismic attributes and rock-physics templates to well-logs data (trend angle, AVO analysis, etc.). The chapter 3, describes the sequence of steps followed for seismic re-processing as well as the preparation of well logs in the 2D North Viking Graben seismic data. The chapter 4 presents the results and the implication of each technique and templates applied to the interpretation and seismic data characterization coupled with well-logs data analysis. Finally, the chapter 5 presents the conclusions about our analysis and interpretation. The appendix A shows comments about the geology of the Viking Graben field. This appendix presents the geological concepts of the graben. The appendix B presents the mathematical formalism of the Gassmann's model for fluid substitution, as well as, and the steps to apply it on real data.

2 THEORETICAL FRAMEWORK

2.1 Standard Seismic Processing

Seismic signals are the result of convolution of the wave signal generated by source with successive reflection coefficients from subsurface interfaces. In this way, the convolution can be thought as the process in which the input waveform (wavelet) is changed along the propagation's pathway by the reflection coefficient of the earth. The modification of the phase signal and amplitude magnitude is proportional to the sign and the magnitude of the reflection coefficient. The wavelet is reversed when there is a velocity value inversion, i.e., negative reflection coefficient. Beyond that, the reflected amplitude is directly proportional to the reflection coefficient magnitude. Thus, as a result of the convolution, the incoming signal's imprint brings information about the subsurface.

Mathematically, a convolution is an operator (symbolized by “*”) which transforms two functions r and w (in our case, respectively, the reflection coefficient and wavelet) in a third function s (recorded signal). The mathematical expression that represents the convolutional model of the earth is (in time domain),

$$s(t) = r(t)*w(t)+ n(t), \quad (2.1)$$

where $r(t)$, $w(t)$ and $n(t)$ are the seismic reflection coefficient, the source seismic wavelet and the noise. In frequency domain we have,

$$S(\omega) = R(\omega)W(\omega)+ N(\omega). \quad (2.2)$$

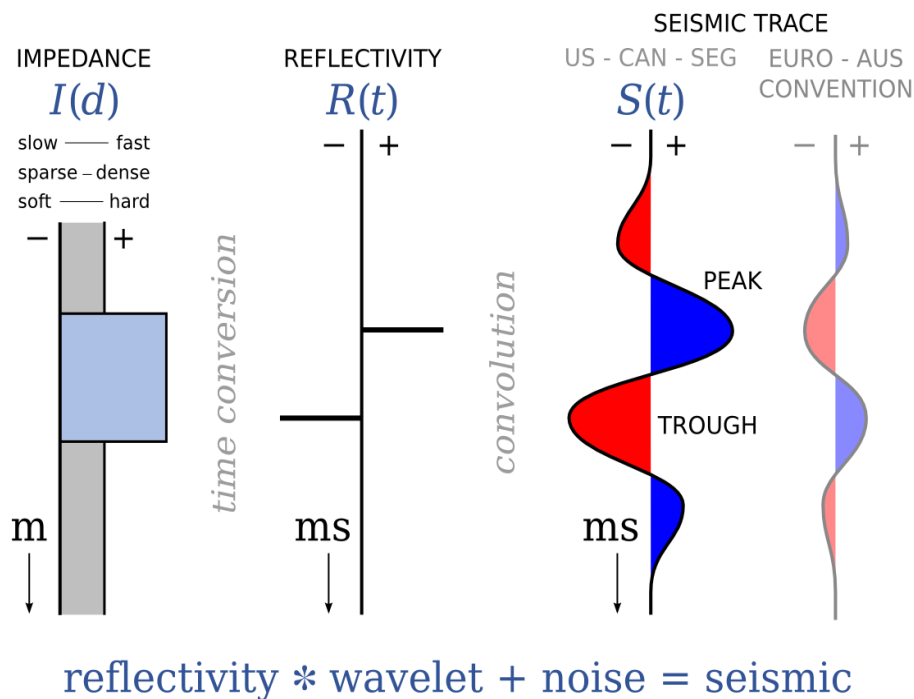
Figure 2.1 shows the illustration of convolutional model of the earth. The seismic signal is related to the source-wavelet and reflection coefficient of the earth. Beyond that, there are environment noise that are present in all seismic traces. Mathematically, the acoustic reflection coefficient from zero-offset case is given by

$$R(\theta = 0) = \frac{V_{P2}\rho_1 - V_{P1}\rho_2}{V_{P2}\rho_1 + V_{P1}\rho_2} , \quad (2.3)$$

where the indices 1 and 2 in the velocity and density mean the elastic properties in the medium 1 (above to the interface) and the medium 2 (below to the interface).

After obtaining the seismic records in the field (signals and noises), the next step lies on the seismic and signal processing through specific programs on computers with sufficient capacity. A fundamental mathematical tool for this purpose, is the Fourier Transform (Fourier, 1824), which changes the seismic traces from the time domain (which are values of amplitude in time domain) to the frequency domain (which are values of amplitude in frequency domain).

Figure 2.1: Illustration of the convolutional model of seismic trace.



Source: seismic amplitude and interpreter's Handbook (Simm; M. Bacon, 2014)

The transformation is done by approximating the shape of the trace with an integration of a series of harmonic functions (sines and cosines) or Fourier Series of variables amplitude, and then passing to the calculation and representation of the frequency spectrum (also expressible as an integration, but now differential frequency).

The seismic processing involves the election and subsequent application of the appropriate parameters and algorithms applied to the seismic data in the field (raw data) in order to obtain quality seismic sections. The fundamental goal of all multi-signal process is isolate, in the records, the reflections from the other seismic events that overlap them (ambient noise, ground roll, airwave, etc.). Currently, due to the large increase in the data volume (more instrumental capacity) and the development of new algorithms (more computing power), mastering processing techniques is the mainstay of geophysical prospecting.

Another decisive factor in the seismic reflection processing is the need to preserve the frequency range, by optimal filtering the seismic data and the selection of speeds that enhance the horizons and anomalies, since most of the geological structures are almost at the limit of detectability and seismic applying filters to suppress non-events to reflections (coherent and incoherent noise) often fall in the same frequency range, so any reduction in this range results in less definition of the seismic section. It is also a provision that any algorithm used during processing must preserve as much as possible the original reflections, so that its application does not create "artifacts" that can be considered as spurious reflections. Indeed, the whole object of seismic data processing is to manage seismic data recorded in the field into a coherent cross-section of significant geological horizons in the earth's sub-surface. In this work, we make the use of the final product of seismic processing following by the usage and analysis of well-log data set.

2.1.1 Usual Seismic Processing Work

It is well known that seismic processing can be made based on different workflows with different ways. A basic seismic processing can be presented as follows:

- Geometry Correction
- Trace Edition
- Statics Corrections
- Deconvolution

- Gathers Analysis
- NMO Correction
- Velocity Analysis
- Stacking
- Migration

The sequence above were adopted in our seismic processing to acquire a suitable velocity model (in time and depth domains) as well as a migrated section (also, in time and depth domain). In the next chapter we will make a reference to the seismic steps process performed in this work. More information about seismic processing workflows are available in vols. 1 and 2 of Yilmaz (1987).

2.2 Well Log Data

Well-loggings, also known as borehole loggings, is the practice of making a detailed record (a well-log) of the geologic formations penetrated by a borehole. The log may be related either by visual inspection of samples brought to the surface (geological plugins) or by the measurements of petrophysical parameters made by instruments lowered into the hole (geophysical logs). The oil and gas industry uses wireline logging to obtain a continuous record of the formation's rock properties. Wireline logging can be defined as the acquisition and analysis of geophysical data performed as a function of well bore depth, together with the provision of related services (BOLT, 2012).

Wireline logging is performed by lowering a logging tool - or a string of one or more instruments - located on the end of a wireline into an oil well (or borehole) and recording petrophysical properties using a variety of sensors. Logging tools developed over the years measure the natural gamma-ray, electrical, acoustic, stimulated radioactive responses, electromagnetic, nuclear magnetic resonance, pressure and other properties of the rocks and their contained fluids.

The measured cable depth can be derived from a number of different measurements, but is usually either recorded based on a calibrated wheel counter or (more accurately) using magnetic marks which provide calibrated increments of cable length. The measurements must then be corrected for elastic stretch and temperature. There are many types of wireline logs and they can be categorized

either by their function or by the technology that they use. "Open hole logs" are run before the oil or gas well is lined with pipe or cased. "Cased hole logs" are run after the well is lined with casing or production pipe. Wireline logs can be divided into broad categories based on the physical properties of rocks.

Depending on the type of measurement there are different types of well log:

- Resistive Logs:
 - Induction
 - Induction Double
 - Double Laterolog
 - Microspherical
 - Microimages Resistive Training
- Radioactive Logs:
 - Compensated Neutron
 - Compensated Lithodensity
 - Gamma Ray Spectroscopy
 - Natural Gamma Ray
- Acoustic Logs:
 - Porosity Sonic
 - Dipole Sound Images
 - Ultrasonic Images
 - Sonic Logs (V_P and V_S)

Because the well data obtained from ExxonMobil only exhibited some logs, we analyzed the following well-data: induction (water saturation), natural gamma ray (shale volume), density, sonic porosity and sonic logs (V_P and V_S). For a better interpretation of well data, it is sometimes necessary to filter the data for environments with low S/N ratio. In other occasions it was necessary to reconstruct the records. For example, S-wave velocity recording is a problem in seismic processing. However, most of techniques used in reservoir characterization uses seismic attributes that needs information of S-wave velocity (V_S). In this way it is important to find ways that from P-wave velocity we are capable to acquire S-wave velocity. For this task, there are many ways to obtain S-wave velocity from P-wave

velocity using empirical formulations.

In this work, we used many techniques and empirical equations from rock-physics for the analysis of the data set, one of these techniques come from the Castagna' equations (CASTAGNA et al., 1985), with which the new well log of the S-wave velocity was created, which relating the P wave velocity changes through linear and nonlinear relationships

$$V_S^{(1)} = \frac{V_p - 1.36}{1.16}, \quad (2.4)$$

and

$$V_S^{(2)} = -0.1236V_p^2 + 1.6126V_p - 2.3057, \quad (2.5)$$

where, V_p are the P-wave velocity. Here, it is worthy to say, that the well-logs available in Viking Graben data sets, both of them has S-wave velocity available. We are invoking the Castagna' equations (CASTAGNA et al., 1985) only to estimate S-wave velocity in regions where we do not have these information.

Other parameter used in our analysis is the porosity. The well-log porosity was not available in the Viking Graben data sets. Usually, because the calculation of porosity is performed by indirect methods, adjustments are needed for best results, which can avoid errors in the interpretation. In this work, the sonic porosity was estimated by the Wyllie's equation (GREGORY et al., 1958), (in equation 2.6)

$$\Phi_{sonic} = \left(\frac{\Delta_p^{log} - \Delta_p^{matrix}}{\Delta_p^{fluid} - \Delta_p^{matrix}} \right) C_f, \quad (2.6)$$

where C_f , Δ_p^{log} , Δ_p^{matrix} , Δ_p^{fluid} and ϕ_{sonic} , are the compaction factor (fractional), sonic log read in zone of interest ($\mu\text{sec}/\text{ft}$. or $\mu\text{sec}/\text{m}$), sonic log read in 100% matrix rock ($\mu\text{sec}/\text{ft}$. or $\mu\text{sec}/\text{m}$), sonic log read in 100% water ($\mu\text{sec}/\text{ft}$. or $\mu\text{sec}/\text{m}$) and porosity from sonic log (corrected for compaction if needed) respectively. The values used for this study were obtained empirically, which are: $C_f = 1.3$, $\Delta_p^{matrix} = 50 \mu\text{sec}/\text{m}$, $\Delta_p^{fluid} = 238 \mu\text{sec}/\text{m}$.

Although in both well-logs we have the availability of the density log. In the case of seismic, where the properties of the well are extrapolated for regions far to the well, it is necessary to estimate the density for the entire seismic section region.

One possibility of doing this, would be through empirical relations between density and velocity. One of the empirical relationships more known and used routinely in the case of seismic processing, is the empirical Gardner's equation (GARDNER et al., 1974), in which mathematically, the density as function of the P-wave velocity is given by,

$$\rho = \alpha V_p^\beta, \quad (2.7)$$

where $\alpha = 0.23$ and $\beta = 0.25$ for velocity in ft./s and $\alpha = 0.31$ and $\beta = 0.25$ for velocity m/s.

2.3 Rock Physics Attributes

In reflection seismic, a seismic attribute is a quantity extracted or derived from seismic data that can be analyzed in order to enhance information that might be more subtle in a traditional seismic image. Consequently, this can leading to a better geological or geophysical interpretation of the data. Examples of seismic attributes can include travel time, amplitude, phase, frequency content and/or combination of these attributes. In most exploration and reservoir seismic surveys, the main objectives are, firstly, the correctly imaging of structures in time and depth and, second, the correctly characterization of the amplitudes of the reflections. Assuming that the amplitudes are accurately rendered, a host of additional features can be derived and used in interpretation. Collectively, these features are referred as seismic attributes (YOUNG; LOPICCOLO, 2005).

Beyond those one, other attributes commonly used include: coherence, azimuth, dip, instantaneous amplitude, response amplitude, response phase, instantaneous bandwidth, AVO, and spectral decomposition. A seismic attribute that can indicate the presence or absence of hydrocarbons is known as a direct hydrocarbon indicator (SHERIFF, 2002). Attributes can be obtained from typical post-stack seismic data volumes, and these are the most common types. On the other hand, additional information can be obtained from attributes of the individual seismic traces prior to stacking, in a pre-stack analysis. The most common of these is the variation of amplitude with offset (or amplitude versus offset also called by AVO), which is often used as an indicator of fluid type. The interpretation of any attribute is non-unique and calibration to well data is required to minimize the ambiguities

present. (DEY-SARKAR; SVATEK, 1993)

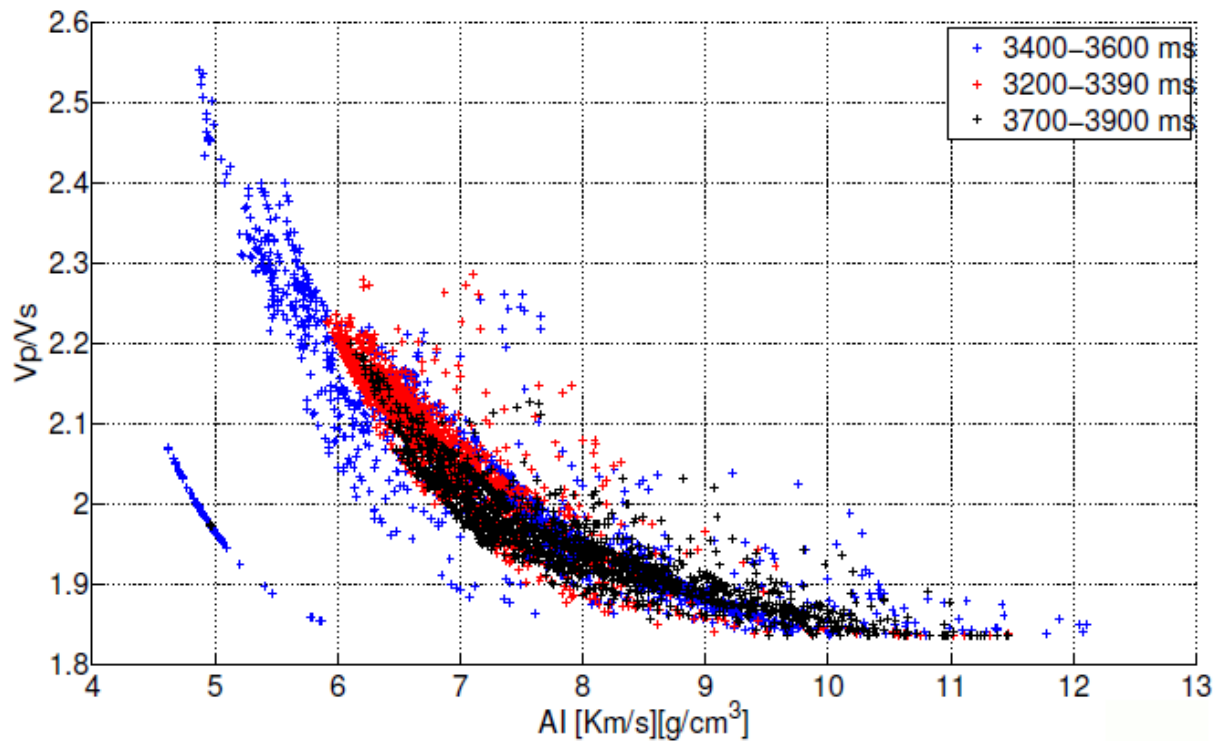
2.3.1 Rock-Physics Template

The conventional seismic interpretation and amplitude versus offset (AVO) inversion workflows provide an important information for hydrocarbon explorationists. Extending this workflow to quantitatively assess potential rock fabric and grain micro-structure, they provides new opportunity to improve reservoir characterization studies. Rock physics is intrinsically linked from sedimentology properties to seismic attributes. In general, this is performed through the implicit and explicit assumptions about grain and matrix relationships that are used to describe the material. The conventional applications of such models are primarily related to clastics sequences in which rock fabric and texture are related to grain size and sorting and have compressional and shear velocity expressions. Avseth et al. (2005) proposed a technique they called the rock physics template (RPT), based on the theory by Dvorkin and Brevik (1999), in which the fluid and mineralogical content of a reservoir could be estimated on a crossplot of V_P/V_S ratio.

In this method, they compute a theoretical template consisting of values of V_P/V_S ratio versus acoustic impedance-AI (AI=velocity vs density) and compare this template to results derived from both well logs and the inversion of pre-stack seismic data. The RPT involves computing the V_P/V_S ratio and P-wave impedance of various rock types based on their mineralogy, porosity, fluid type, pressure and grain contacts. Avseth et al. (2005) shows that we can interpret the various clusters on a rock physics template in terms of their mineralogy, fluid content, cementation, pressure and clay content. Figure 2.2 shows an example of crossplot between V_P/V_S ratio and P-wave impedance (or acoustic impedance) from well log data. The V_p (sonic) and ρ (density) logs were measured and the V_s (dipole sonic) log was computed using the Gardner relationship (GARDNER et al., 1974) mud-rock line over the shales and wet sands and the Gassmann equations (GASSMANN, 1951) in the gas sands.

Figure 2.3 shows the relationship of V_P/V_S ratio as function of caustic impedance. The points related to three depth intervals are represented by colors blue, black and red.

Figure 2.2: Graph relating variation of the Poisson's ratio and the change in acoustic impedance where the type of fluid in relation to the variation of the porosity, density and depth, the data were classified, filtered and placed in a RPT (AI vs V_p/V_s) for better viewing behavior and classification of elastic parameters (Data from the well-7 of the Oseberg oil field in North Sea).

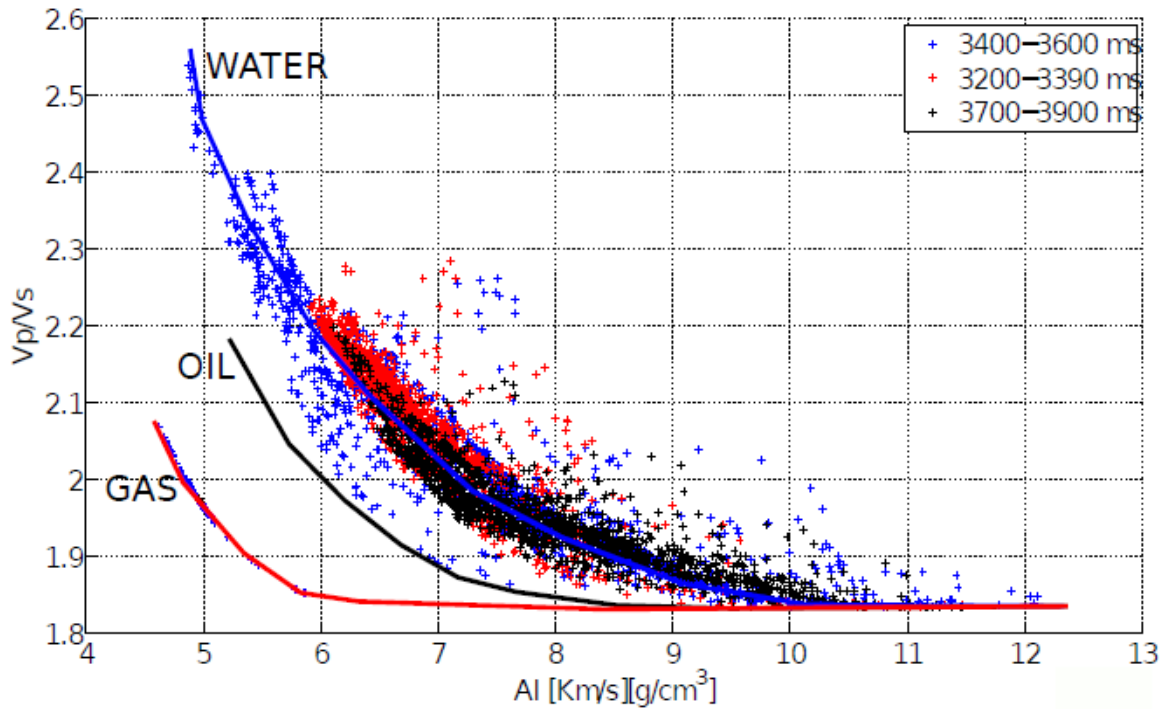


Source: from author

2.3.2 Trend angle

Rock physics has emerged as a tool for geophysicists to characterize reservoir properties as they belong to seismic elastic parameters. In addition, rock physics models have been presented that relate sedimentology and rock fabric to changes in elastic properties. In this paper we have implemented the seismic attribute called by trend angle (AVSETH; VEGGELAND, 2014). The trend angle is a new technique of rock physics that quantifies the angle trend among neighboring data points in a rock physics. On the other hand this method quantifies the interaction of the elastic properties of the fluids with reservoir properties, based on the type of material found by variations in the medium velocities. This attribute is shown conceptually in Figure 2.4 and mathematically at equation bellow,

Figure 2.3: Graphic interpretation of the example of Figure 2.2 where the type of possible fluids contained is different regions from log depends of the degree of porosity, density and depth (data from the well-7 of the Oseberg oil field in North Sea).



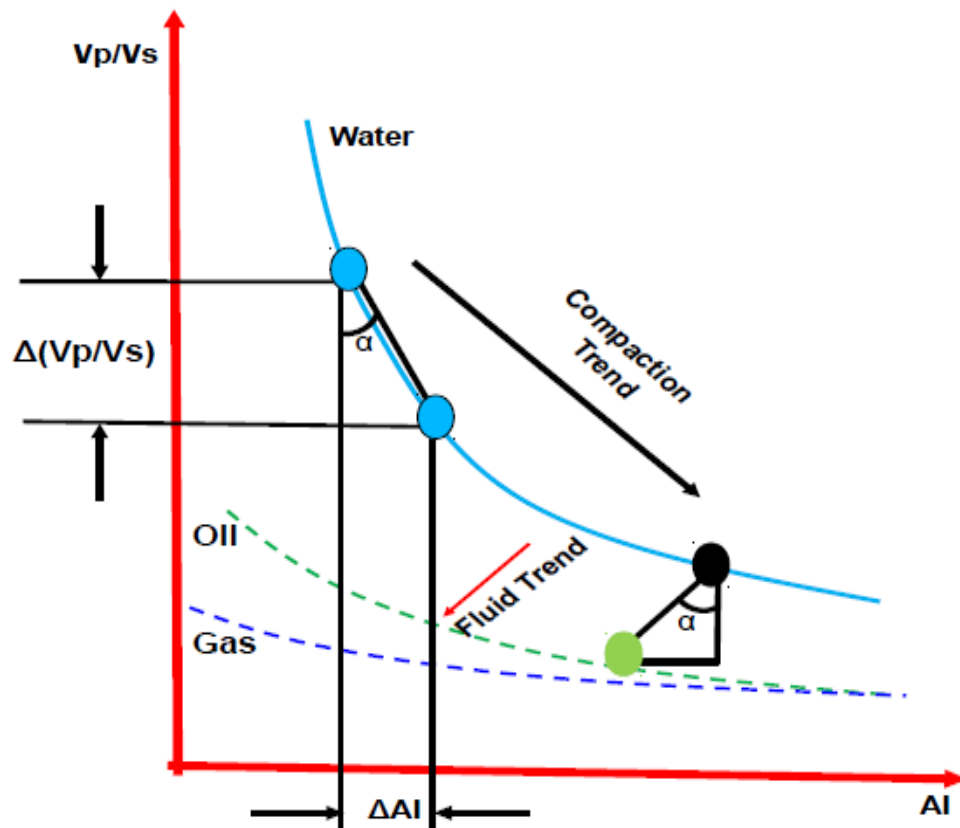
Source: from author

$$\alpha = \arctan \left[\frac{\Delta AI}{\Delta \left(\frac{V_p}{V_s} \right)} \right], \quad (2.8)$$

where ΔAI are variations in acoustic impedances of two adjacent formations, $\Delta(V_p/V_s)$ are variations in the P-wave velocity and S-wave velocity ratio of the same two adjacent formations and α is the attribute value. The minimum and maximum values are between the values of -90 to +90 degrees.

In addition, the units of AI should be in kilometers per second times grams per cubic centimeter to avoid extreme fluctuations between the limits for any point. Alternatively, one could find a trend angle from eigenvector analysis. The concept of the trend angle is similar to the AVO attribute defined by Regueiro and Gonzalez (1995) or the polarization angle defined by Castagna et al. (1985). However, this approach is more easily performed by the relationship between the attribute and changes in rocks-physics properties, because the analysis is performed in the domain AI-versus- V_p/V_s .

Figure 2.4: Illustration of trend angle's definition applied to the elastic parameters, wherein the fluid content variation is shown relative to the porosity and physical parameters variation.



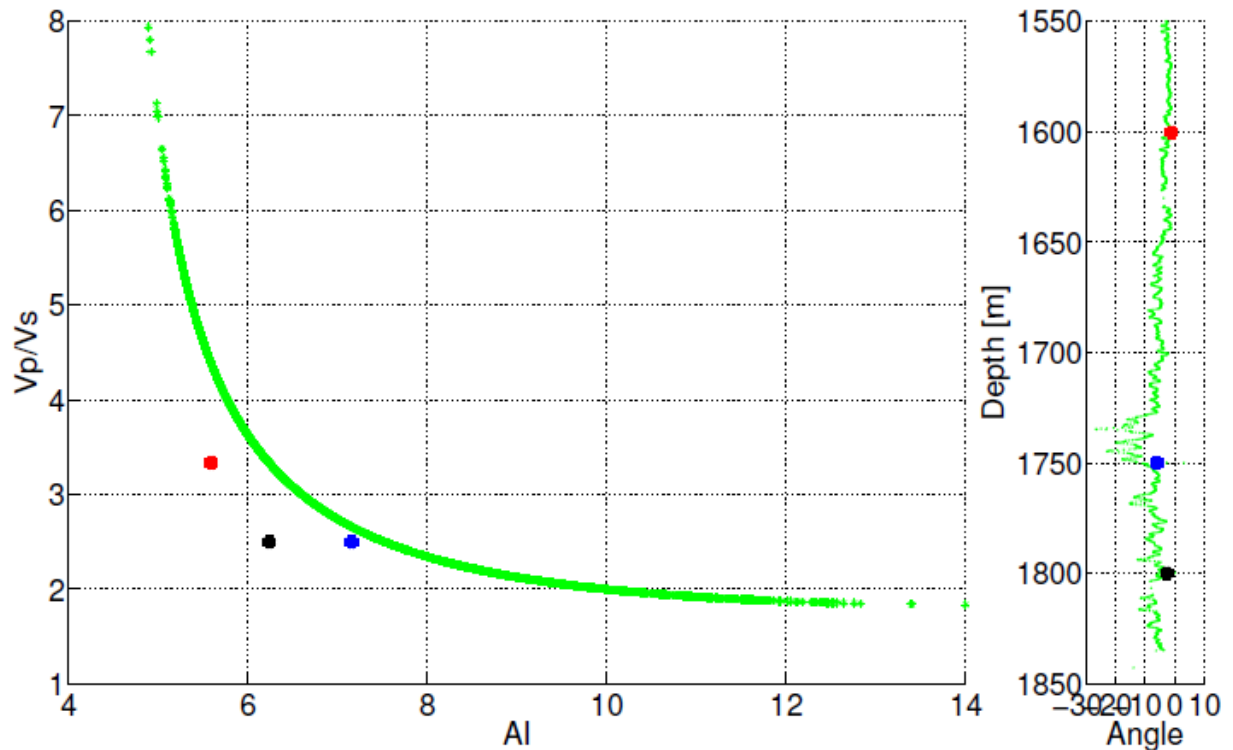
Source: from author

For this work, an example was provided to show the value of this attribute on three synthetic data (see Figure 2.5). We simulated three anomalous points in a range of field data as a function of reducing porosity. The first point (red point) has high porosity and the next points have a low porosity (black and blue points, decreasing toward zero). The p-wave velocity was taken from a real well log and the s-wave velocity was estimated from Castagna's relationship (CASTAGNA et al., 1985), the density from the seismic section was also estimated from the Gardner's relationship (GARDNER et al., 1974). At these two points, we introduce oil into the pore space, using Gassmann theory (GASSMANN, 1951). These data points will create a fluid trend relative to the neighboring data points. We have also introduced extra cement at one data point. This effect causes a movement toward the oil model as V_p/V_s is reduced drastically.

We also plot the data points as a function of depth, where we include the estimated trend angle as a separate log. Here we see that both the oil sands we

simulated are easily detected with the trend angle attribute, including the deeper point. Furthermore, the cement event shows up with a different trend angle, which is closer to the wet-background trend.

Figure 2.5: Example of trend angle applied to the crossplot of the acoustic impedance versus the change of velocity P and S, where we can determine variations in the anomalous data presented (colored dots), inserted in the base data (Data from the well-7 of the Oseberg oil field in North Sea).



Source: from author.

Next we test this attribute on real data (see Figure 2.6). The first step was to select the most suitable location for the test. For this example, it was elected a well with similar characteristics with the wells in the study area, which was the North Sea area.

As shown in the register of gamma ray log of the well-chosen (see Figure 2.7), there are four geological events of progradation and aggradation to the well-marked. Due to the characteristics presented in the log, the portion from 3000 meters up to 4000 meters of depth is ideal for testing the attribute as shown in the Figure 2.6. In the Figure 2.6 we have displayed the AI and Vp/Vs logs along the well trace, where we find a positive value at a depth of approximately 3480 meters, indicating an area with high probability of containing hydrocarbon. Also, the area from 3200-3300 meters presents positive values indicating probable areas containing hydrocarbon.

However, making the comparison with the logs of AI and Vp/Vs, it is noted that these positive values are more related to areas of fracturing, which has the effect of false positives, an effect that can also be noted along trend log angle (Figure 2.6 c). To confirm the results of the attribute trend angle, templates of rock-physics were used, where data of AI versus Vp/Vs were plotted (see Figure 2.2). You can see three trends, which indicate the presence of three types of fluids in the area (water, oil and gas). This would confirm the results of the application of the attribute trend angle (see Figure 2.3).

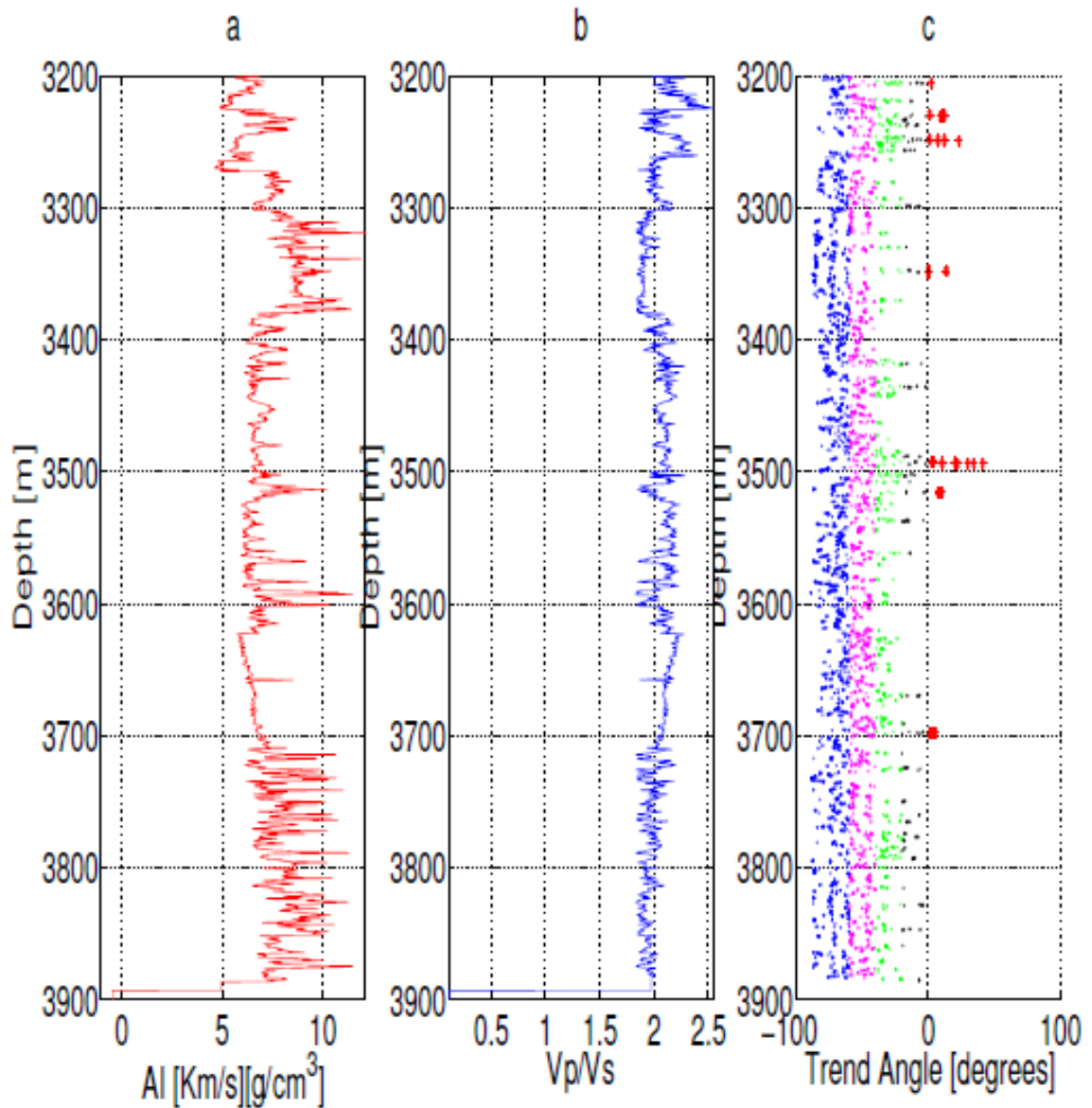
2.3.3 AVO Theory

The AVO (amplitude variation with offset) technique assesses variations in seismic reflection amplitude with changes in distance between shot-points (source locations) and receivers. AVO analysis allows geophysicists to better assess reservoir rock properties, including porosity, density, lithology and fluid content. Around 1919, Knott and Zoeppritz developed a theoretical work necessary for AVO theory (ZOEPPRITZ, 1919).

Given the P-wave and S-wave velocities as well as the density of the two half medium, they developed equations for plane-wave reflection amplitudes as a function of incident angle. Bortfeld (1961) simplified Zoeppritz (1919)'s equations, making it easier to understand how amplitude reflection depends on incident angle and physical parameters. Koefoed (1955) described the relationship of AVO to change in Poisson's ratio across a boundary. Other approximation of exact Zoeppritz equation is the Koefoed (1955)'s approximation.

The Koefoed (1955) approximation are the basis of AVO interpretation nowadays. The AVO analysis is widely used in hydrocarbon detection, lithology identification, and fluid parameter analysis, due to the fact that seismic amplitudes at layer boundaries are affected by the variations of the physical properties just above and below the boundaries. AVO analysis in theory and practice is becoming increasingly attractive.

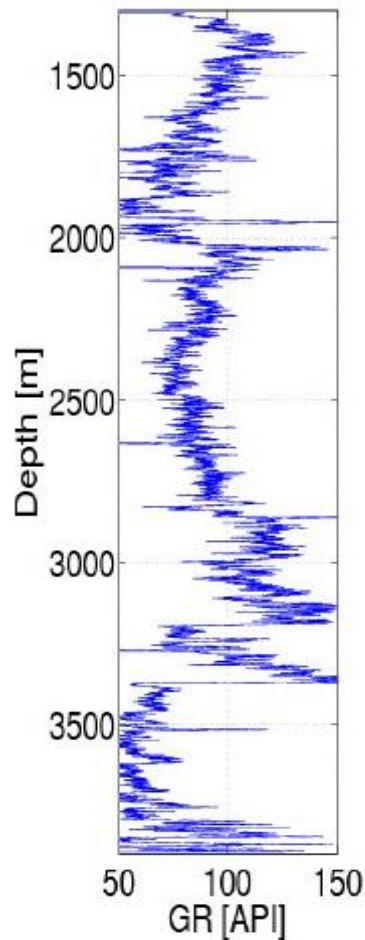
Figure 2.6: Graphic example of trend angle applied to real data, where the target areas were determined. These areas have a high probability of containing hydrocarbon, (a) acoustic impedance plot versus depth (b) ratio of P and S velocities and (c) trend angle depending on the depth (Data from the well-7 of the Oseberg oil field in North Sea).



Source: from author.

The main advantage of AVO analysis is to obtain subsurface rock properties using conventional surface seismic data. These rock properties can then assist in determining lithology, fluid saturated, and porosity. It has been shown through solution of the Knott energy equations (KNOTT, 1899) that the energy reflected from an elastic boundary varies with the angle of incidence of the incident wave (MUSKAT; MERES, 1940).

Figure 2.7: Gamma ray log showing the geological events and variations in the clay content, which can be inferred as target areas (data from the well-7 of the Oseberg oil field in North Sea).



Source: from author.

This behavior was studied further by Koefoed (1955). As mentioned before, the AVO analysis has a simple and important goal: determine the density, P-wave velocity, and S-wave velocity of the earth (Poisson's ratio) and then infer the lithology and fluid content from these parameters. However, there are two difficult problems: the first one is, the unambiguously of some parameters and the second one relies on the inference of lithology from the physical parameters.

When seismic waves travel into the earth and encounter layer boundaries with velocity and density contrasts, the energy of the incident wave is partitioned at each boundary. Specifically, part of the incident energy associated with a compressional source is mode converted to a shear wave (after the critical angle), then both the compressional and shear wave energy are partly reflected from the boundary and partly are transmitted through each of these layer boundaries. The fraction of the

incident energy that is reflected depends upon the angle of incidence. Analysis of reflection amplitudes as a function of incidence angle can sometimes be used to detect lateral changes in elastic properties of reservoir rocks, such as the change in Poisson's ratio. This may then suggest a change in the ratio of P- wave velocity to S- wave velocity, which can imply in a change in fluid saturation within the reservoir rocks.

Starting with the motion's equation (second Newton's law) and Hooke's law, one can derive and solve the wave equations for plane-wave approximation in isotropic media. Then, using the equations of continuity for the vertical and tangential components of stress and strain at a layer boundary, plane wave solutions and Snell's law that relates propagation angles to wave velocities, one obtains the equation for computing the amplitudes of the reflected and transmitted P- and S- wave. Due to the complexity of the Zoeppritz (1919)'s equations, many authors developed approaches to these equations:

- The Bortfeld Approximation (BORTFELD, 1961),
- The Aki, Richards and Frasier Approximation (AKI; RICHARDS, 1980),
- Shuey's Approximation (SHUEY, 1985),

$$R_{\theta} = R_p + \left[R_p A_0 + \frac{\Delta\sigma}{(1-\sigma)^2} \right] \sin^2\theta + \frac{\Delta\alpha}{2\alpha} [\tan^2\theta - \sin^2\theta], \quad (2.9)$$

Where

$$\sigma = \frac{\sigma_1 + \sigma_2}{2}, \Delta\sigma = \sigma_1 - \sigma_2, A_0 = B - 2(1 + B) \frac{1-2\sigma}{1-\sigma}, B = \frac{\frac{\Delta\alpha}{\alpha}}{\frac{\Delta\alpha}{\alpha} + \frac{\Delta\rho}{\rho}}. \quad (2.10)$$

- The Smith and Gidlow Approximation (SMITH; GIDLOW, 1987),

There are numerous expressions for the linear approximation of Zoeppritz (1919)'s equations, each with different emphasis. While Bortfeld (1961) emphasized the fluid and rigidity terms which provided insight when interpreting fluid-substitution problems, Aki and Richard's equation (AKI; RICHARDS, 1980) emphasized the contribution of variations in the P- and S- wave velocities and density. (SHUEY, 1985) after take into account the contributions of Koefoed (1955) and uses the amplitude dependence on Poisson's ratio, reached a simplified equation related to

Aki and Richards equation (AKI; RICHARDS, 1980) in terms of Poisson's ratio. One of the Shuey's (SHUEY, 1985) main contributions is that he identified how various rock properties can be associated with near, mid, and far angle ranges. The AVO response equations expressed above (in equation 2.9) can be simplified further and written as follows for angles of incidence lower than 30 degrees. The angular dependence of P-wave reflection coefficients is now expressed in terms of two parameters, the AVO intercept (A), the AVO gradient (B) and the angle of phase (C). This mathematical relation is expressed by

$$R_{\theta} = A + BC, \quad (2.11)$$

where A represents the normal incidence P-wave reflectivity or intercept term, B is the gradient term containing the AVO effects and C is a constant related with the squared of the angle of phase (MCGREGOR, 2007).

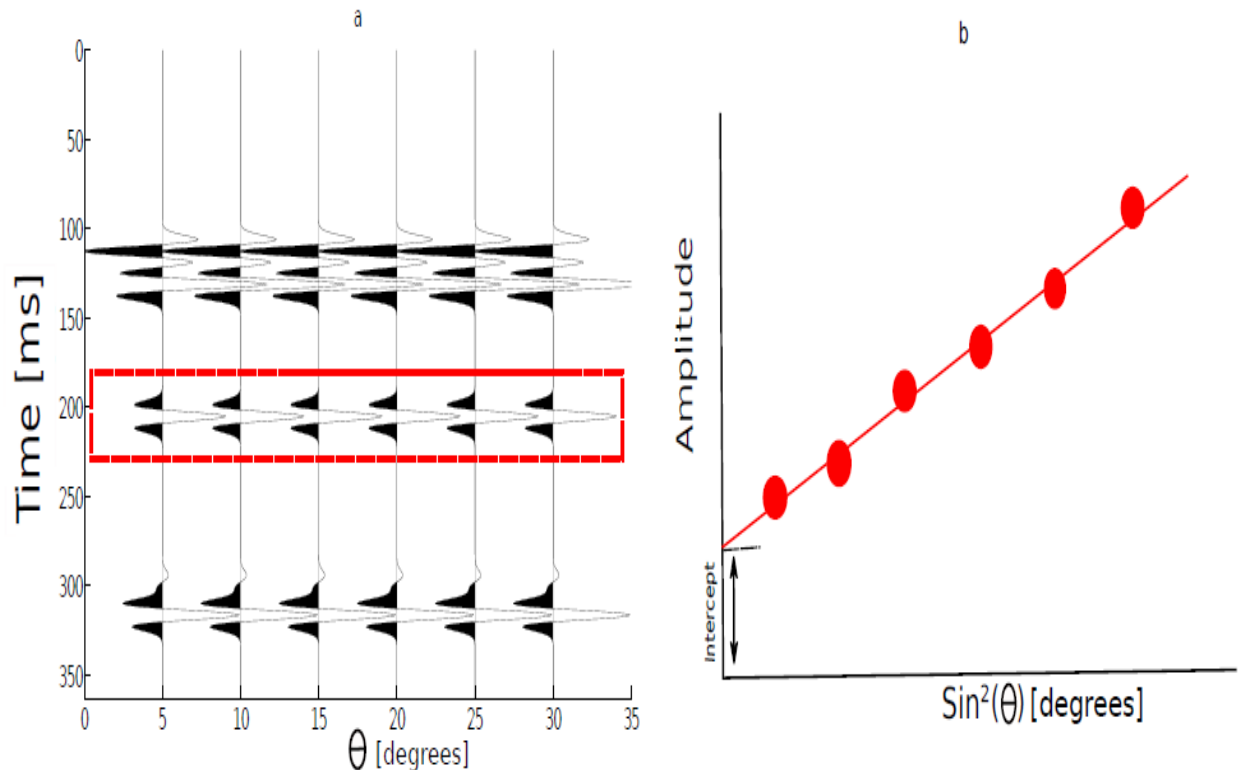
It should now be apparent that amplitudes for any event across a seismic gather can be plotted against incidence angle as shown in the Figure 2.8. This allows the intercept amplitude to be computed for any event in the gather and the computation of the zero-offset or intercept stack. This is more representative of the compressional impedance than the full stack in which the amplitude variation with offset are simply averaged out. This, in essence, is why the AVO analysis and the AVO interpretation have become key processes. The stacking process was designed to average out amplitude variations caused by changes in Poisson's ratio (which can be directly related to the P- and S- velocities) and in density.

2.3.3.1 AVO classification

The original AVO classification scheme proposed by Rutherford and Williams (1989) was limited to gas sands underlying shale which exhibit a subset of the range of possibilities now recognized (see Figure 2.9a):

- Class I - high impedance sands - are mature sand that have been exposed to moderate to high compaction (RUTHERFORD; WILLIAMS, 1989). Seismically, reflection amplitudes decrease with offset and may result in a polarity reversal if sufficient offsets are recorded.

Figure 2.8: Example of the theory of AVO applied to synthetic data. This illustration shows the change in amplitude with the variation of the incidence angle of the wave in the reflector, (a) synthetic seismogram and (b) plot of magnitude of amplitudes as function of incidence angle.



Source: from author

- Class II - near zero impedance contrast sands - possess near-zero impedance contrast between the sand and encasing materials and are moderately compacted sands (RUTHERFORD; WILLIAMS, 1989). This type of gas sand has very low amplitude reflections at near offsets and significantly higher amplitude reflections at far offsets. This offset-dependent seismic response is opposite from "normal" seismic response, therefore processing flows designed for average earth materials are rarely effective in detecting the unique characteristics of class 2 gas reservoirs.

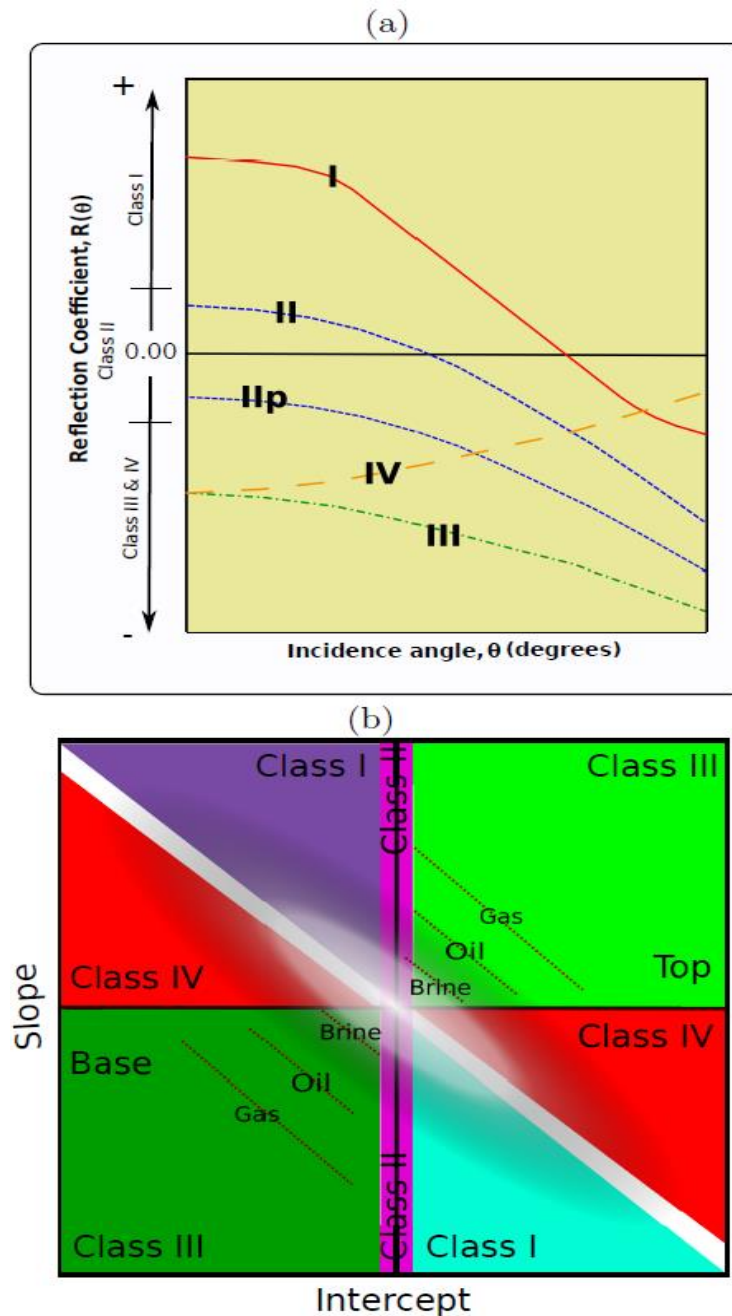
- Class IIb - classification II b is a special type of classification II, because the gas-sand content contained in this class, it can have low amplitude and an intercept with a negative sign (RUTHERFORD; WILLIAMS, 1989). The polarity change, from the classification II to IIb is usually not detectable, because it occurs at a near offset where the signal is below the noise level.

- Class III - low impedance sands - class of gas sands has lower impedance than the encasing medium and is usually unconsolidated (RUTHERFORD; WILLIAMS, 1989). Seismically, reflections appear at offset ranges and without polarity changes. In some cases, deeper layers are not imaged due to limited or no transmission of energy through the base of the confining layer.

- Class IV - lower impedance gas sands - A class IV AVO response has a trough that dims with offset (CASTAGNA et al., 1998). In fact, for this class the introduction of gas causes its reflection coefficient to become more positive with increasing offset, yet decrease in magnitude with increasing offset.

Figure 2.9 shows a scheme of AVO classification and the plane-wave reflection coefficients for the gas sand classification (CASTAGNA et al., 1998). In other words, the relation of gradient versus intercepts is directly related to changes in rock properties, such as changes in lithology and fluid (MCGREGOR, 2007). The gradient section shows areas where AVO anomalies are present as high amplitude events. In the absence of a gradient, the section is quiescent. The gradient section led directly to the interpretation methods commonly used in the industry where the gradient section functions as a screening tool. Gathers are examined in those areas high graded from the gradient section analysis. The traditional workflow is then to analyze the events on the gathers by trying to match the response with model gathers.

Figure 2.9: Graphical definition of AVO classification in AVO analysis chart. In a general words, this graphics are showing the classification of the fluids by varying physical properties: (a) plane-wave reflection coefficients at the top from Rutherford and Williams (1989) classification of gas sand. Class IV sands have a negative normal-incidence reflection coefficient, but decrease in amplitude magnitude with offset (from Castagna et al. (1998)) and (b) AVO classification scheme for identifying the magnitude and class of a seismic reflection. The polarity convention in this display denotes a decrease in acoustic impedance by a peak.



Source: from author modified from (CASTAGNA et al., 1998; RUTHERFORD; WILLIAMS, 1989)

3 METHODOLOGY

As mentioned before, in this work, we conducted a reservoir characterization analysis on the exploration field North Sea region. More specifically, we performed a reservoir analysis in the Viking Graben seismic and well logs data set. The sequence of processing steps performed in this study, is described in the following section. We used several flowcharts to show the main stages carried out in our analysis. Figure 3.1 shows the general flowchart used in this work. It shows the seismic processing stages as well as the well-log processing stages. Beyond that, it shows that there is a moment where both are combined.

3.1 Processing Sequence of the Seismic Data

- **PROCESSING OF SEISMIC DATA:** in this stage (after performing the data extension revision) the seismic data were loaded and the seismic processing was made using the "ProMax 2D" software.

- **PROCESSING SEQUENCE (SEISMIC DATA)** (see Figure 3.2)

- **Data Loading:** to start at this stage, the seismic data acquired in the field are loaded in ProMax 2D program.

- **Geometry Setting and Correction:** at this stage, the field data, like latitude, longitude, altitude, label, shot-point number, etc. were loaded.

- **Editing Data Loaded:** at this stage the seismic data was revised (corrupted traces) and cut at 3000 ms (original size 6000 ms), because the subsequent section the S/N ratio was very low.

- **Velocities Analysis:** at this stage of the processing sequence was a complete review of the frequencies present in the seismic data, and the predominant frequency was determined, which is able to make a process for increasing the S/N ratio, it was also created the velocity model (table of velocities) used for the time-depth conversion and in the stage of migration (YILMAZ, 1987).

- **Multiple Filtering:** at this stage applied a filter to remove horizons that were repeated in seismic data, due to the arrangement of the geological sequences (horizons), this was done to improve the S/N ratio.

- **NMO (normal moveout) Correction and Stacking:** at this stage, the NMO correction to the seismic data was made using the velocity model obtained earlier. Also we use this velocity model to perform stacking operation.

- **Migration:** at this last of conventional seismic processing, we use the velocity model (obtained above). This stage is important because in this moment the reflectors are positioned at correct location (if velocity model are nearly to the true one) and cross-talk events are removed. Beyond that, this migration provides good handling of steep dips, up to 90 degrees (YILMAZ, 1987).

- **AVO analysis:** in this stage the AVO attributes were acquired (intercept and gradient). Using this attributes we construct the AVO maps. The AVO analysis to seismic section was performed for the location of the target areas in the section.

- **Data Exportation:** in this this stage we prepare and export all tables (seismic migrated section and AVO attributes) then be used in other software, e.g., “MatLab”. In the “MatLab” software we carry out the analysis and integration of the seismic data with the well-logs data.

3.2 Processing Sequence of the Well-Log Data

- **PROCESSING OF WELL DATA:** in this stage the well data were loaded and codes for filtering and processing was created in MATLAB software.

- **PROCESSING SEQUENCE (WELL DATA)** (see Figure 3.3)

1. **Data loading:** we start this stage loading the well data related to the two wells, which are located in the target zone.

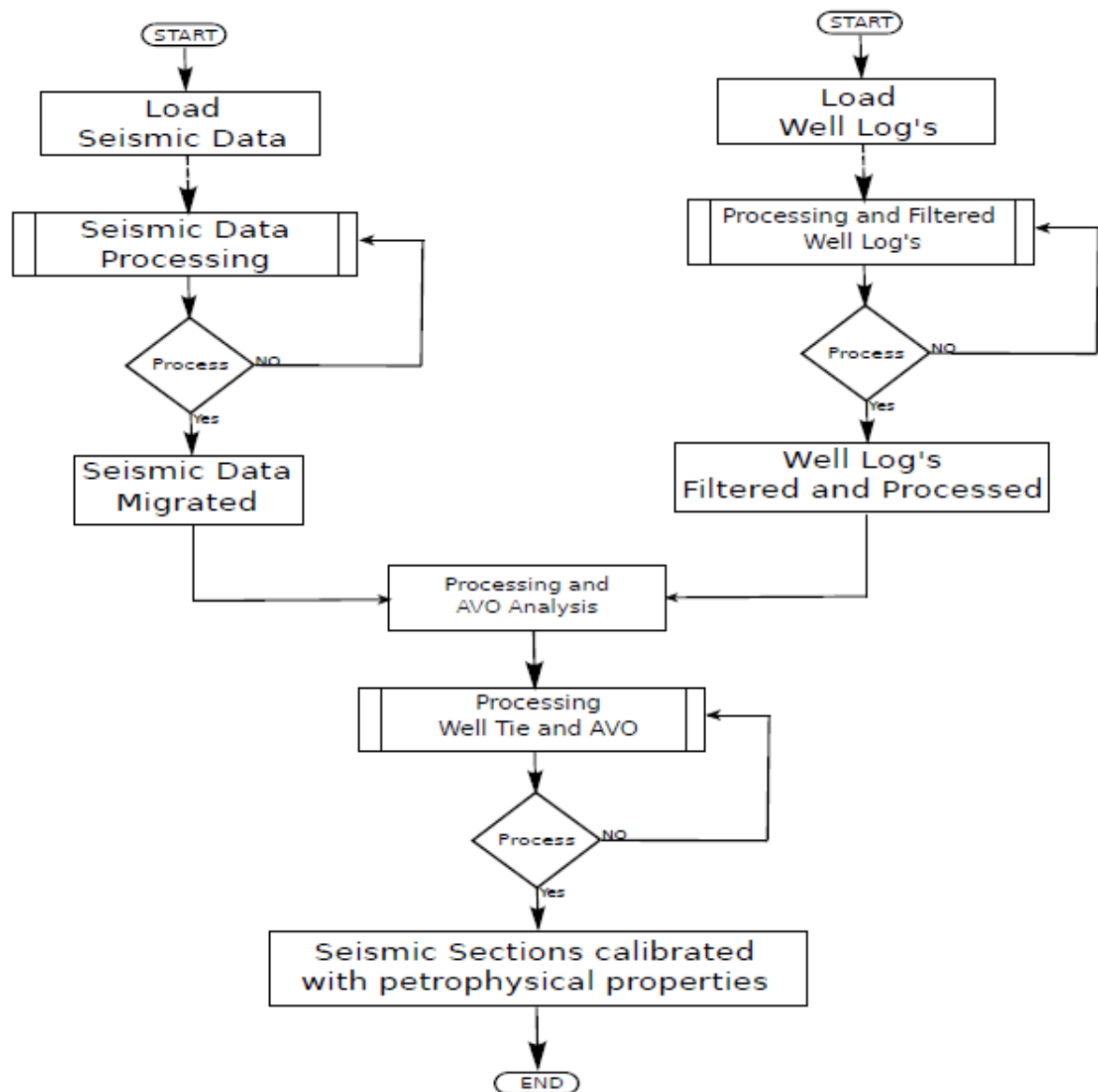
2. **Review, Filtering and Removal of Bad Data:** in the second stage, was made a full revision and filtering of well-logs in order to eliminate the bad data. For example long sections with gaps or very large anomalous data, were revised to increase the S/N ratio in the data well. This was performed, because some well logs contain errors along to the data. In some logs, it was necessary to create new well logs based on empirical equations.

3. **Creation of m-File:** in the third stage, was created the m-files for compilation, filtering and creation, by mathematical formulation, of new logs (density, velocity, porosity, etc.).

4. **Processing New Tables and Logs (density, porosity, velocity, etc.):** in the fourth stage, was made a compilation, filtered and creation of new logs, from the well data, to perform the analysis and interpretation of well-log data.

5. **Well-Logs Characterization:** at the fifth stage, after generation, compilation and filtering the well-logs, the characterization of them was performed (acoustic impedance, Poisson ratio, etc.).

Figure 3.1: Workflow chart applied to the seismic and well-logs data processing.

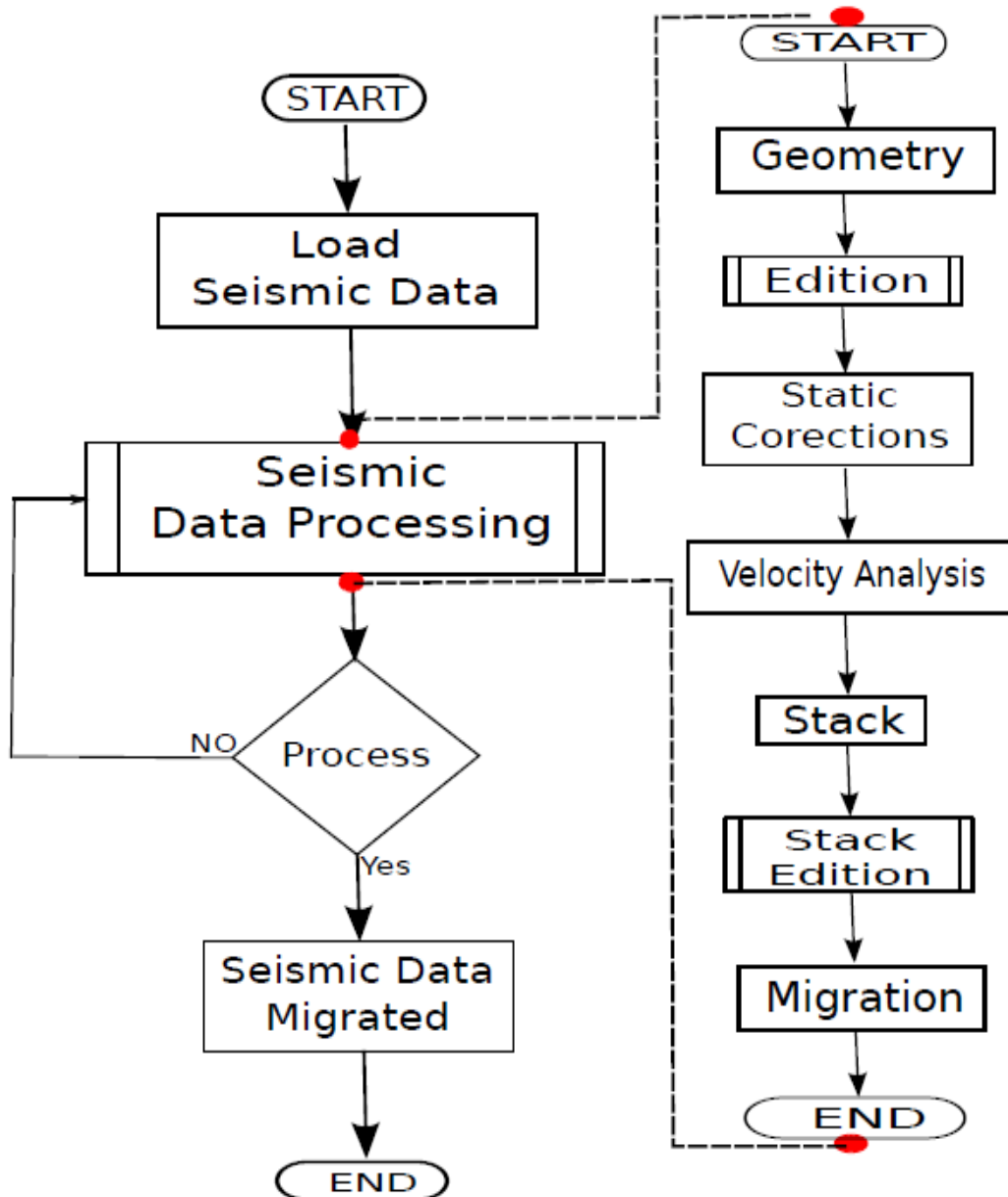


Source: from author

6. Identification and Delimitation of Anomalous Zones: in the sixth stage, the extraction of the seismic attributes was performed, and the results was shown in logs and rock-physics templates.

7. Analysis of Anomalous Zones Finally: in the seventh stage, a different analysis of well-logs by deferent techniques were performed, for determining the rock-physics property changes of the wave.

Figure 3.2: Basic seismic processing step performed in our seismic data.

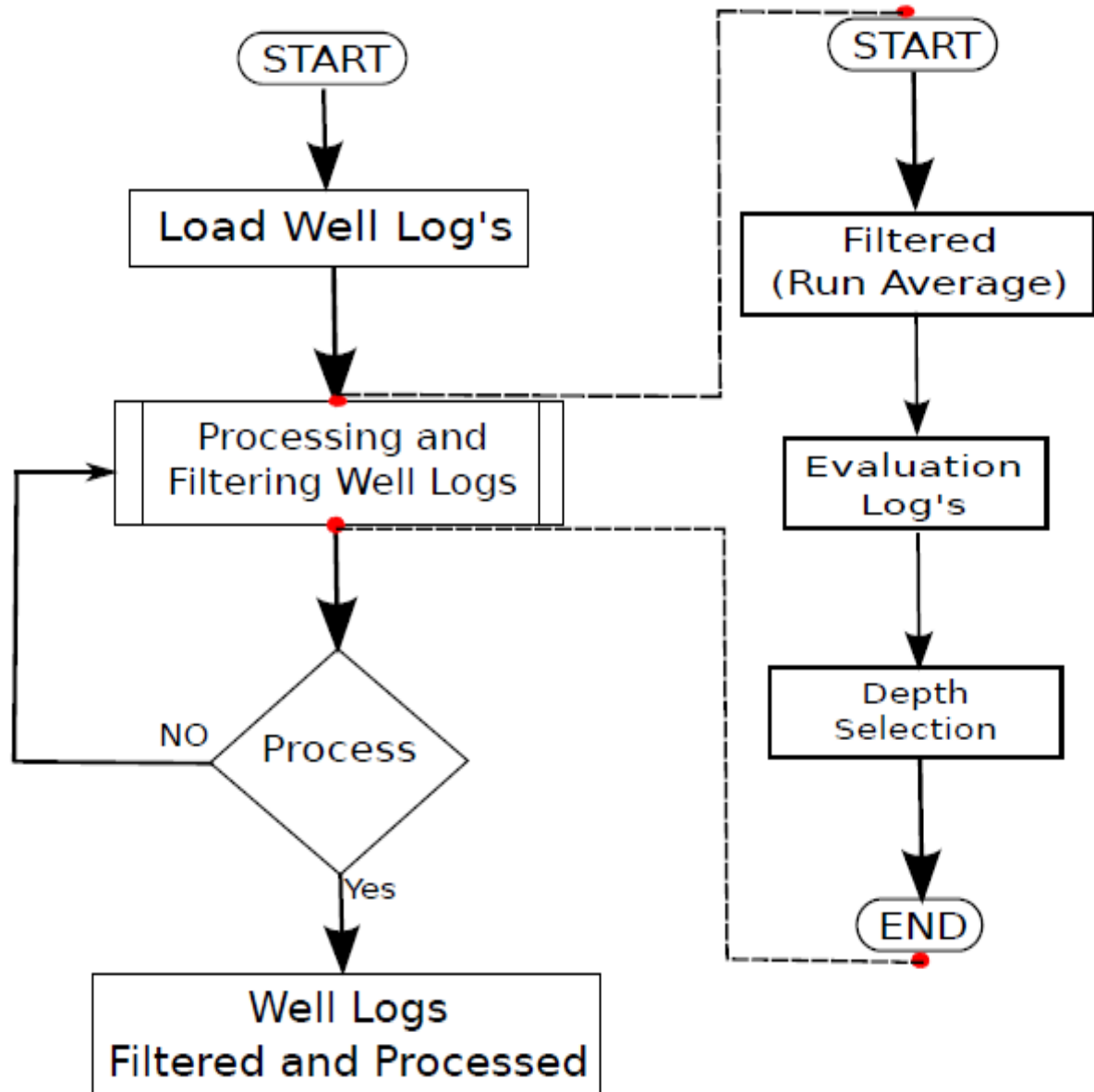


Source: from author

- **PROCESSING THE RESULTS:** the processing results will be used to correlate the seismic data with the new well logs. This will be used to generate synthetic seismograms and create new maps of physical properties.

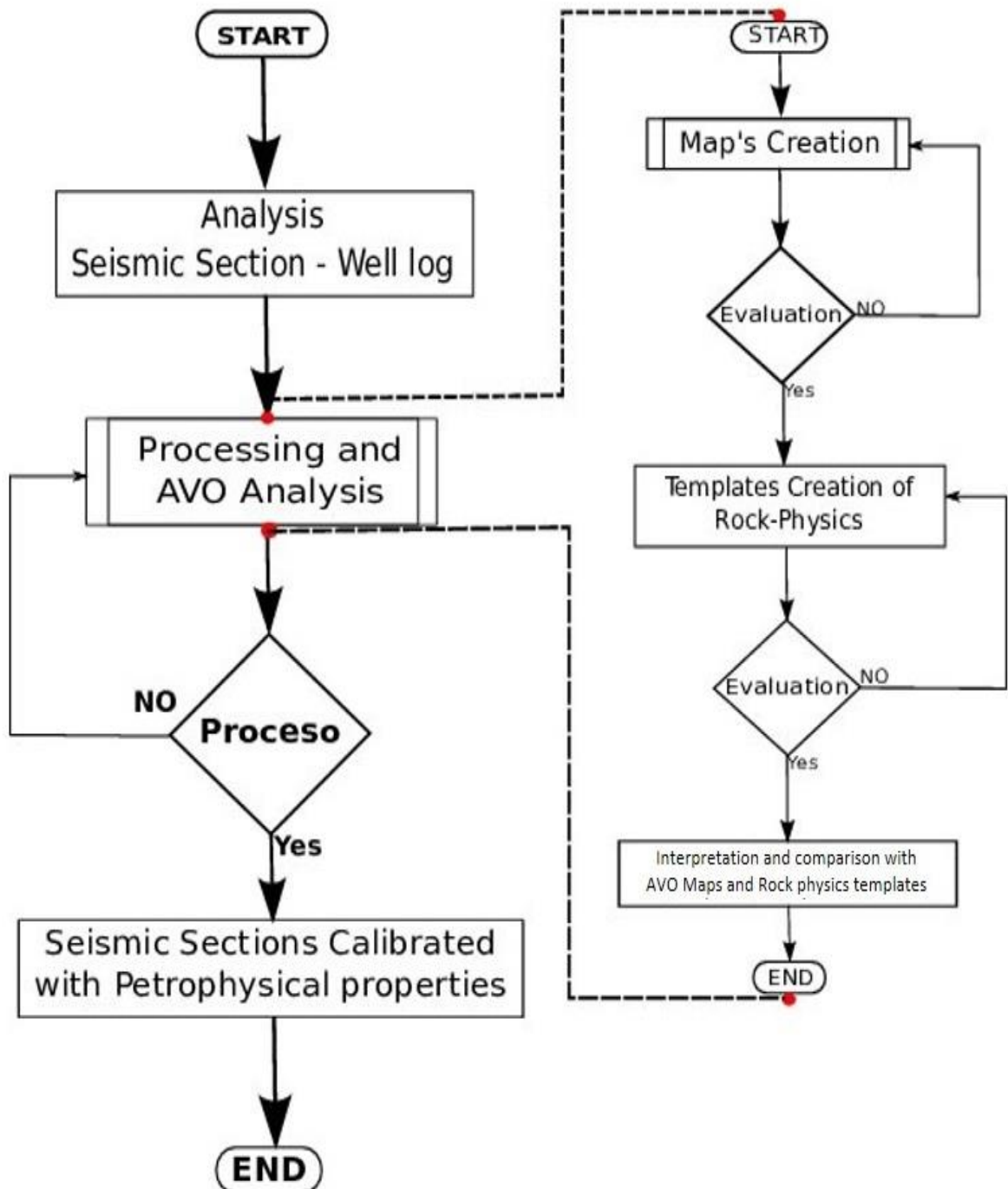
- **ANALYZING THE RESULTS** (see Figure 3.4): in the final stage the analysis and interpretation (seismic section and well data), of the maps and records of the physical properties obtained from the anomalous zones it will be performed.

Figure 3.3: This workflow chart shows all stages performed in the well-log data processing.



Source: from author

Figure 3.4: This workflow chart shows the point in our analysis that information from seismic section and well-logs are combined to provide an interpretation about this reservoir.



Source: from author

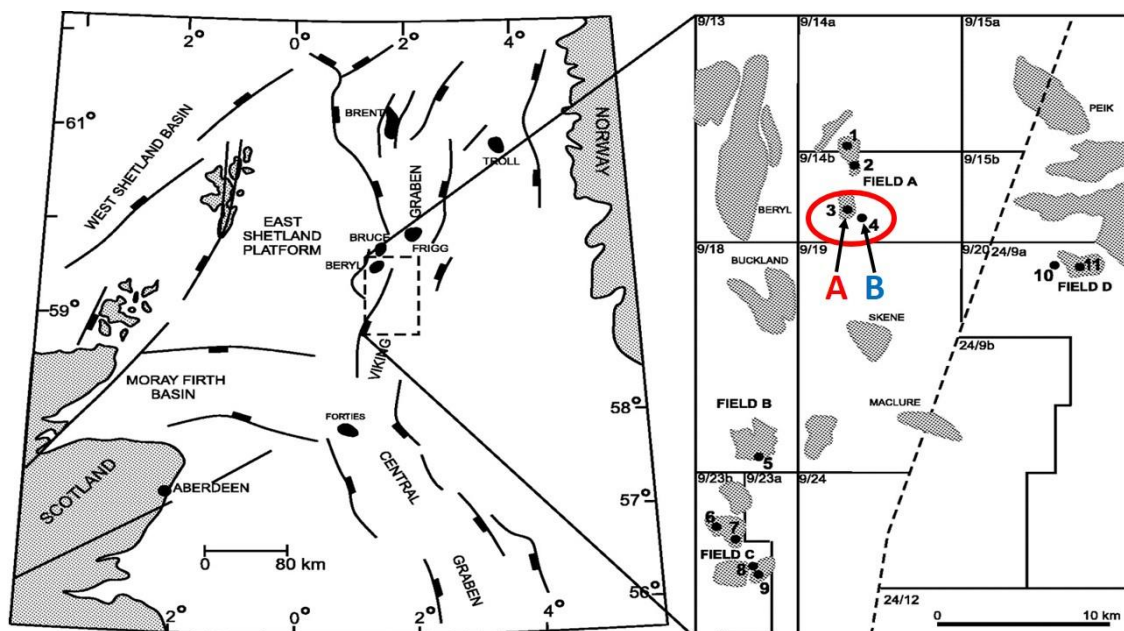
4 RESULTS

4.1 Location

The Viking Graben is a north-south trending linear trough straddling the boundary between the Norwegian and UK sectors of the northern North Sea (see location in Figure 4.1). The east Shetland platform, with Tertiary strata resting directly on Devonian redbeds, lies to the west of the graben, to the east is the Vestland Arch, a narrow fault-bounded ridge (GLENNIE, 1982).

The Viking Graben was formed during late Permian to Triassic rifting, extensional episodes and accompanying continued sedimentation through the Jurassic into the early Cretaceous. Normal basin subsidence and filling became the primary depositional mechanism by the late Cretaceous (ROBERT et al., 1992). The stratigraphy of the reservoir rocks in this area is shown in (Appendix A). Reservoirs occur in the Frigg, Cod, Staffjord, and Brent Formations. In the Figure 4.2 we can see a significant unconformity occurs at the base of the Cretaceous (labeled base Cretaceous unconformity - BCU). Jurassic syn-rift sediments are uncomfortably overlain by Cretaceous and Tertiary basin fill (MADIBA; MCMECHAN, 2003).

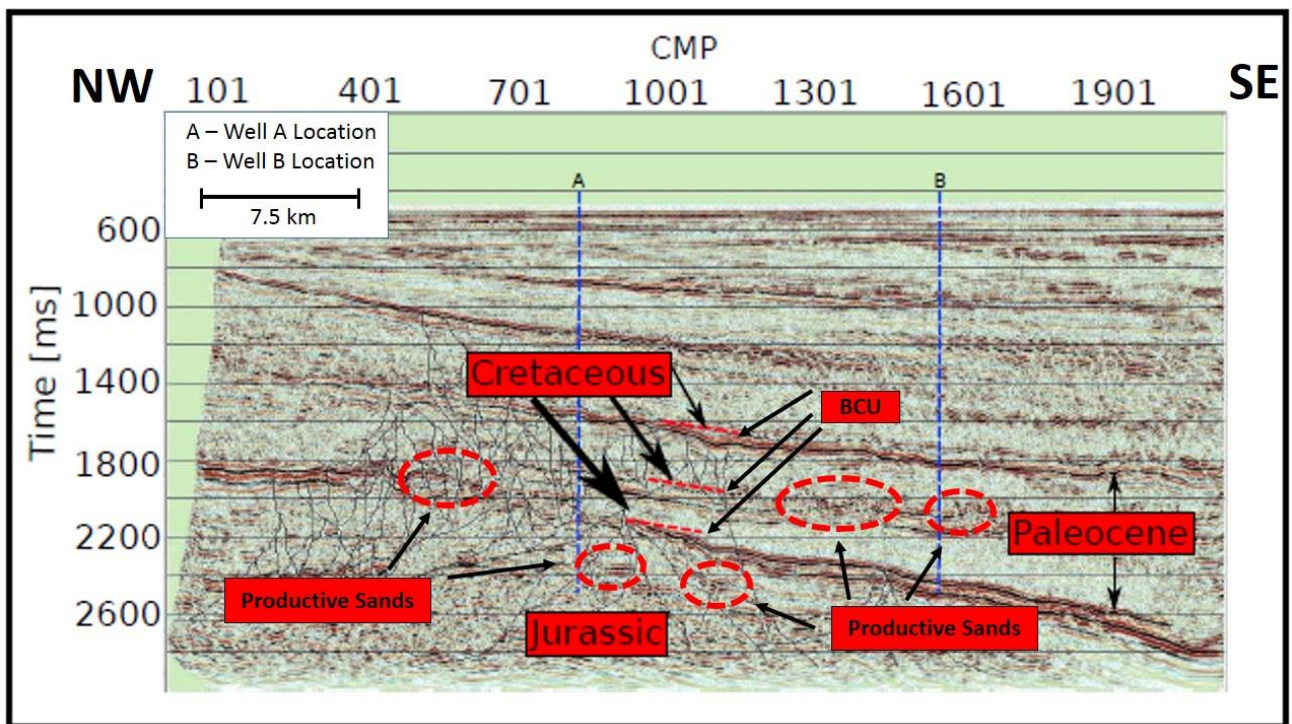
Figure 4.1: Map of the Viking Graben field area.



Source: Jonk; Hurst; Duranti; Parnell; Mazzini and Fallick (2005), modified from (Brown, 1990).

The objectives in the primary reservoir of the north Viking Graben presents clastics sediments of the Jurassic syn-rift (lying below the unconformity). The strata of the Jurassic area in the North Sea area occurs for most part, in the basins fault-bounded, this is related to the development of the graben system. The transgressive system has periods, in the Jurassic, of regression that provided the coarse clastic input that forms the reservoir intervals (MADIBA; MCMECHAN, 2003).

Figure 4.2: Time migrated and interpreted seismic section of the study area, where the main geological structures, faults, anomalies and geological faces are shown.



Source: from author

The Jurassic was a period of active faulting, hydrocarbon traps are usually fault-bounded structures, but some are associated with stratigraphic truncation at the BCU (BROWN, 1990). The depositional environments of the Jurassic reservoirs range from fluvial to deltaic and shallow marine. Productive sands have been encountered in diverse local structural positions (see Figure 4.2), including the crests of tilted fault blocks, the down-thrown side of normal faults, and arched-over salt-induced (BROWN, 1990). A second reservoir target in the North Viking Graben is a Paleocene deepwater clastics. The Paleocene interval is undisturbed by the rift tectonism and dips into the basin (see Figure 4.2). Over much of the basin, the

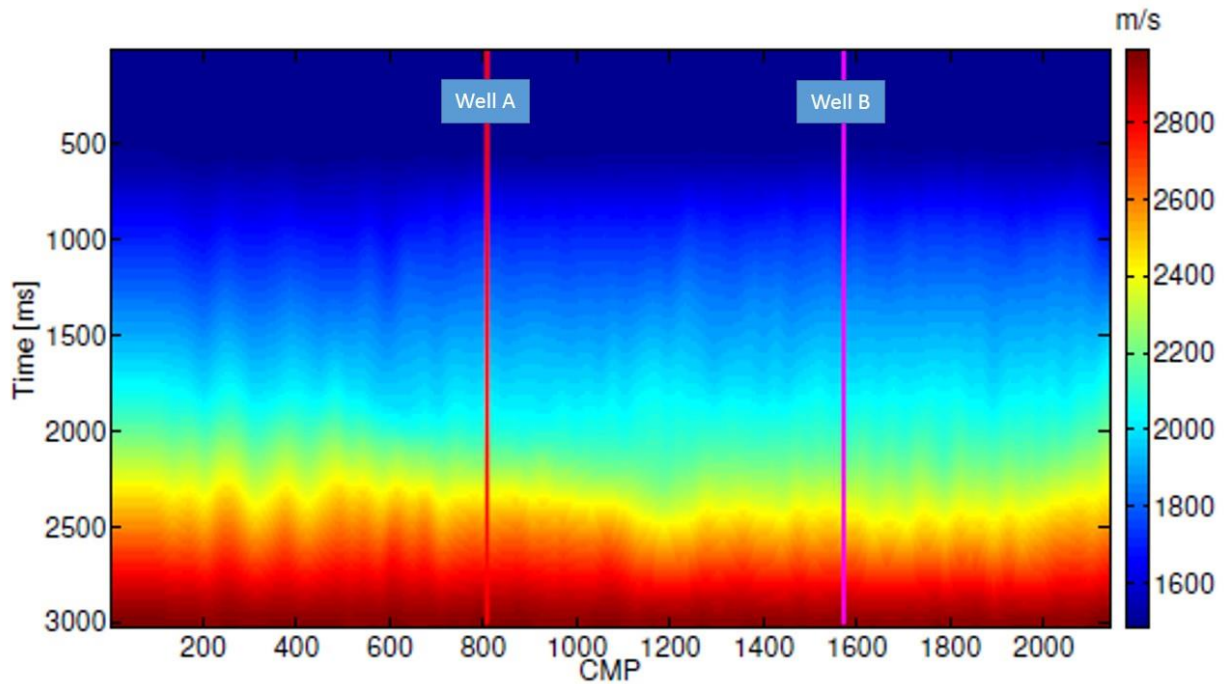
Paleocene section was deposited in an environment slope (and so contains turbidities or slump sediments). Here, the sandstone reservoirs are associated with regressive pulses and the hydrocarbon traps are usually depositional mounded structures or stratigraphic pinch outs. (BROWN, 1990)

4.2 Seismic Data Preparation

There are two difficulties with the hydrocarbon characterization in the Viking Graben dataset. The first one, is the complexity itself of the Viking Graben region. The second and most important, is the discrimination of hydrocarbon-bearing sands from shale and the separation of gas sands from water-saturated matrix. To overcome the difficulties presented, a carefully processing and reprocessing of seismic data were performed. The operations involved with the processing among other things, that we have mentioned in previous chapters, constituted in repositioning of the data in the true geometry, data filtering (because the data present an environment with low s/n ratio) and the creation of a feasible velocity to migration. An affordable velocity model was reached through the velocity picking every 5 CMP. In this way, a velocity model with the best sampling rate was achieved. Figure 4.3 shows the best velocity model reached with our NMO correction (normal moveout correction) analysis. As it showed in Figure 4.3, the velocity model created, has variation in the velocities as expected in the area of the Graben, in the model also can be seen that the variations in the contrast of velocities from 2000 ms to 3000 ms have less separation, this is the result of having an environment highly fractured, due to strong tectonic movements during the formation of the study area.

Figure 4.4 shows the result of the time migrated section. The migration was performed using the Kirchhoff operator and the velocity model showed previously. The red lines in Figure 4.4a show the well positions (wells A and B). As it can see, the well A is located in the middle of the Graben with many faults, which provides a favorable environment for structural traps, creating areas with possibility of containing hydrocarbon. Figures 4.4b and 4.4c show the seismic traces of each well. The high variations in the amplitude magnitude show that are impedance changes, caused by the change in the lithology of the area.

Figure 4.3: P-wave velocity model, used to reach the migrated seismic section. As it can be seen the lateral and vertical anisotropy are present in the area.



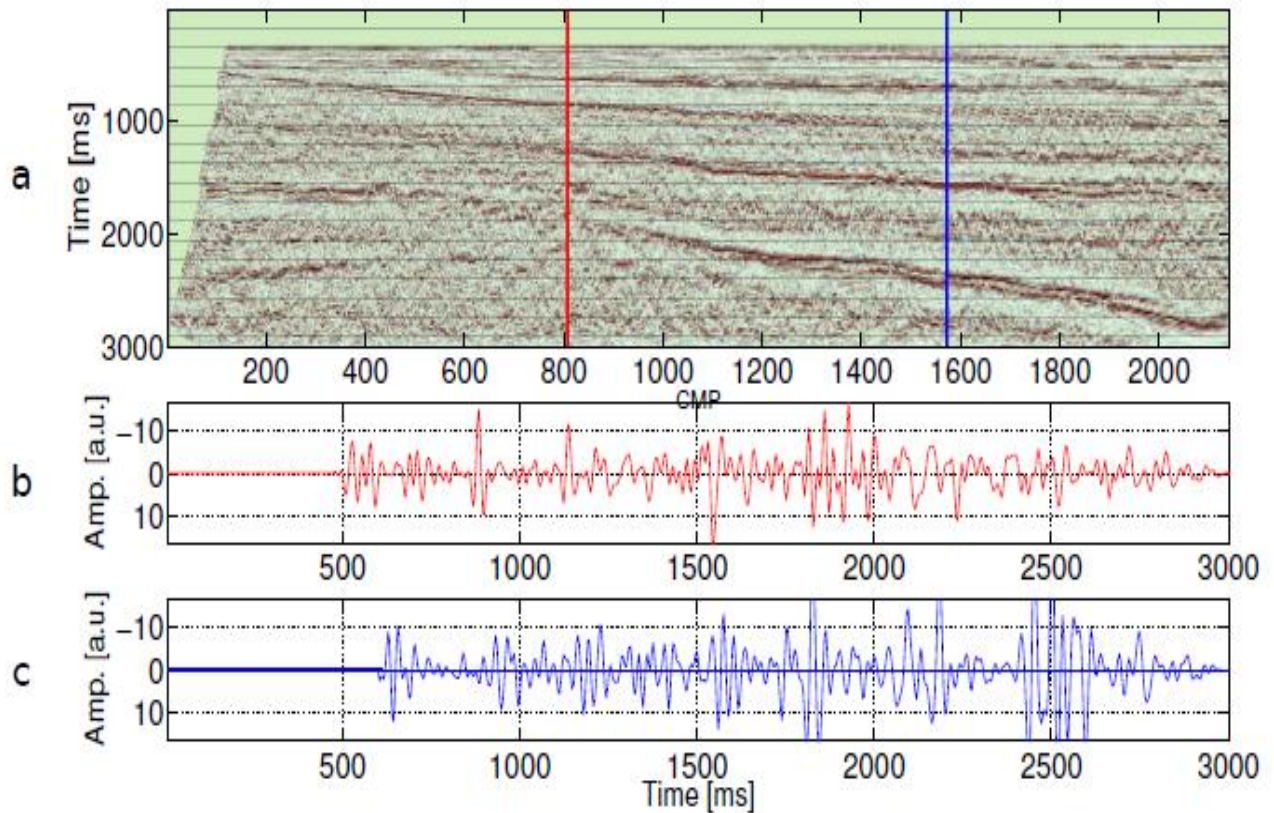
Source: from author

4.3 V_s and Porosity Predictions

Due to in the well log of the S-wave velocity has showed gaps, was necessary to create a new well logs, for both wells (see Figures 4.6 and 4.7), for which the two different types of mathematical relationships from Castagna et al. (1985) were taken, the first is a linear relation, which the relation of V_p velocity with a V_s velocity by a numerical constant ($V^{(1)}$) (in equation 2.4), and the second is a quadratic relationship, which relating the V_s velocity and V_p velocity by three numerical constants ($V^{(2)}$ in equation 2.5).

In Figure 4.5, the logs from the well A and B are shown, where it can be seen that in the initial part that the calculated velocities and the original velocity do not exhibit coincidence, especially in the uppermost part, this is due to compaction factor, but in the target areas the coincidence is greater, so for to eliminate the gaps present and increase the accuracy of the results, we was worked with the log of the S-wave created from Castagna et al. (1985)'s relationship V_{cs} (in equation 2.5).

Figure 4.4: Time migrated section and seismic traces related to the well locations (CMP 808 and CMP 1572), where the structural variations present on the sub-surface are shown: (a) time migrated seismic section, (b) seismic trace from well A and (c) seismic trace from well B.

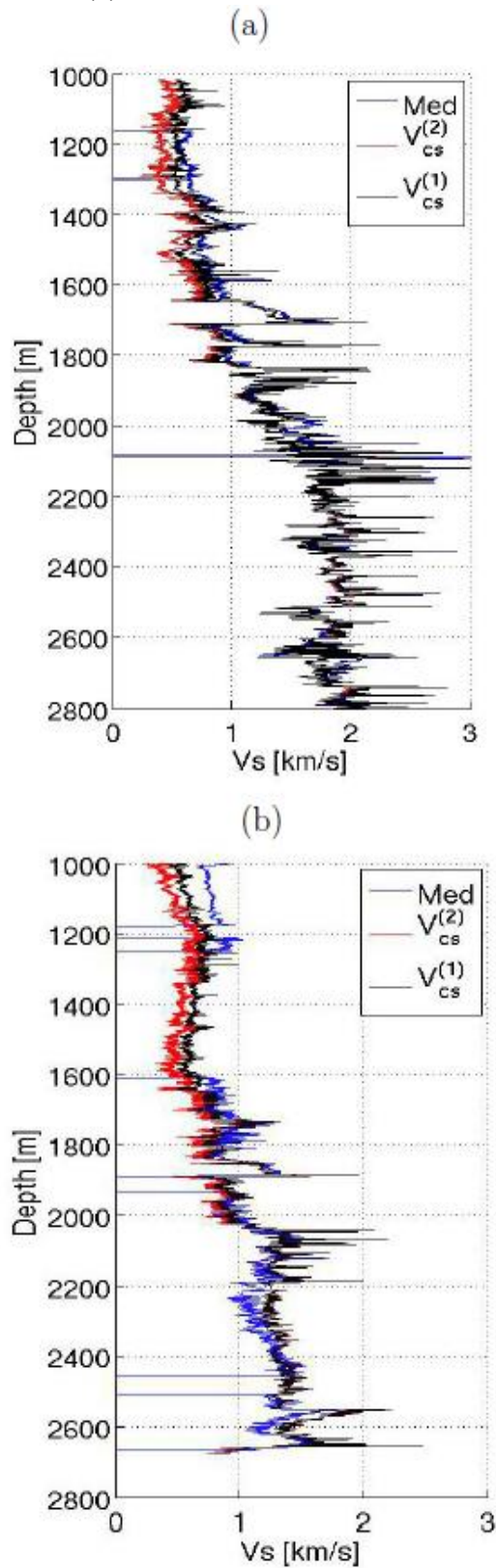


Source: from author

In addition to determine the target zones, it was necessary to use the following well logs: gamma ray, porosity, P-wave velocity and S-wave velocity (depicted in Figures 4.6 and 4.7) as well as the density, impedance and reflection coefficient logs, which are shown in Figure 4.10 for the well A and of the well B in the Figure 4.11. The reflection coefficient was evaluated by equation 2.5. The density and P-wave velocity were used to calculate the impedance log and this last was used to calculate the reflection coefficient log. The sonic porosity was estimated by Wyllie's equation (GREGORY et al., 1958) (see equation 2.6).

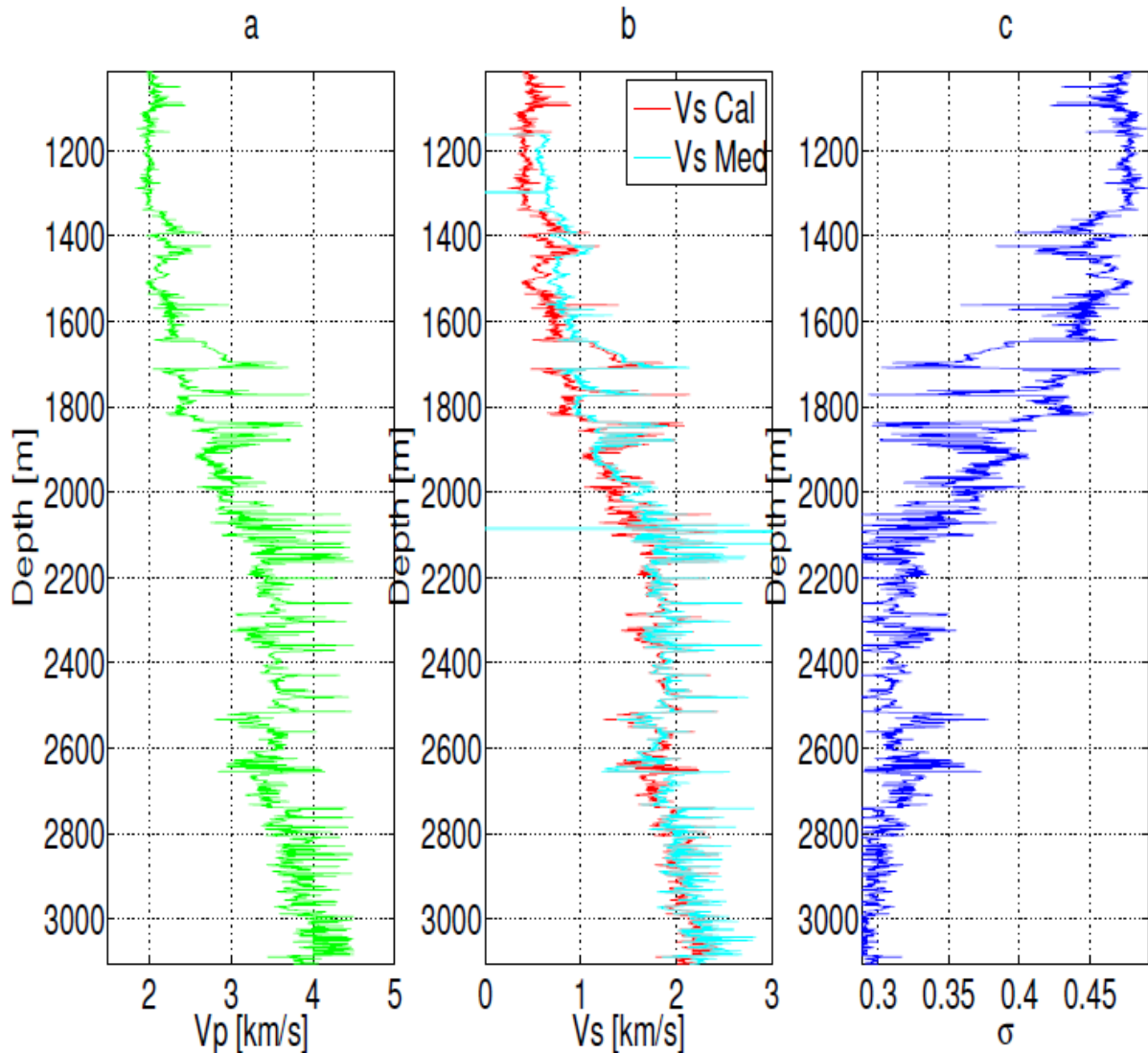
Other important task using the S-wave empirical relations, was to obtain S-wave velocity model for interval of seismic section. This was important for implementing the analysis by attributes, in the Figure 4.12, the velocity model for the S-wave is shown, which was obtained directly from the processing velocities (P-wave velocity) by CASTAGNA et al. (1985) 's equation (see equation 2.5)

Figure 4.5: Comparison between S-wave velocity logs measured and estimated by the Castagna et al. (1985)'s equations: (a) well A and (b) well B.



Source: from author

Figure 4.6: From well A: (a) P-wave velocity log, (b) S-wave velocities measured (med) and calculated by the Castagna et al. (1985)'s equation 2.5, (c) poisson ratio estimated from Vs using the Castagna et al. (1985)'s equation.

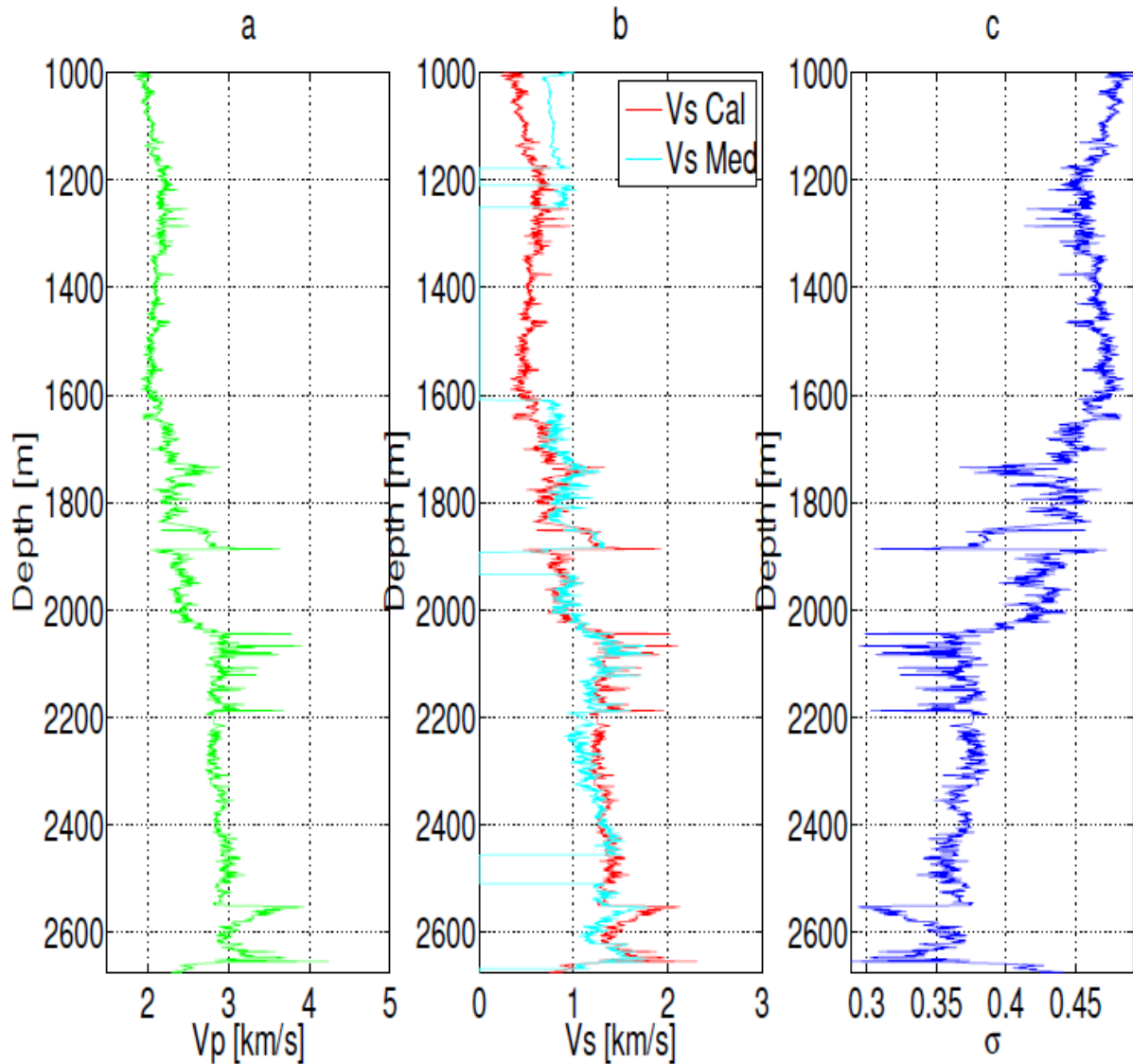


Source: from author

4.4 Data Interpretation

For the interpretation of the results obtained in the re-processing of seismic data, were applied three different methods, the angle trend, AVO analysis and RPT analysis (Rock Physics Template). The methodology of the trend angle to the data set was applied in order to check the anomalies found in the re-processing section, by the other hand the methodologies of AVO analysis and the RPT analyzes were applied in order to classify the fluid content of the anomalies found and eliminate ambiguity results.

Figure 4.7: From well B: (a) P-wave velocity log, (b) S-wave velocities measured (med) and calculated by the Castagna et al. (1985)'s equation 2.5, (c) poisson ratio estimated from Vs using the Castagna et al. (1985)'s equation.



Source: from author

4.4.1 Trend Angle Analysis

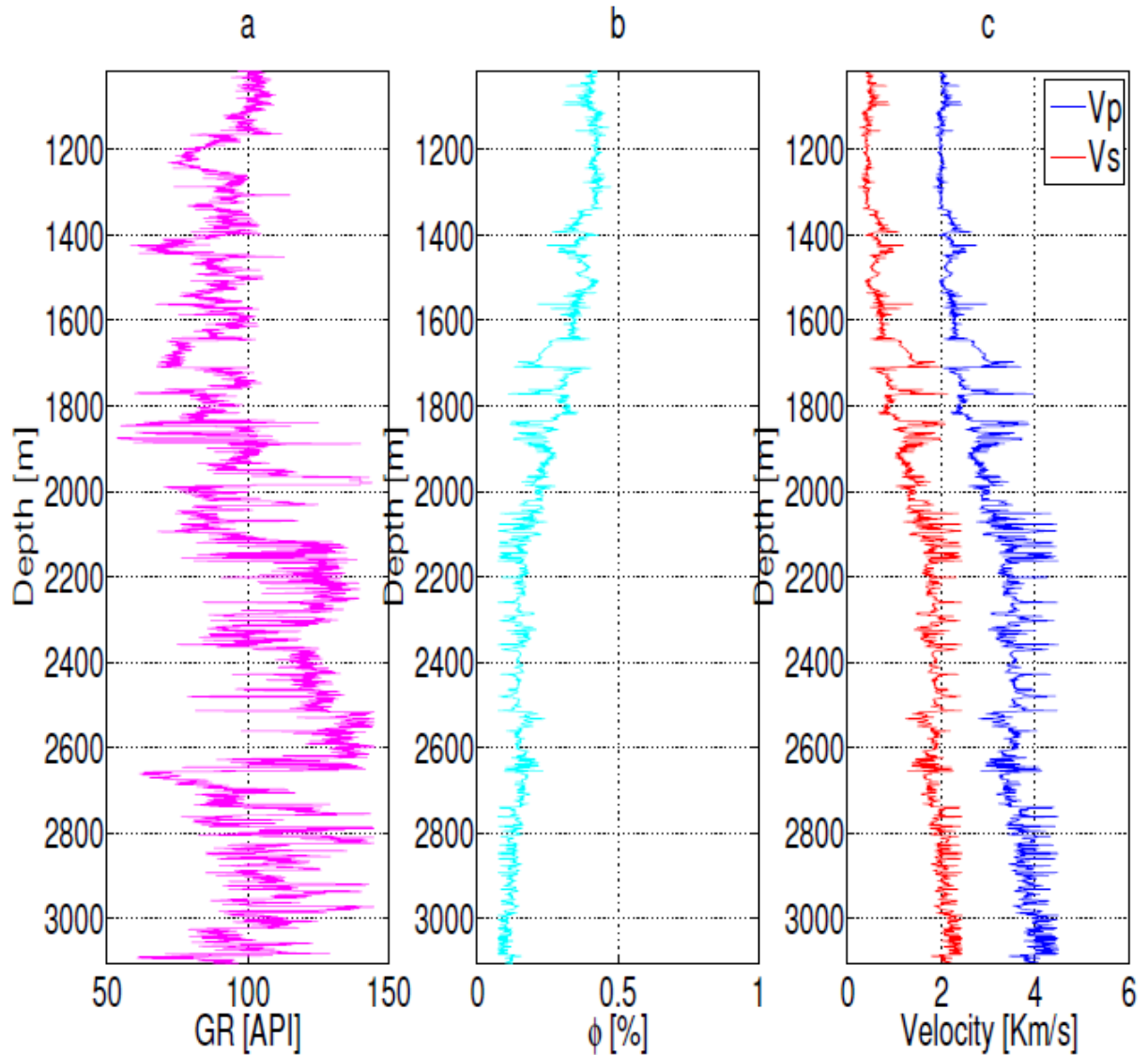
In the present work, it was applied, in well logs (A and B) and seismic section, a new attribute of rock-physics, which provides information on the interaction of fluids with the rock matrix. This approach provides a new way of discretization of the fluid contained in the sub-surface, which quantifies the trend angle in the data and highlights the anomalies of the fluids, even at low values of V_p/V_s (as can be seen in Figures 4.13 and 4.14).

During application of the techniques of re-processing was found an amplitude anomaly (in CMP 600) showing a bright-spot on the impedance map at time approximately in 2000 ms (see Figure 4.15a). In addition, the same anomalous zone appears as an area of low amplitude on the AVO map (see Figure 4.24b), intercept map (see Figure 4.25b) and gradient map (see Figure 4.25a). As the result the V_p/V_s ratio could be used to separate between unconsolidated clastic sediments ($V_p/V_s \geq 2.0$) and consolidated or gas-filled unconsolidated clastic sediments ($V_p/V_s \leq 2.0$) (GREGORY, 1977).

This anomaly could represent sands interblended with shale, because of the impedance and V_p/V_s values have a gradation with sand/shale ratio (as shown in Figure 4.22). As a validation of the results found in the maps of AVO and reflectivity was made an analysis by attributes (trend angle), as result is shown a low V_p/V_s ratio and a trend angle variation from -2 to 2 degrees, suggesting a gas sand (OSTRANDER, 1984) or limestone (HILTERMAN, 2001) with the unconsolidated gas-sand interpretation (GREGORY, 1977) being supported by the low values on the Φ (as can be seen in Figure 4.22), would therefore confirm the presence of the anomalous zone present in the CMP 600, which has high probability of contain hydrocarbon, as is shown in Figure 4.15b, further showed that the fractured environments have a very low influence on the trend analysis angle.

As mentioned before, in our approach we are relating the seismic attribute to changes in rock-physics properties, because we operate in the AI-versus- V_p/V_s crossplot domain (see Figure 4.17a and b). Thus as it seen in Figure 4.17 while a lower AI value and higher values in V_p/V_s , great will be the value of porosity. The Figure 4.17 is a template that outlines the effect of the matrix (cement) within the basin, gas-saturated sands are typically well separated from brine-saturated sand in the rock-physics crossplot of V_p/V_s versus AI. This effect could reduce the fluid sensitivity, this would cause, in the model, an overlapping between brine and oil data. As result, this can cause a well know ambiguity between poorly sorted loose sands with hydrocarbons and well-sorted cemented sandstones saturated with water. (AVSETH et al., 2005), however the AI will increase, so trend in a rock-physics template will be different from a fluid trend (see Figure 4.17).

Figure 4.8: Well logs from well A. (a) gamma ray log, (b) estimated porosity log and (c) P-wave and S-wave velocities, where the mainly geological events are shown and the areas with better porosity rate.

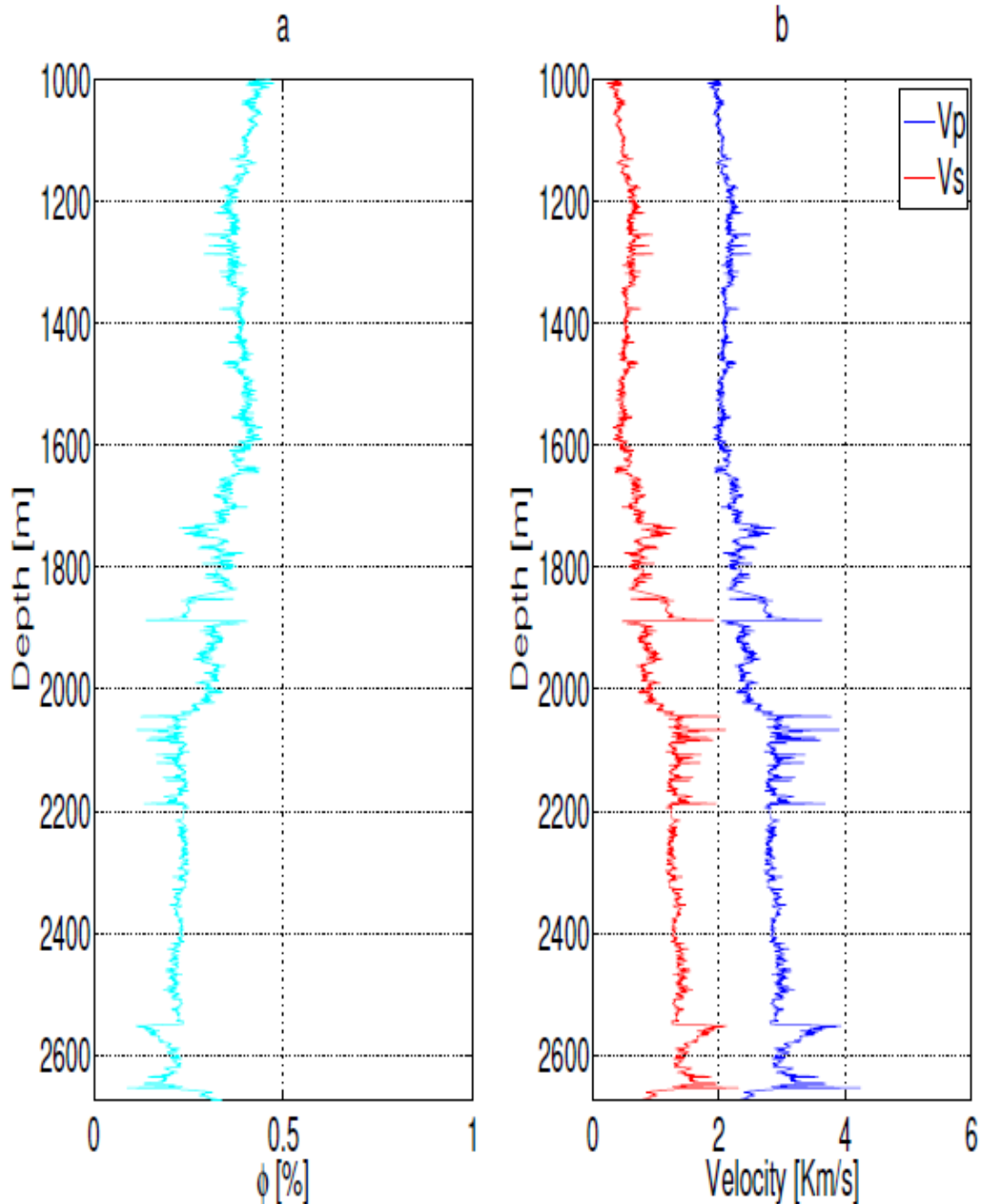


Source: from author

The corresponding trend angles are estimated between each point shown in Figure 4.13 and are displayed in color. We also plot the data points as a function of depth (as shown in Figure 4.13a) where we include the plot of trend angle as a separate log (see Figure 4.13c). In this log two possible zones with gas-sands are easily detectable from the matrix, because are the maximum picks in the right side. In addition to test the effectiveness of the attribute trend angle, in the seismic section, were applied techniques of reflectivity and AVO analysis which is shown in Figure 4.24b and Figure 4.24c, where we can confirm the anomalous zones. In Figure 4.13c we can observe two anomalous zones (2400 and 2780 m.) which are generated by

the possible presence of compact material (shale), which would indicate a sealing area.

Figure 4.9: Well logs from well B. (a) estimated porosity log and (b) P-wave and S-wave velocities, where mainly the porosity events are shown and the areas with better velocity ratio.

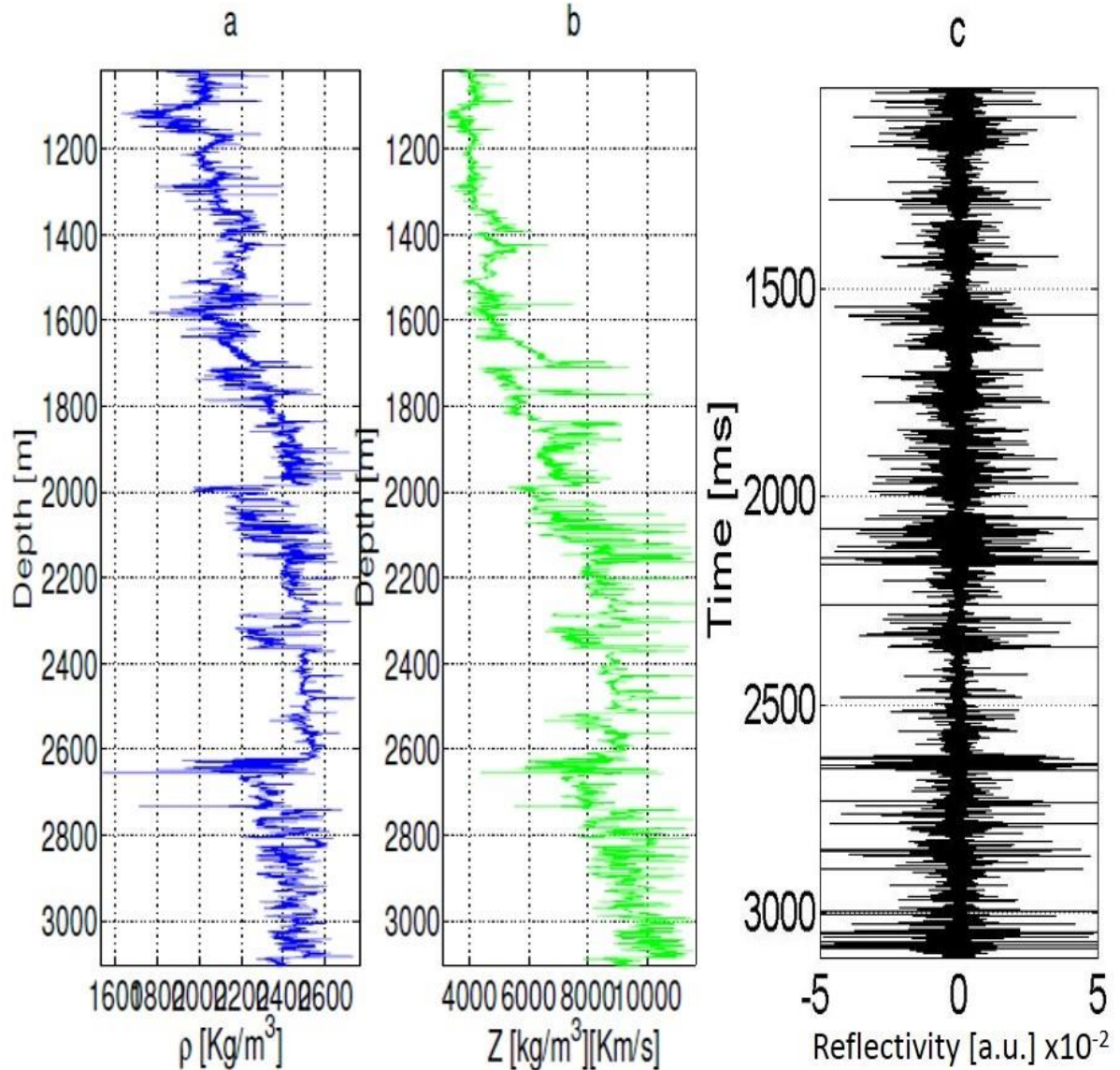


Source: from author

As we can see in the figure 4.18, the primary fluid contained in the well B is the brine, so you can also see a small area with a potential of hydrocarbon content (Figure 4.18a), but this phenomenon is due to the high rate of porosity caused by

highly fractured environment (as shown in Figure 4.18b).

Figure 4.10: From (a) density log and P-wave log shown in Figure 4.6, the (b) acoustic impedance log was calculated and (c) the coefficient reflection log were estimated for well A.

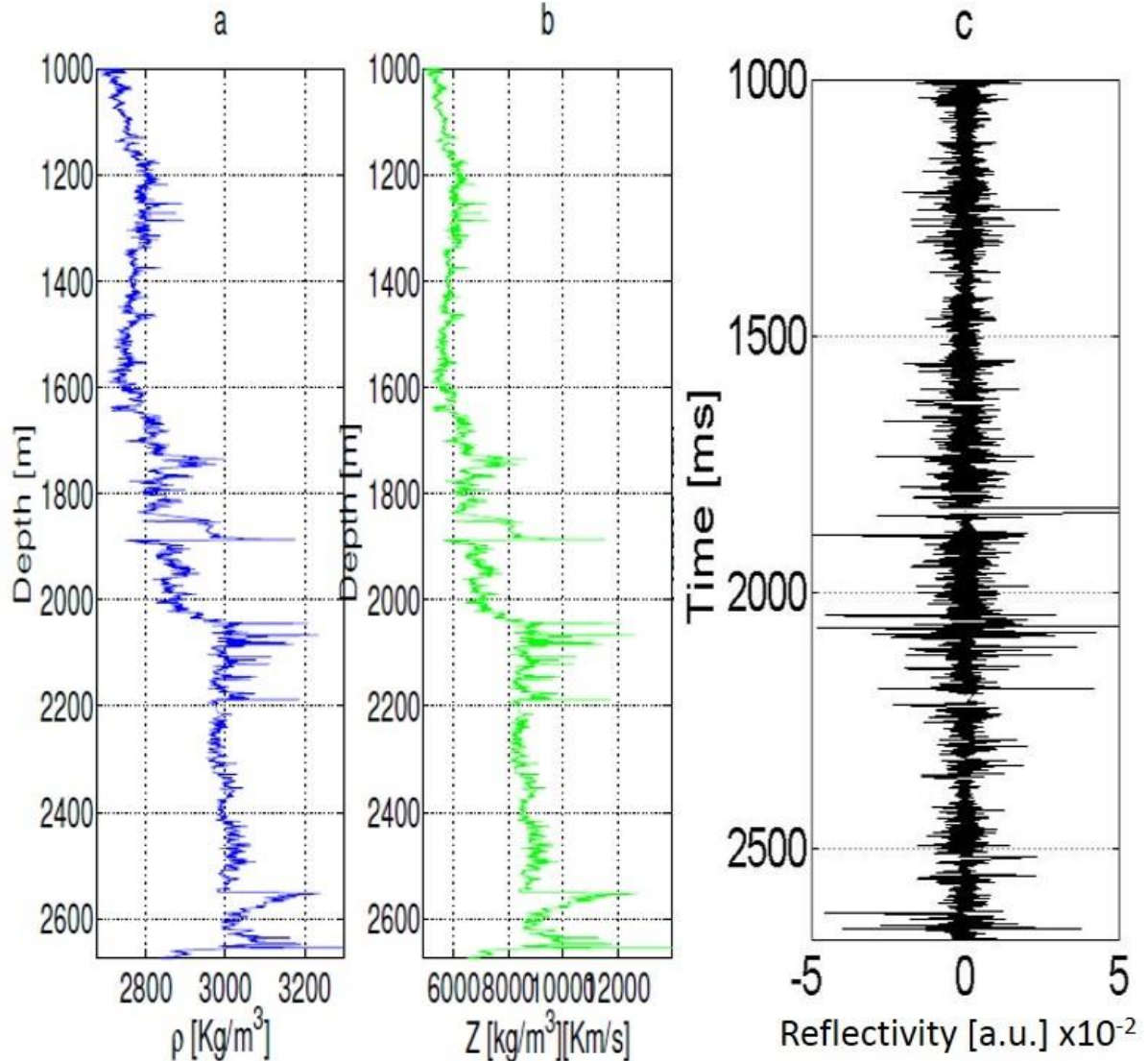


Source: from author

In order to classify the behavior of the P- and S- velocities, an analysis of velocities is done by crossplotting the velocities of the possible target areas (Andrew; Bezdán, 2001), which shows three areas with high possibility to contain gas-sand (see Figure 4.16a) for the well A, in the A and C areas you can see the presence of gas sand in between 1600-1800 and 2600-2800 meters, this phenomenon is possibly because the area has a high rate of fracture. In the Figure 4.16b, is shown the analysis of the velocities, where we can see two anomalous zones present in the

Paleocene and the base of Cretaceous, which are caused by the high index of porosity of the fractured environment

Figure 4.11: From (a) density log and P-wave log shown in Figure 4.6, (b) the acoustic impedance log was calculated and (c) the coefficient reflection log were estimated for well B.

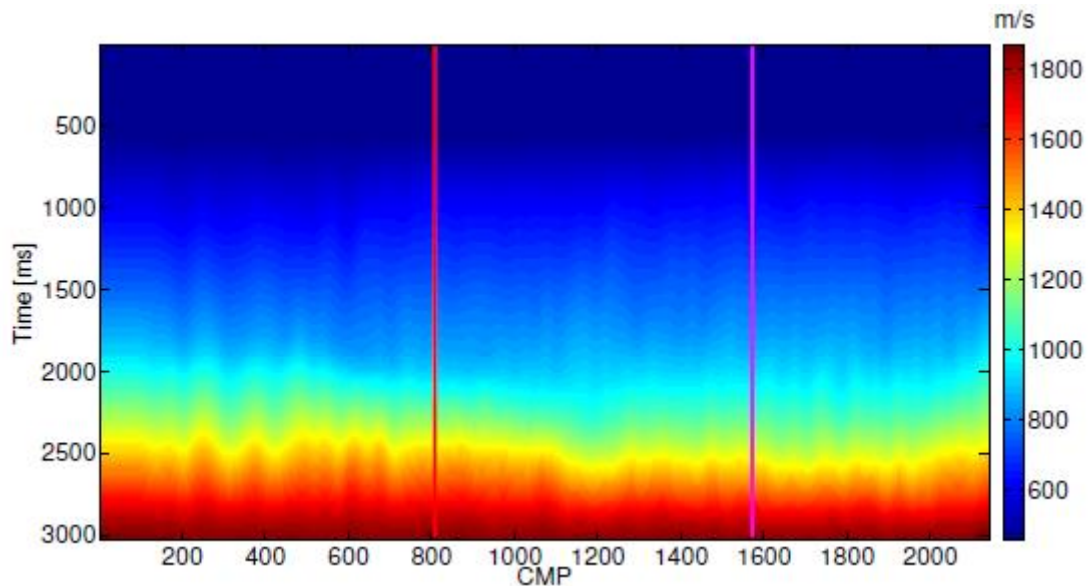


Source: from author

Castagna et al. (1985) shows that water-saturated sandstones, siltstones, and shales fall approximately along a line in crossplot of V_p versus V_s , whereas gas-saturated sandstones stand out as outliers to the main trend (as shown in Figure 4.16). In the present data, we make similar observations. Brine-sands and limestones show much higher P-impedances than oil-sands and gas-sands. For the shales it is difficult separating the oil-sands and gas-sands, since they have some overlapping impedance values. However, gas-sands are known to have anomalous low ratios of

V_p/V_s . Thus, if we can relate the rate of V_p/V_s and the pore-fluid content, we have a first step to separate the lithology and pore-fluid effects (MADIBA; MCMECHAN, 2003).

Figure 4.12: S-wave velocity obtained by P-wave velocity model. This velocity model will be used to application of the trend angle technique and the templates of rock-physics for characterizing the reservoir.



Source: from author

The subsequent mapping of the water contained in the porosity, which is estimated as the sum of all the water components in the pore space (the volume fractions of movable water, bound water, and water trapped in unconnected pores), further improves discrimination between pore-fluids in the sandstone reservoirs.

To find different anomalous zones, we estimate the ratio V_p/V_s and relate with AI (see Figure 4.17). The ratio V_p/V_s is sensitive to the pore-fluid (OSTRANDER, 1984). For a fixed lithology and porosity, V_p/V_s is 10 to 20% lower for gas saturation than for water saturation, but there is some overlap in the ratio V_p/V_s between brine-sands and oil-sands. For example, shales have higher values of V_p/V_s than sands. There is a great number of low V_p/V_s anomalies which are shown in Figure 4.17, especially in the Jurassic section below the unconformity (BCU), some of the low V_p/V_s areas could be either gas-saturated sands or water-saturated limestones (CHACKO, 1989; HILTERMAN, 2001) indicating, that for many stages (specialty carbonates), V_p/V_s is approximately 1.9 and relatively insensitive to porosity. In

contrast, in rocks with lower porosity (as shown in Figure 4.17b) in which more pore-filling minerals are present, the sensitivity to fluid is lower. However, fluid sensitivity can decrease dramatically with the presence of contact cement. As can be seen in Figure 4.17b is possible identify four zones, which indicate the type of fluid and the kind of porosity present.

4.4.2 Gassmann Fluid Substitution Analysis

Another technique to validate the results obtained by the application an analysis by attributes (trend angle) is the technique of Gassmann, which evaluates different scenarios where is measured the interaction of the velocities (P and S) with the density. As results, was found two areas with a high probability of containing hydrocarbon (as shown in Figure 4.19 and Figure 4.20).

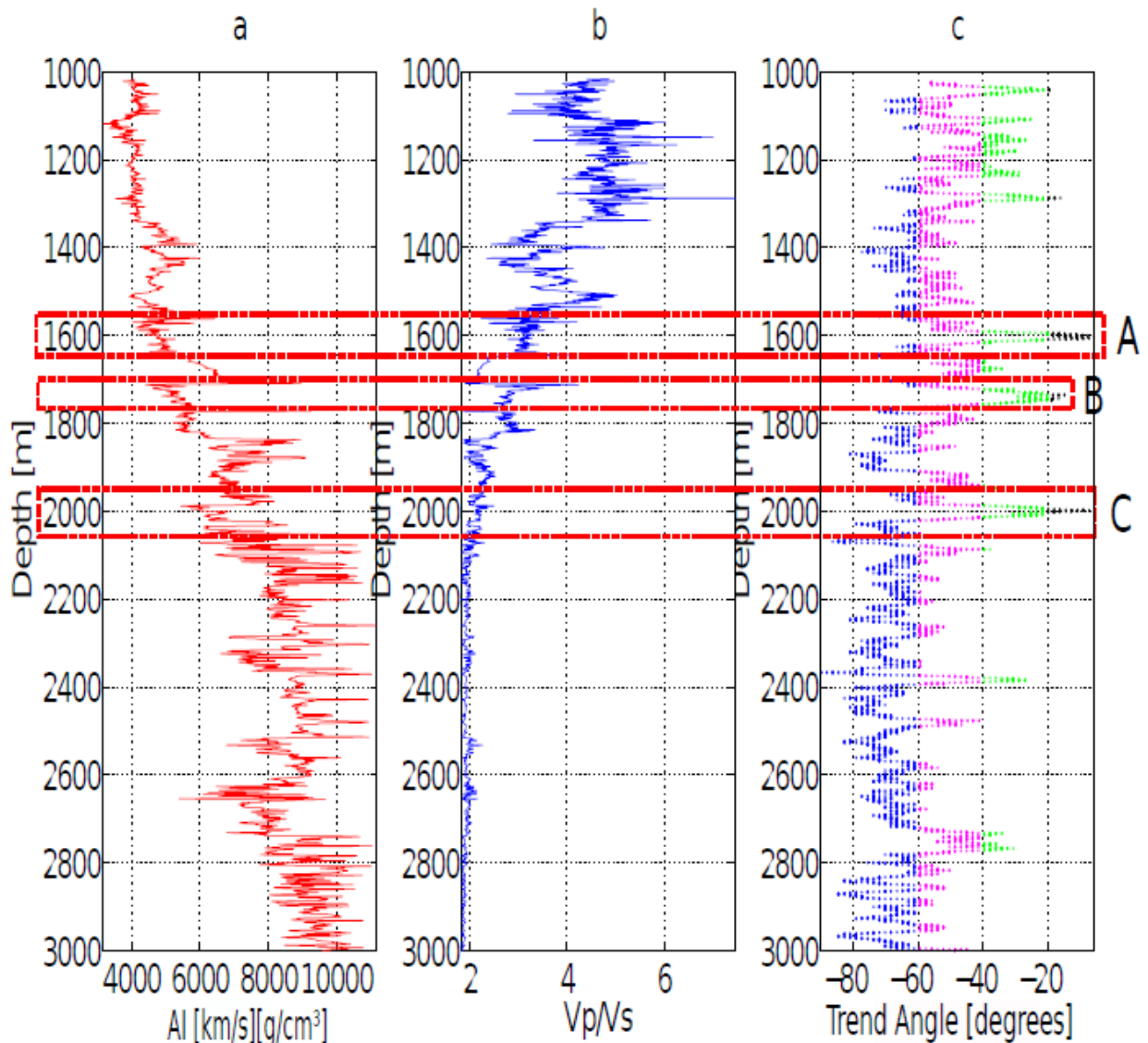
As result of application of the Gassmann technique, the P-wave velocities and S-wave velocity are slightly different to the original, so for validate the results previously described, an analysis by attributes (trend angle) was applied, as see in the Figures 4.19 and 4.20, the anomalous zones previously described were found and the emergence of new zones with high probability of containing hydrocarbon, although these areas are more highly fractured linked to its environment (see Figure 4.21). Other geologic/reservoir configurations, is defined (see Figure 4.23a), $\phi \leq 0.19$ and $V_p/V_s \leq 2.2$ are the criteria that delineate potential reservoirs in this area, with decreasing Φ indicating a higher gas/oil ratio, and decreasing V_p/V_s indicating a higher sand/shale ratio. As these criteria were locally calibrated, they appear to be valid locally, they should not be applied to other data sets, which may exhibit significantly different relationships. However, the overall procedure should be generally applicable.

4.4.3 V_p/V_s - ϕ Relationship

The work of Lee and Collett (2008) helped to generate crossplot of ϕ versus V_p/V_s over the time interval of interest (1.5 to 2.8 s) to calibrate the V_p/V_s - ϕ relationship at the wells (see Figure 4.22a). In general, this calibration will have to be done separately for each sedimentological package in a geological formation.

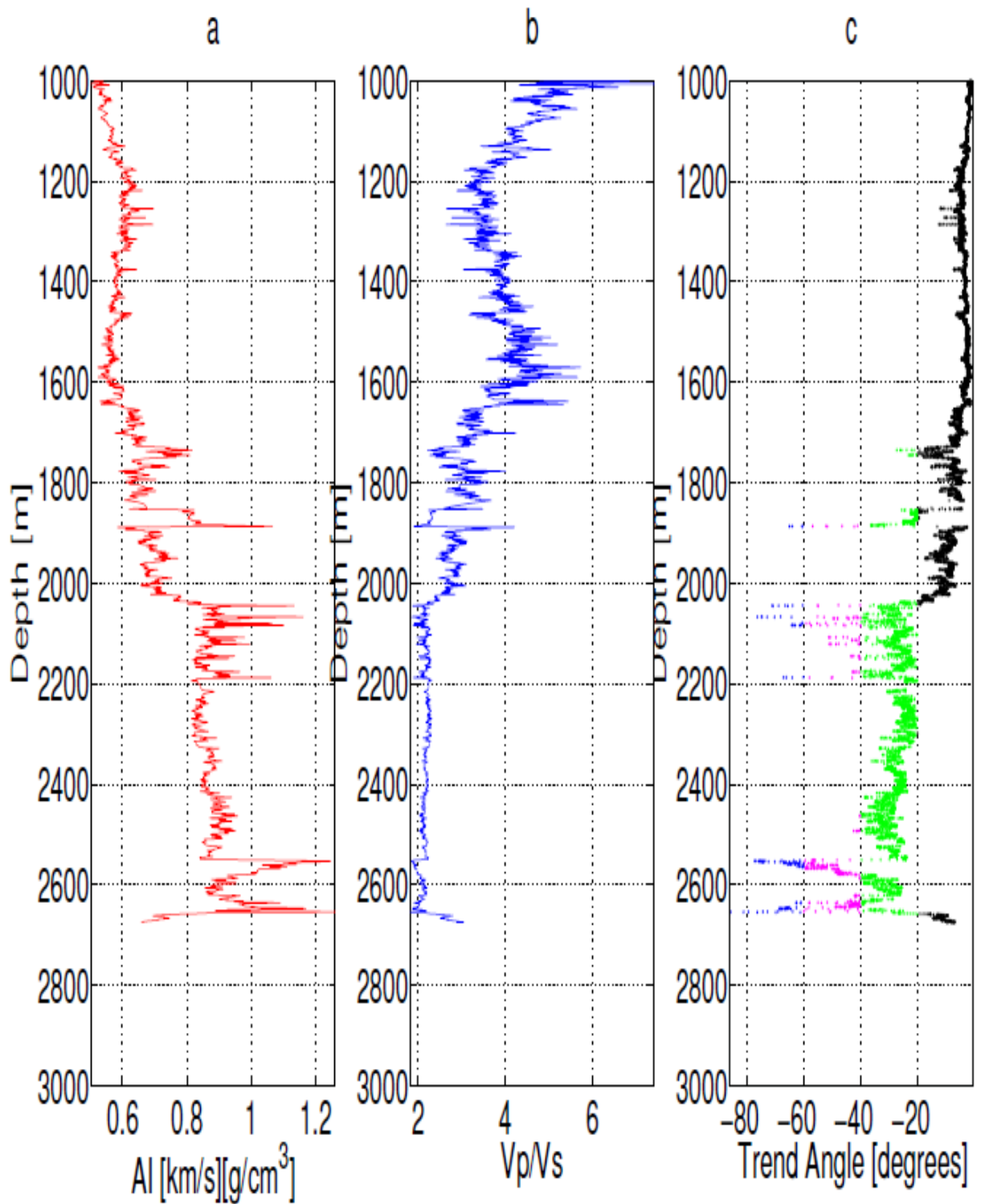
However, here the relationships for the Jurassic and Paleocene sections are similar so a single calibration is sufficient as shown in crossplots of ϕ versus V_p/V_s (see Figure 4.23a). In the other hand, the porosity in shallow areas can be seen that contain only water (GREGORY, 1977), in addition in the graph is highlighted that the gas-sand saturation occurs in the deeper sediments, besides the ratio V_p/V_s increases with increasing porosity and also shown that V_p/V_s could effectively be used to separate water-saturated and gas-saturated sediments as porosity increases.

Figure 4.13: Logs, from well A, showing the three main anomalous zones found by the trend angle technique, which are compared with the logs of acoustic impedance and Poisson's ratio, (a) acoustic impedance plot versus depth (b) ratio of P and S velocities and (c) trend angle depending on the depth.



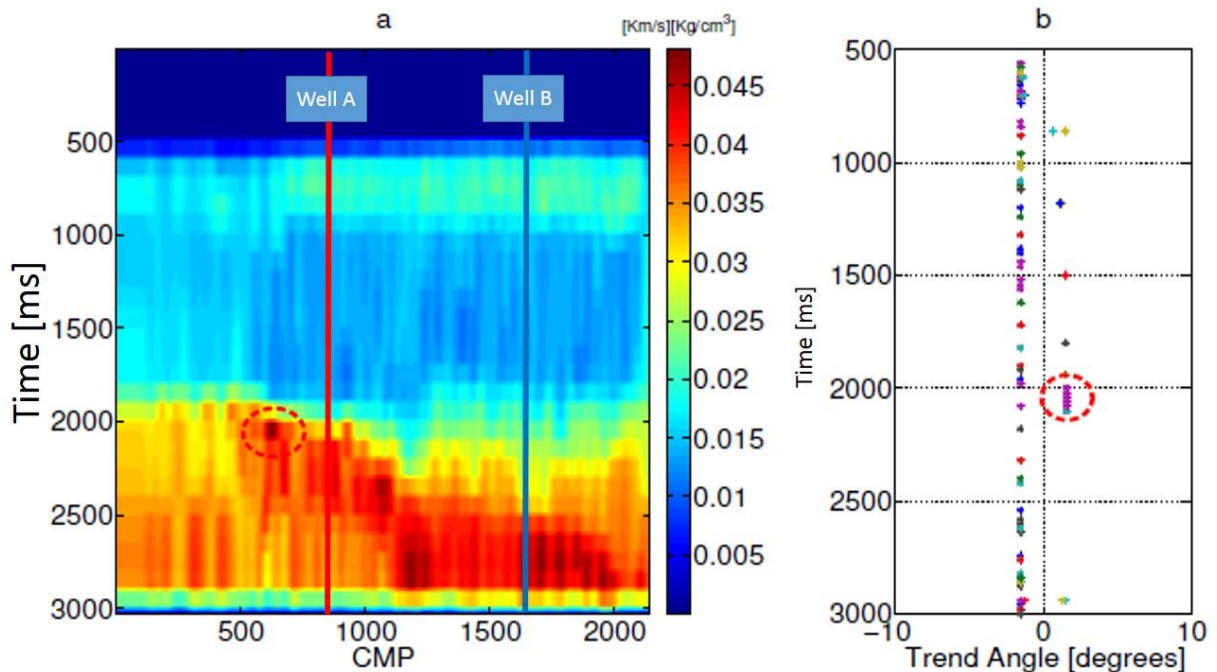
Source: from author

Figure 4.14: Logs, from well B, showing the three main anomalous zones found by the trend angle technique, which are compared with the logs of acoustic impedance and Poisson's ratio, (a) acoustic impedance plot versus depth (b) ratio of P and S velocities and (c) trend angle depending on the depth.



Source: from author

Figure 4.15: The application of angle trend technique in the anomalous zone present in approximately 2000 ms and CMP 600, the log presented was performed by creating a pseudo-well, where were found the physical parameters necessary for the application of the technical trend angle: (a) impedance map and (b) trend angle log applied between CMP 500 to CMP 700.



Source: from author

Figure 4.22a shown the Jurassic sand reservoirs (from 2.0 seg. to more) correspond to $V_p/V_s \leq 2.3$, higher V_p/V_s values correspond to shales (WANG, 2001), unconsolidated water-filled sands and water-filled carbonates (CHACKO, 1989; HILTERMAN, 2001). Comparing the Figure 4.22a and Figure 4.23a we can see that the Jurassic reservoir sands (at $V_p/V_s \leq 2.2$) all have total porosity approximate of 22% with error of 4%. Higher porosities occur in the shallower part of the section (at higher V_p/V_s as shown in Figure 4.23a), is believed to be for the environment highly fractured.

The $V_p/V_s - \phi$ plane still does not produce a unique interpretation in many situations. However, the critical distinction, which is between hydrocarbon-bearing sands and all other geologic/reservoir configurations, is defined (see Figure 4.23a). The $\phi \leq 0.19$ and $V_p/V_s \leq 2.2$ are the criteria that delineate potential reservoirs in this area, with decreasing ϕ indicating a higher gas/oil ratio, and decreasing V_p/V_s indicating a higher sand/shale ratio. As these criteria were locally calibrated, they appear to be valid locally, they should not be applied to other data sets, which may

exhibit significantly different relationships. However, the overall procedure should be generally applicable.

4.4.4 AVO analysis

In this study, the AVO analysis technique was applied for CMP sections of wellbore A and B (shown in Figure 4.26 and Figure 4.28), also the AVO analysis was applied to the seismic section in order to relate the results (see Figure 4.24), consequently three anomalous areas were obtained, two anomalous zones near-wellbore A, and at the last in the CMP 600 and as a result of this the anomalous zones encountered during application of analysis by attribute (trend angle) were confirmed.

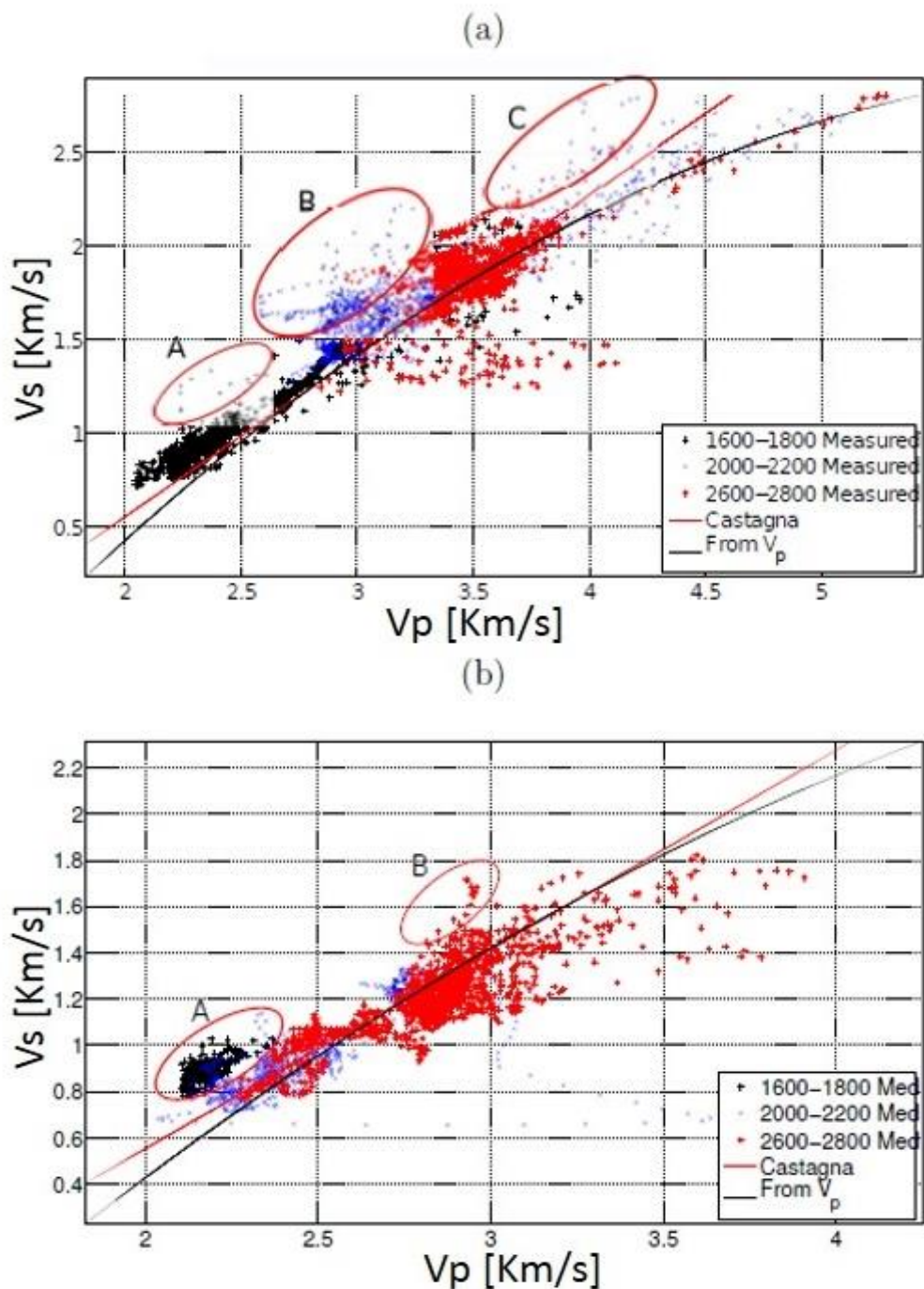
Figure 4.30 and Figure 4.31 shows the CMP 808 and CMP 1572 (well A and well B respectively), showing three anomalous zones A, B and C, to which was applied an analysis of amplitude to determine the nature of the anomalies, as a result of this the anomalies A and C are areas with high potential to contain hydrocarbon (as shown in Figures 4.32 and Figure 4.33 for Well A, and Figures 4.35 and 4.36 for well B), and moreover, the anomaly B is a seal area, this is estimated due to the behavior of the amplitude. (As can be seen in Figure 4.34 for well A, and Figure 4.37 for well B).

For the Figure 4.27 and Figure 4.29 a comparison between the synthetic seismogram, the seismic section seismogram and the AI log are shown, in order to relate the good well tie obtained by vary the distance of the offset (ranging from 5 to 30 degrees), as a result of this we can see that the amplitudes decrease indicating the presence of an area with different physical properties.

As shown in Figure 4.26 we can see that the AVO analysis of data from the well A confirms the presence of hydrocarbon, due to the crossplot that shows anomalous points belongs to the class IV of AVO classification indicating the presence of gas sands, though also can be seen that most of the data belongs to class II (in classification of the AVO analysis seen in point 2.3.3.1), which indicates the presence of formation water present. By the other hand, for the Figure 4.28 it is possible to confirm the presence of formation's water in the well B because of the crossplot shape, although there are some anomalies belongs to class IV, due to the fractured environment which generates this phenomenon called "false positive",

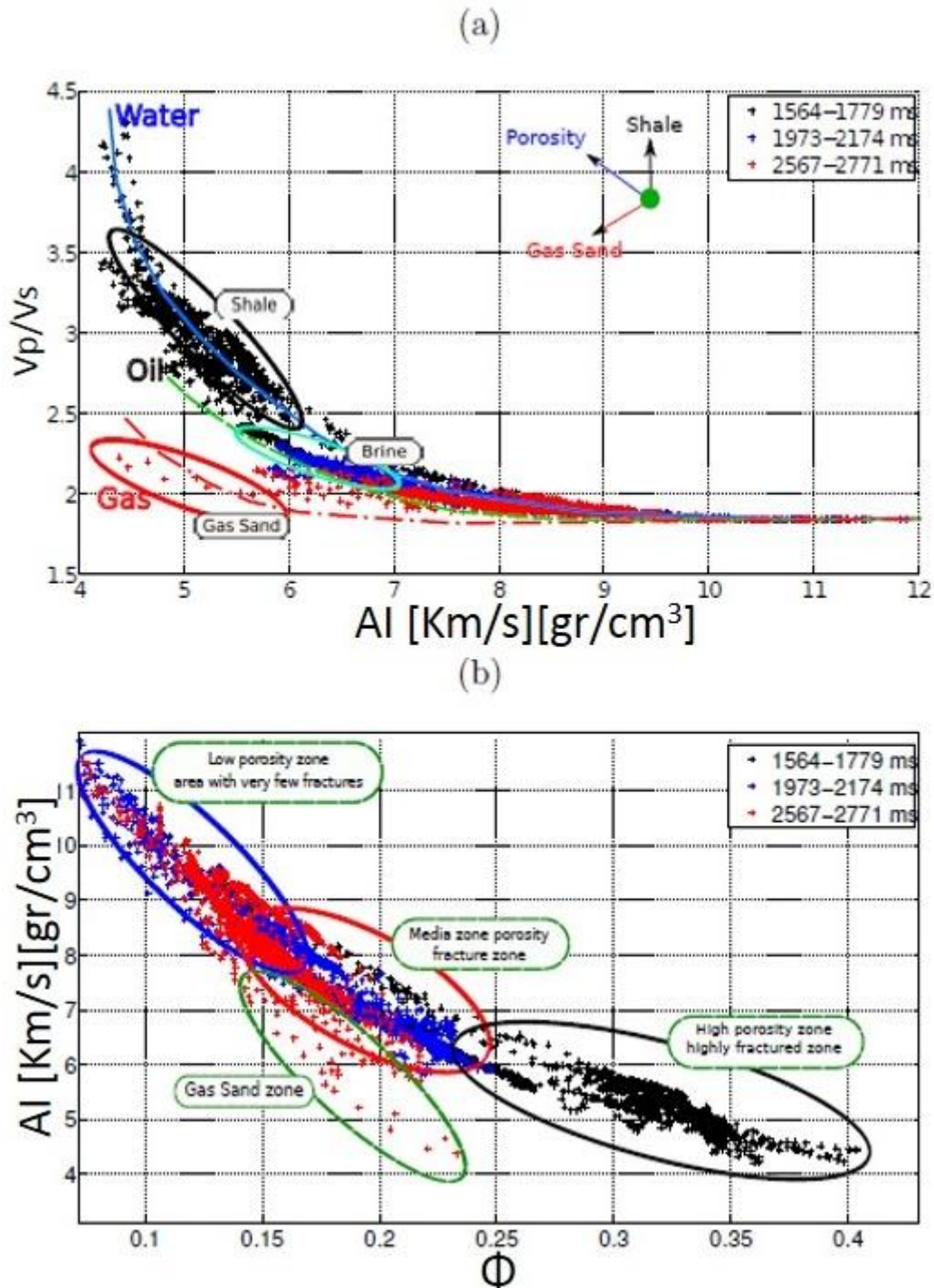
therefore to confirm the results obtained from the AVO analysis in the well A, an AVO analysis to the seismic section was performed (specifically in the area of the well A), which confirmed the results showing that in the area near of well A there is a high probability of containing hydrocarbon (see Figure 4.24a).

Figure 4.16: Chart showing the comparison between different velocities calculated and measured velocities (in situ), showing three anomalous areas with a high probability of containing gas sand: (a) for well A and (b) for well B.



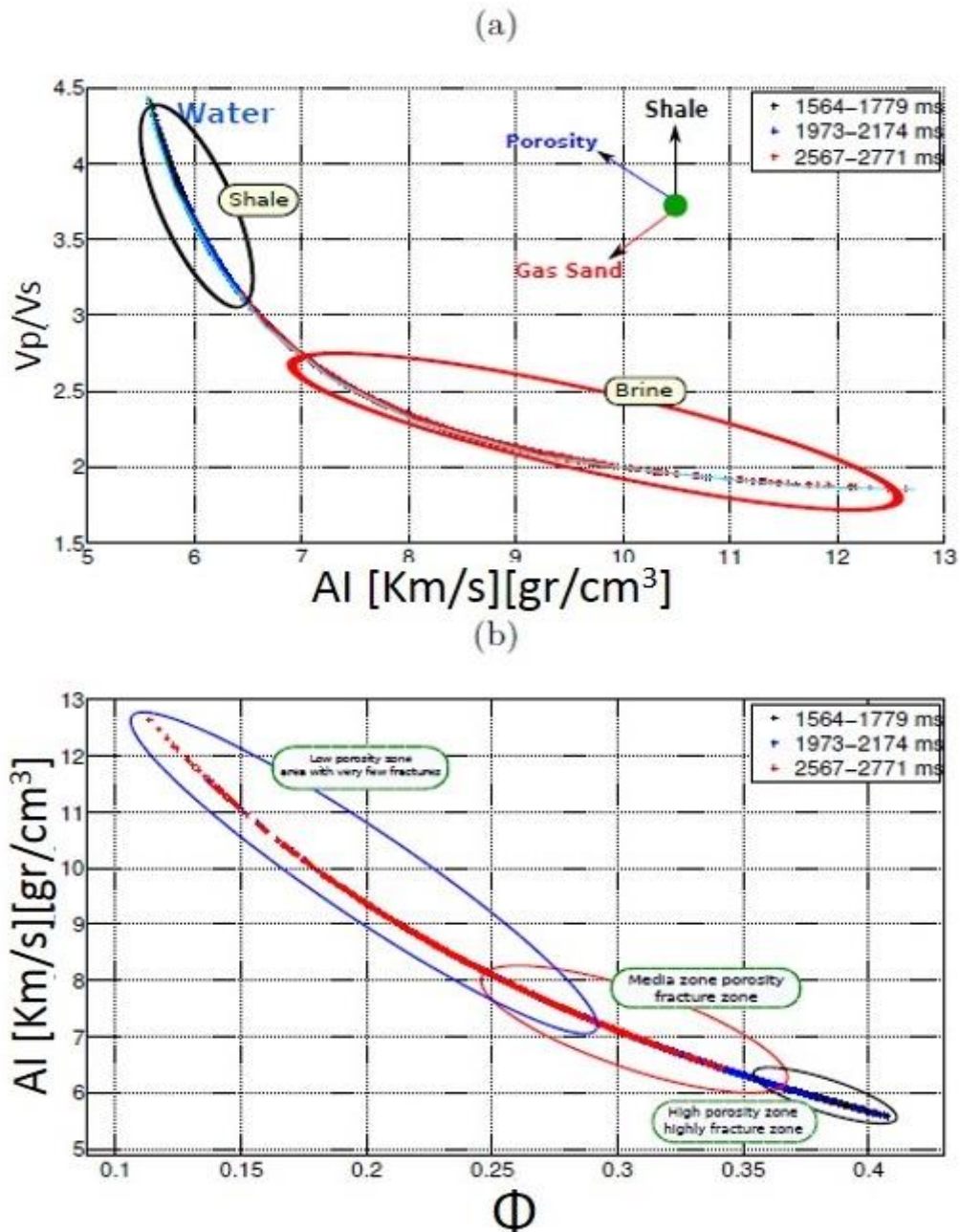
Source: from author

Figure 4.17: From well A: (a) template that shows the behavior of the physical properties compared to the elastic properties, where the type of fluid present is classified and (b) template relating the acoustic impedance with the content of porosity, where we can determine the type of environment present related to each depth level.



Source: from author

Figure 4.18: From well B: (a) template that shows the behavior of the physical properties, into the well B, with the elastic properties and (b) template, showing relating between the acoustic impedance with the porosity.



Source: from author

Figure 4.24 a, show the AVO analysis from the seismic section shows the increase in the P and S velocities within Poisson's ratio, in other words the presence of hydrocarbon is confirmed, due to the crossplot form, that shows anomalous points belongs to the class IV, indicating the presence of gas sands. This also confirms the presence of formation water or brine. Figure 4.24b, show the map of the AVO

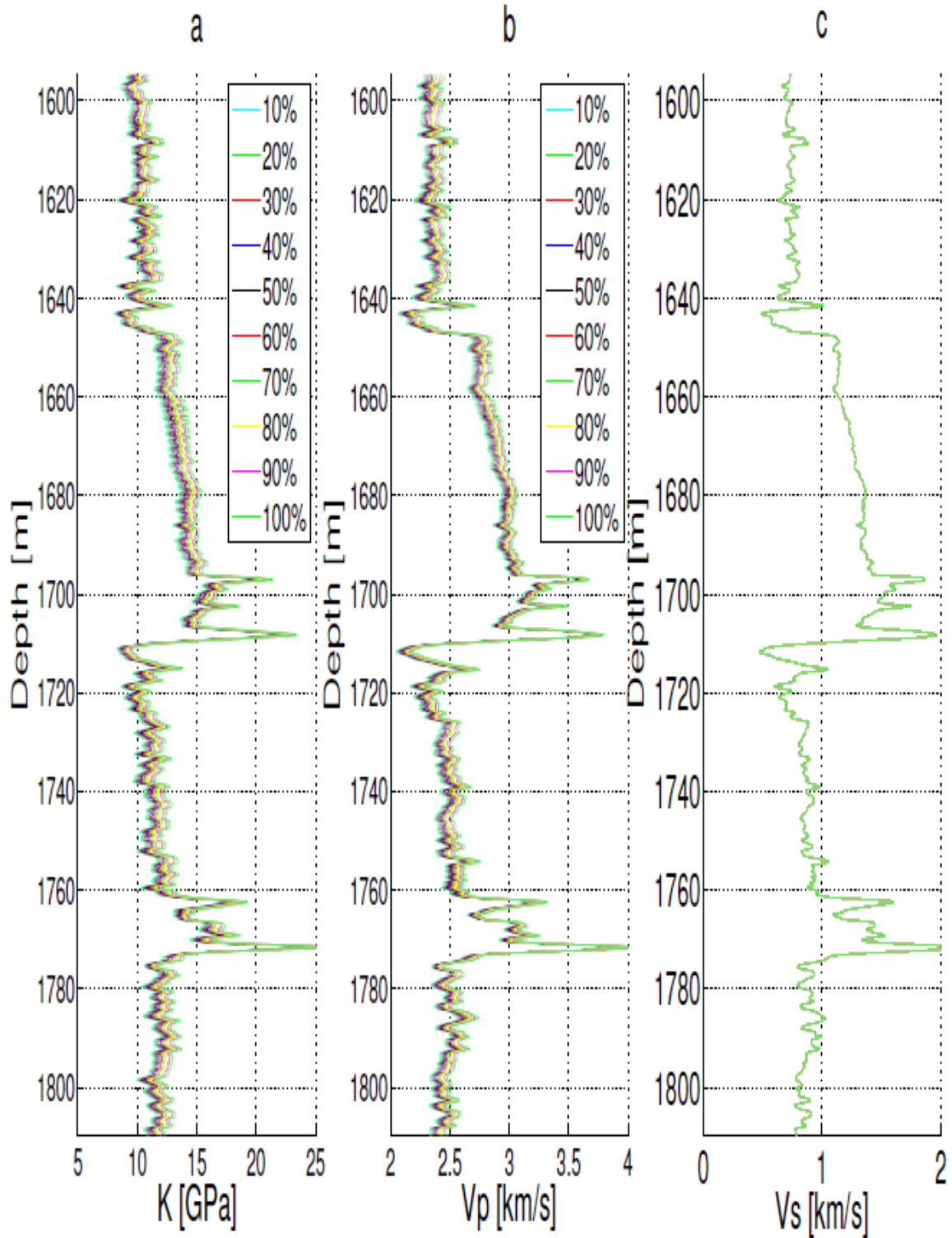
analysis from the seismic section depicted in Figure 4.4. This analysis was performed using the PROMAX software. The color contrasts are related to the AVO anomalies, in other words, these different colors mean different lithologies and environments. In the area concerning to the Jurassic era (interval between 2000 ms and 3000 ms), it can be seen a highly fractured environment, especially in the vicinity of the well B, where we can see the influence of the Graben was more higher. In the Figure 4.24c, shows the impedance map, which shows the variation in lithology by varying the density, and also shows the diversity of environments present as result of this we can observed the presence of low densities into of the Jurassic zone, which is caused by the fractured environment due to the presence of the graben.

The Figure 4.25, shows the maps of AVO attributes, applied in the seismic section, where the presence of fractures is displayed in regions of the Paleocene and Cretaceous, and the presence of anomalies in the Jurassic region is confirmed, indicating the presence of areas of potential hydrocarbon reservoirs, however as could be determined by applying the technique of angle trend in the well B, the anomalous zones are produced by fracture, unlike anomalous zones in the well A and CMP 600, which are confirmed that are produced by the presence of hydrocarbon (gas-sand).

From Figure 4.32 to Figure 4.36 the trends of amplitudes made to anomalies A, B and C are shown, with which one can infer the classes to which they belong and above all try to find the types of fluids present, as a result of this, in Figure 4.32 and Figure 4.34 can be seen that the amplitude is increasing with increasing offset, so it is very likely what the fluid present is gas, by the other hand in Figure 4.33 shows that decrease the amplitude, suggesting a material with very strong impedance contrast indicating, like a seal. Also can be seen from the graphic that exist a phase shift thus can be inferred that the fluid contained in the formation can be brine.

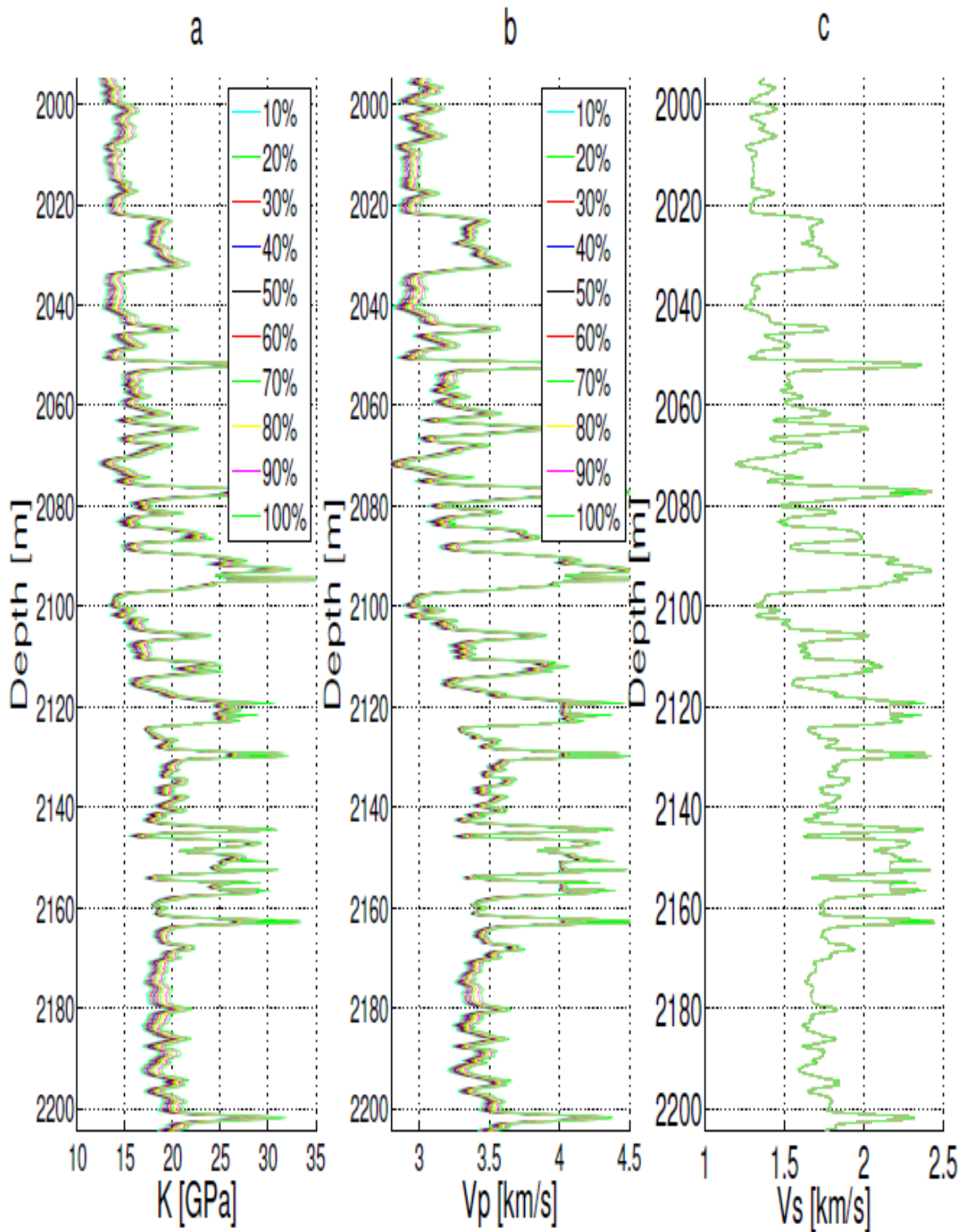
Figures 4.35 and 4.36 shows the results of the analysis of amplitude applied to the formations with stronger reflectivity for the well B, as result of this it is inferred that these formations present a seal behavior, without much fracture. In the Figure 4.37 shows as an AVO crossplot, where an increasing trend of the amplitude is shown, which would indicate the presence of different fluid of brine, but however on the AVO map from the seismic section (see Figure 4.24) no anomalous zone is shown, as the result of this it can be inferred that this effect called "false positive" is due to fractured environment of the well B.

Figure 4.19: Gassmann methodology applied to anomalous zone A (Figure 4.13) shown in the trend angle, where we can see the variation of modulus K at different percentages of saturation: (a) log showing the variation of the bulk modulus, (b) record, where we can see the variation in the P-wave velocity with the saturation change and (c) record showing that there is not variation in the S-wave velocity, generated by the saturation changes.



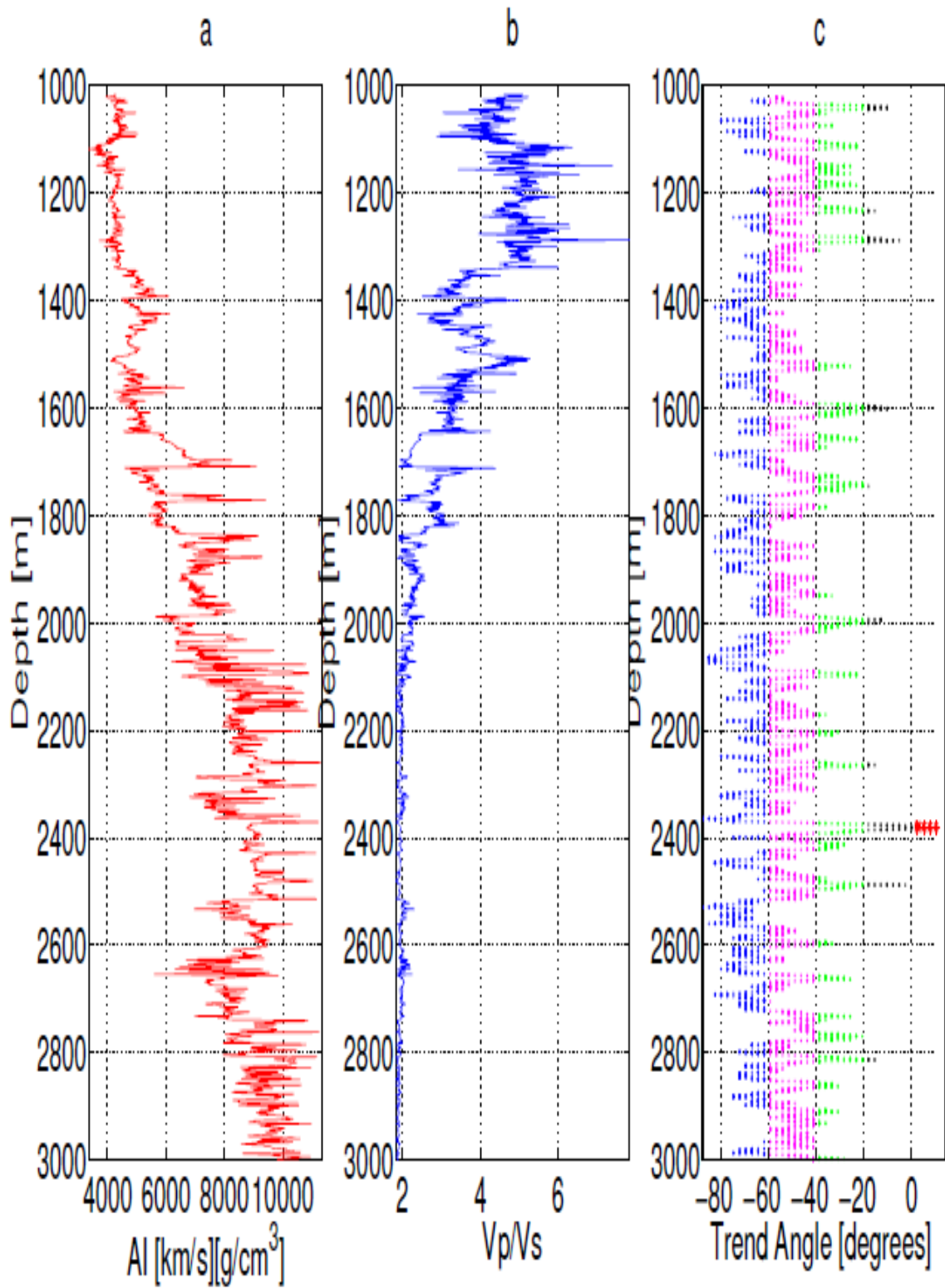
Source: from author

Figure 4.20: Gassmann theory applied to anomalous zone B in the target section shown in the Figure 4.13, where we can see inter-bedded areas containing high porosity zones and low porosity zones: (a) bulk modulus K, (b) record showing the change of the P-wave velocity with the saturation change and (c) record of the S-wave velocity without change by saturation.



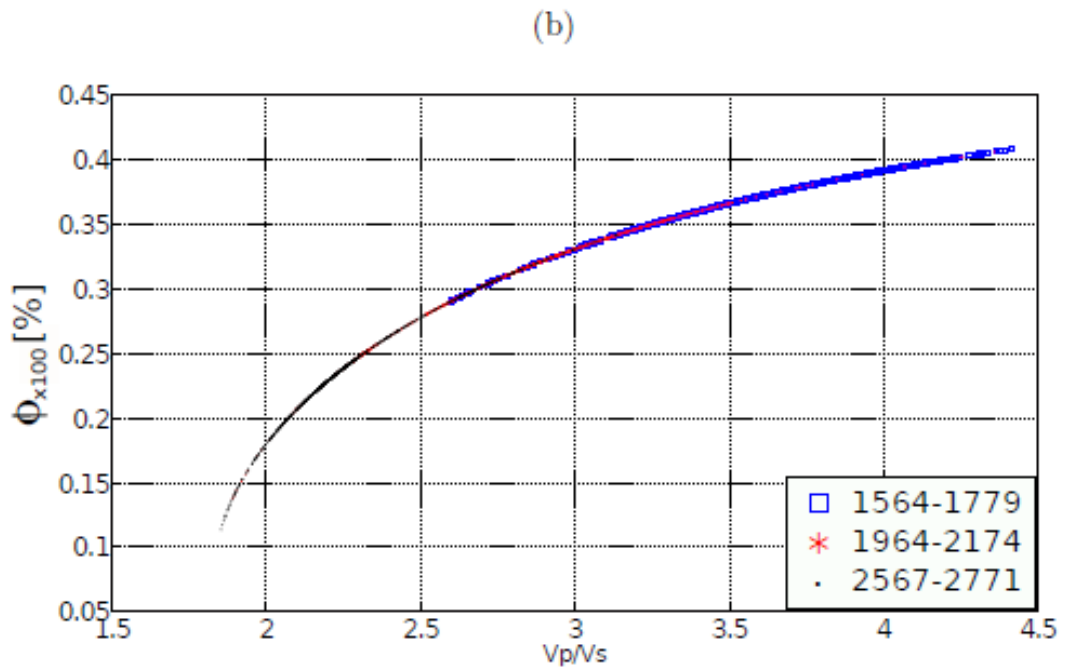
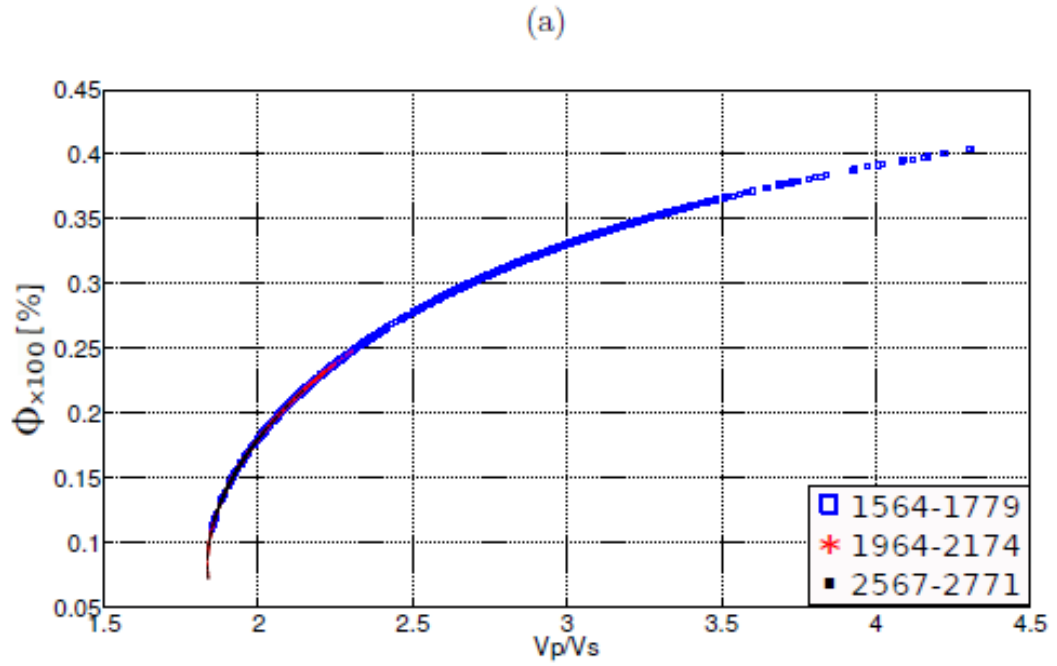
Source: from author

Figure 4.21: Example of trend angle for well A, in case of saturated medium estimated by Gassmann methodology.



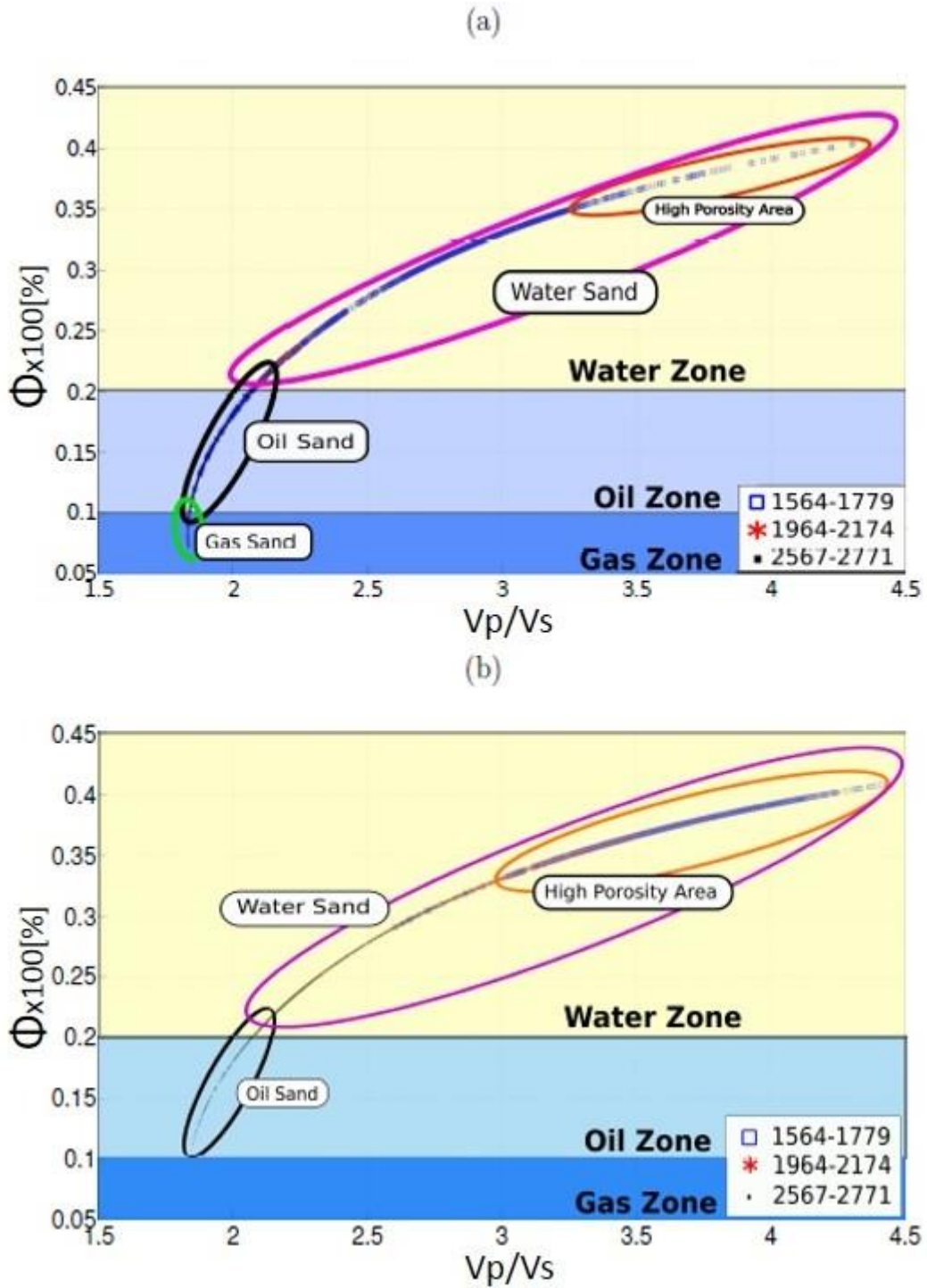
Source: from author

Figure 4.22: Plot showing the variation of V_p/V_s ratio versus porosity for different depth intervals: (a) information is for well A and (b) information from well B.



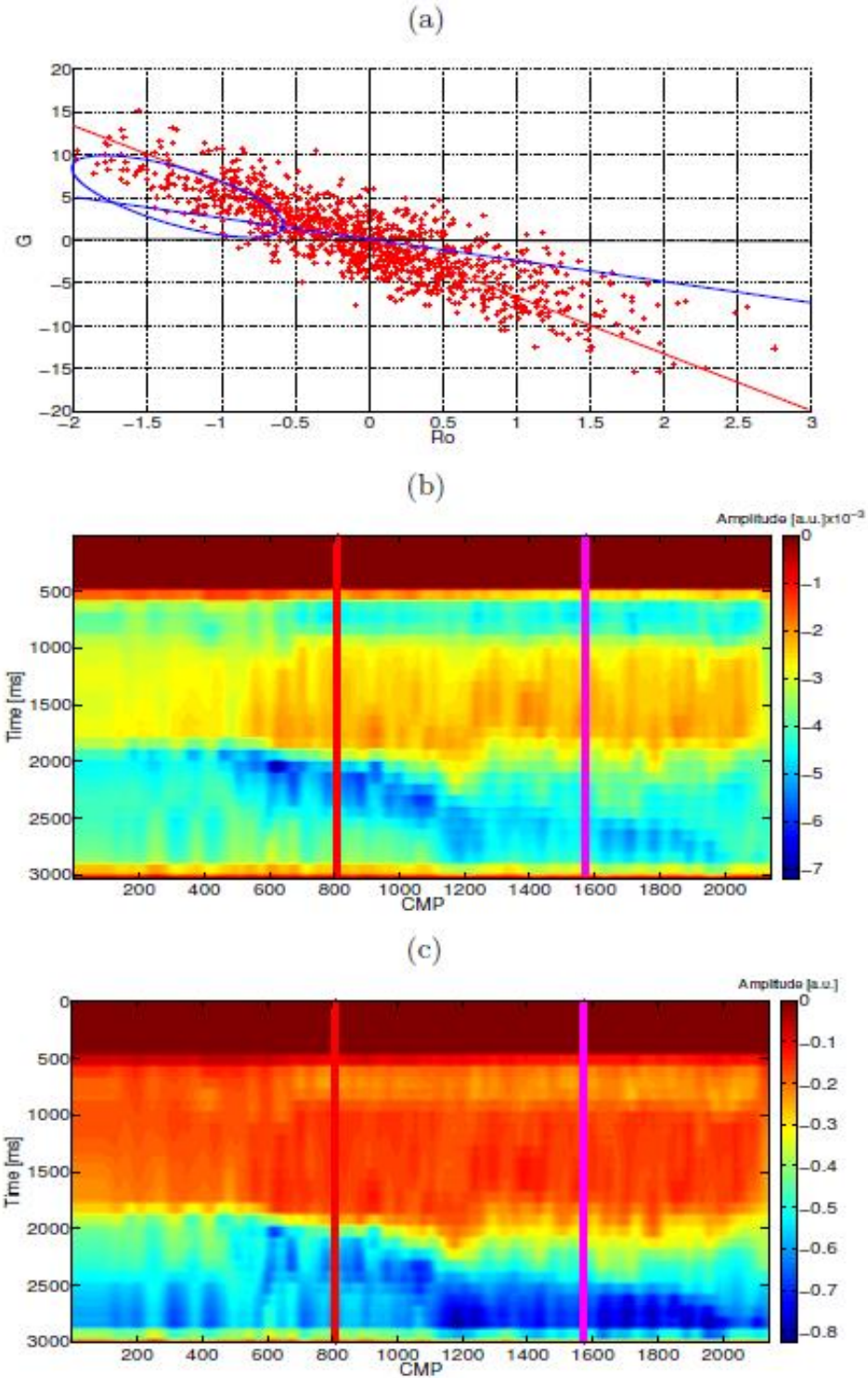
Source: from author

Figure 4.23: Empirical relationship V_p/V_s versus ϕ . This relationship of porosity and V_p/V_s ratio and type of fluid content are showed for different depth interval: (a) well A and (b) well B.



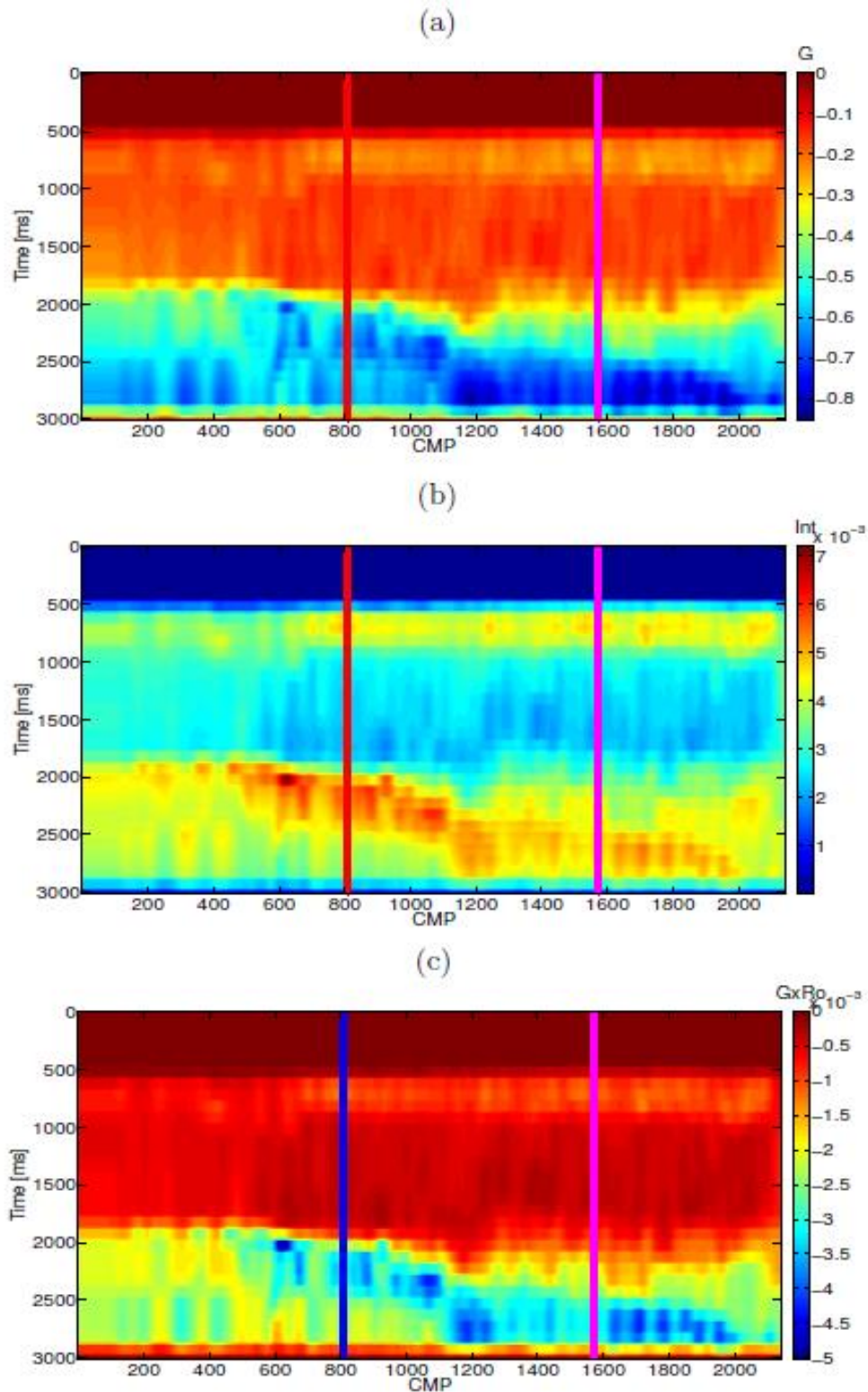
Source: from author

Figure 4.24: (a) AVO analysis from the seismic section, where we can confirm the presence of a fluid with a high potential for gas due to variations position in their physical properties, (b) map of seismic AVO attribute related to seismic section depicted in Figure 4.4. It can be note that anomalous zones are related to areas with high rate of fracturing, (c) reflectivity map showing the anomalous zones present in the CMP 600 as well as anomalous areas close to the well A. We also can see the fractured zones. All results were obtained by PROMAX software.



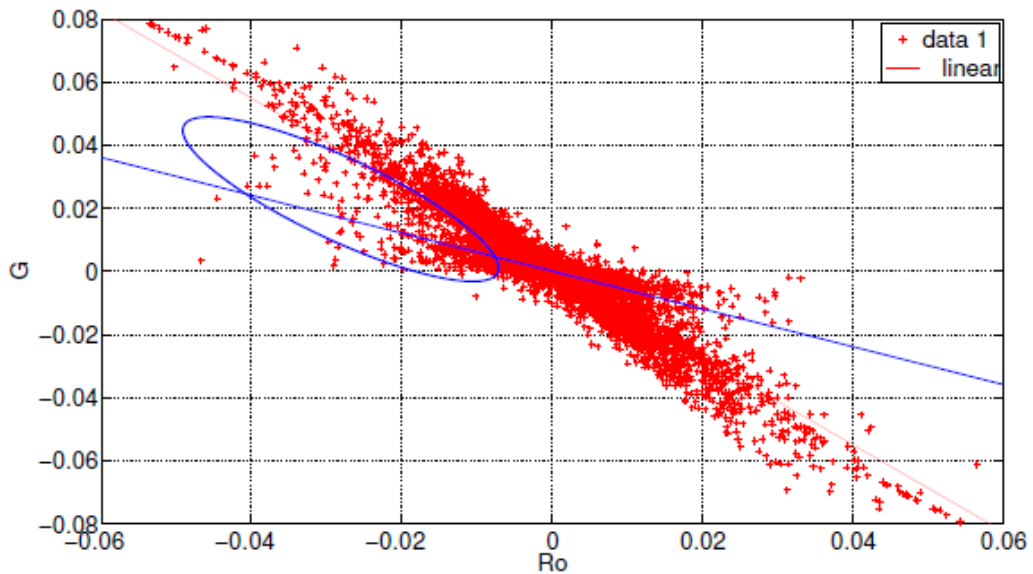
Source: from author

Figure 4.25: (a) Seismic gradient map we can see the anomalous zones is present in the CMP 600 and in the area near the well A, (b) intercept seismic map derived from the application of the AVO technique to seismic section, (c) map of gradient x intercept attribute related to seismic section depicted in Figure 4.4. It can be noted that anomalous zones are related to areas with high rate of fracturing.



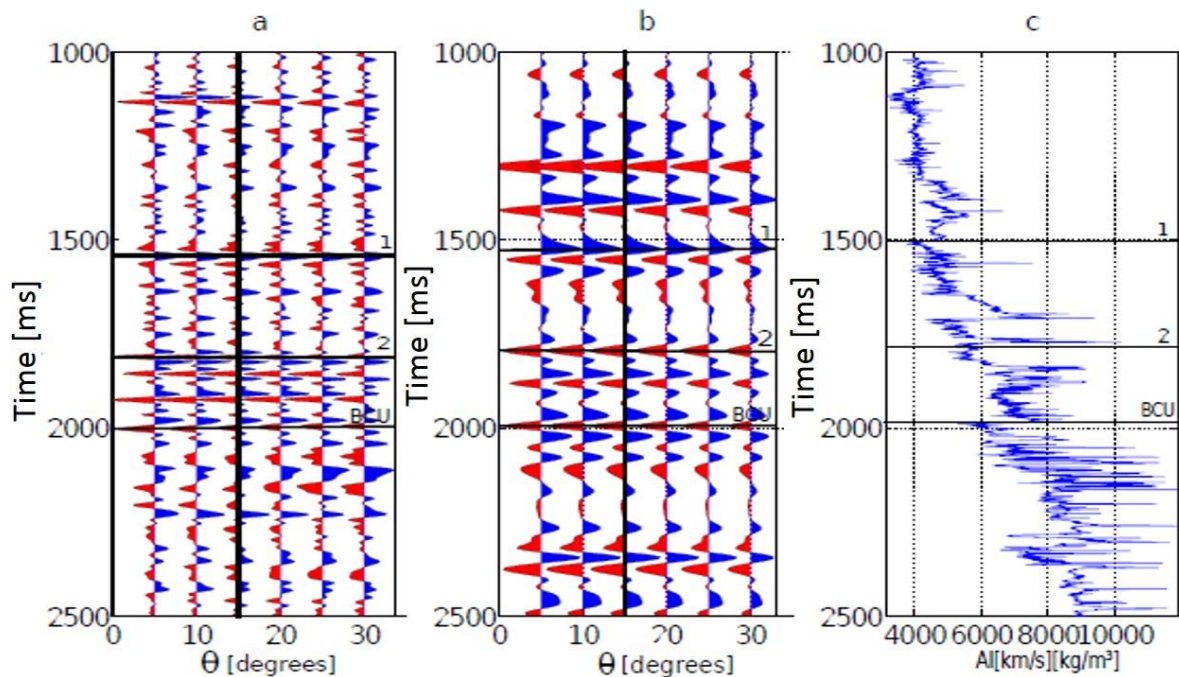
Source: from author

Figure 4.26: AVO analysis from well A, showing the trend of the data, which can infer the presence of gas sand classification of the fluids contained in the well A.



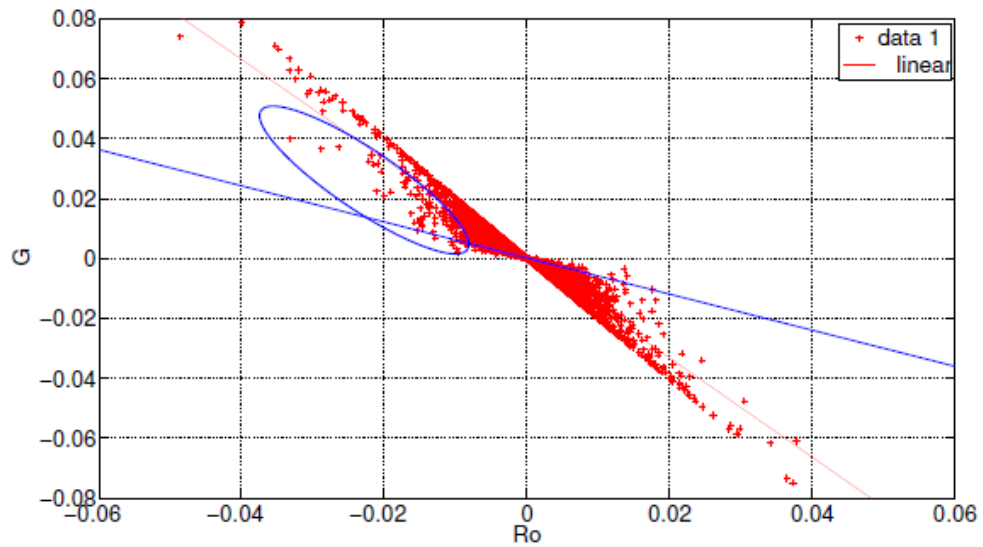
Source: from author

Figure 4.27: Comparison between synthetic seismogram and real seismograms from well A. The geological events are shown (BCU and event 1 and event 2 are cretaceous limits), using the near-angles stack for wavelet estimation (a) real seismogram, (b) synthetic seismogram and (c) acoustic impedance log.



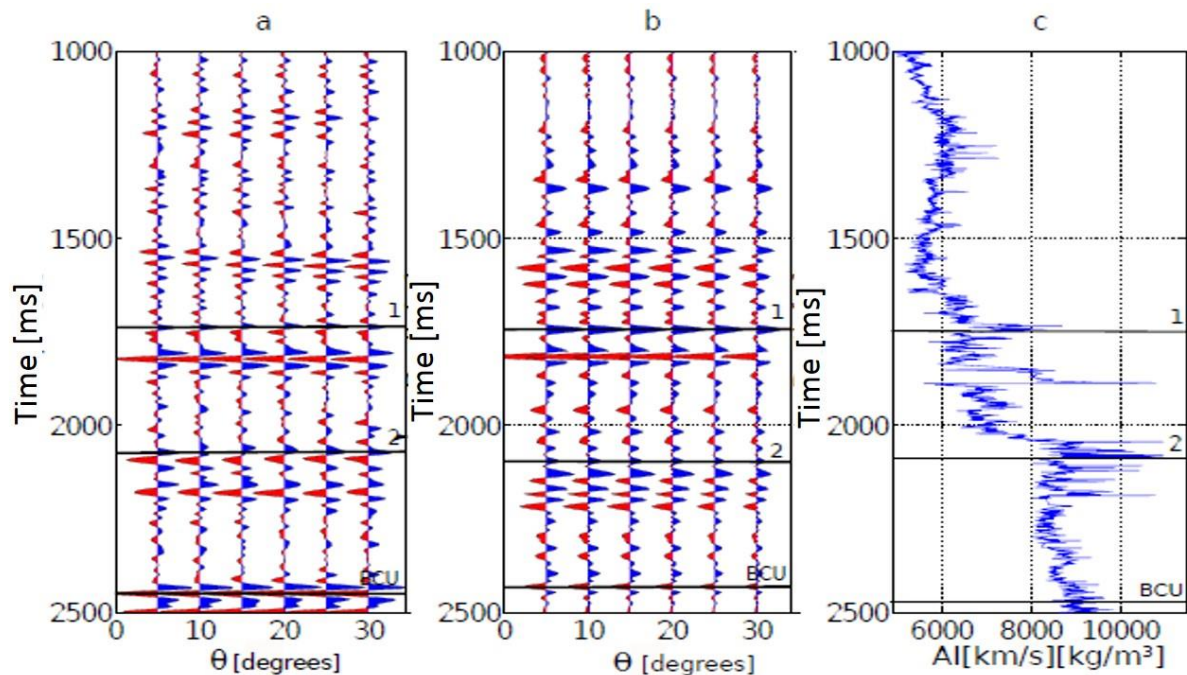
Source: from author

Figure 4.28: AVO analysis applied to the well data B, where the presence of the fluids is mostly water formation, such analysis is inferred from the trend of the data.



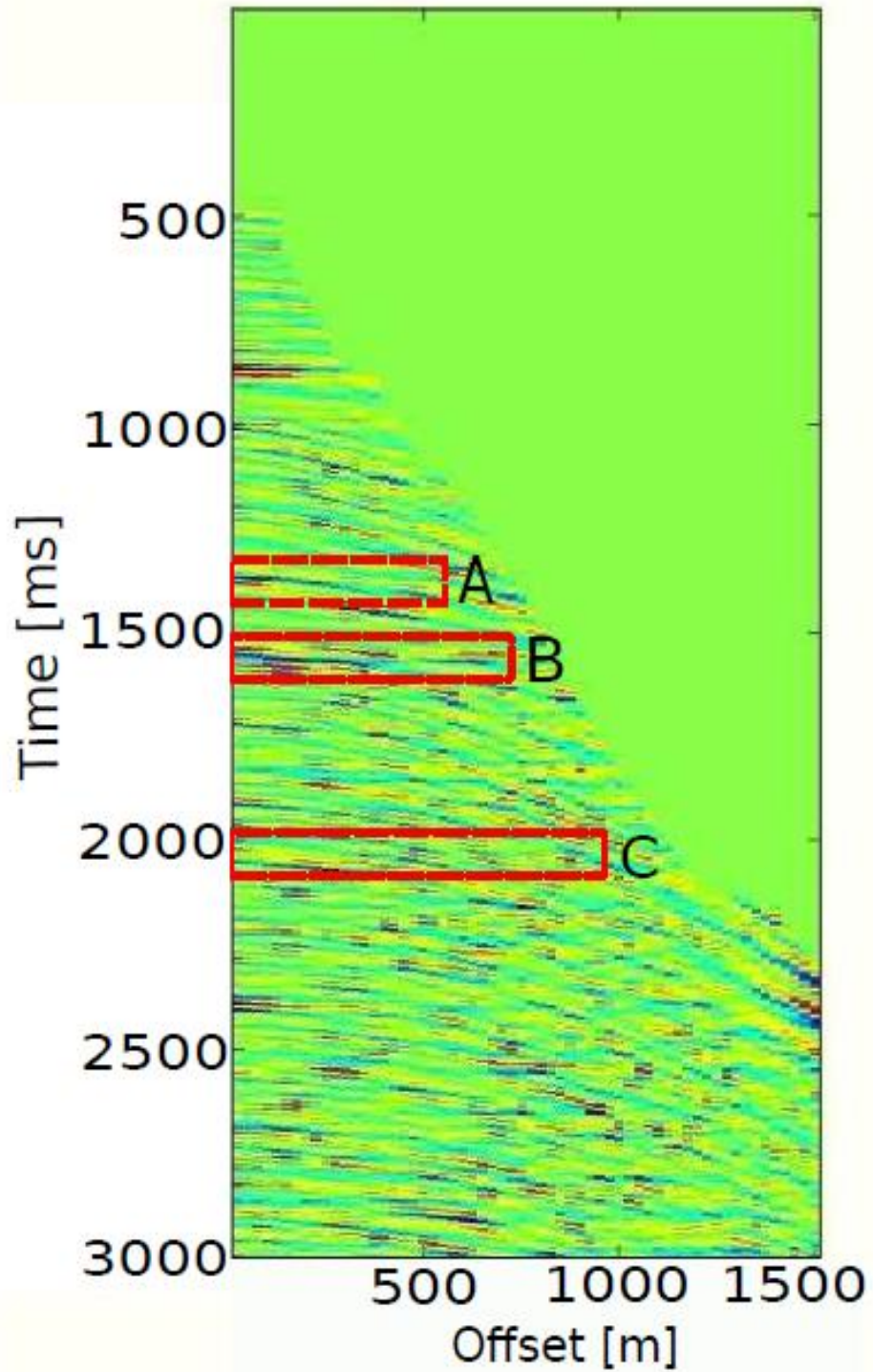
Source: from author

Figure 4.29: Comparisons between the synthetic seismogram and the seismogram from seismic section for well B, (a) real seismogram, (b) synthetic seismogram and (c) acoustic impedance log. Although there are some polarity inversion between the synthetic and real seismic data, most of section are well correlated.



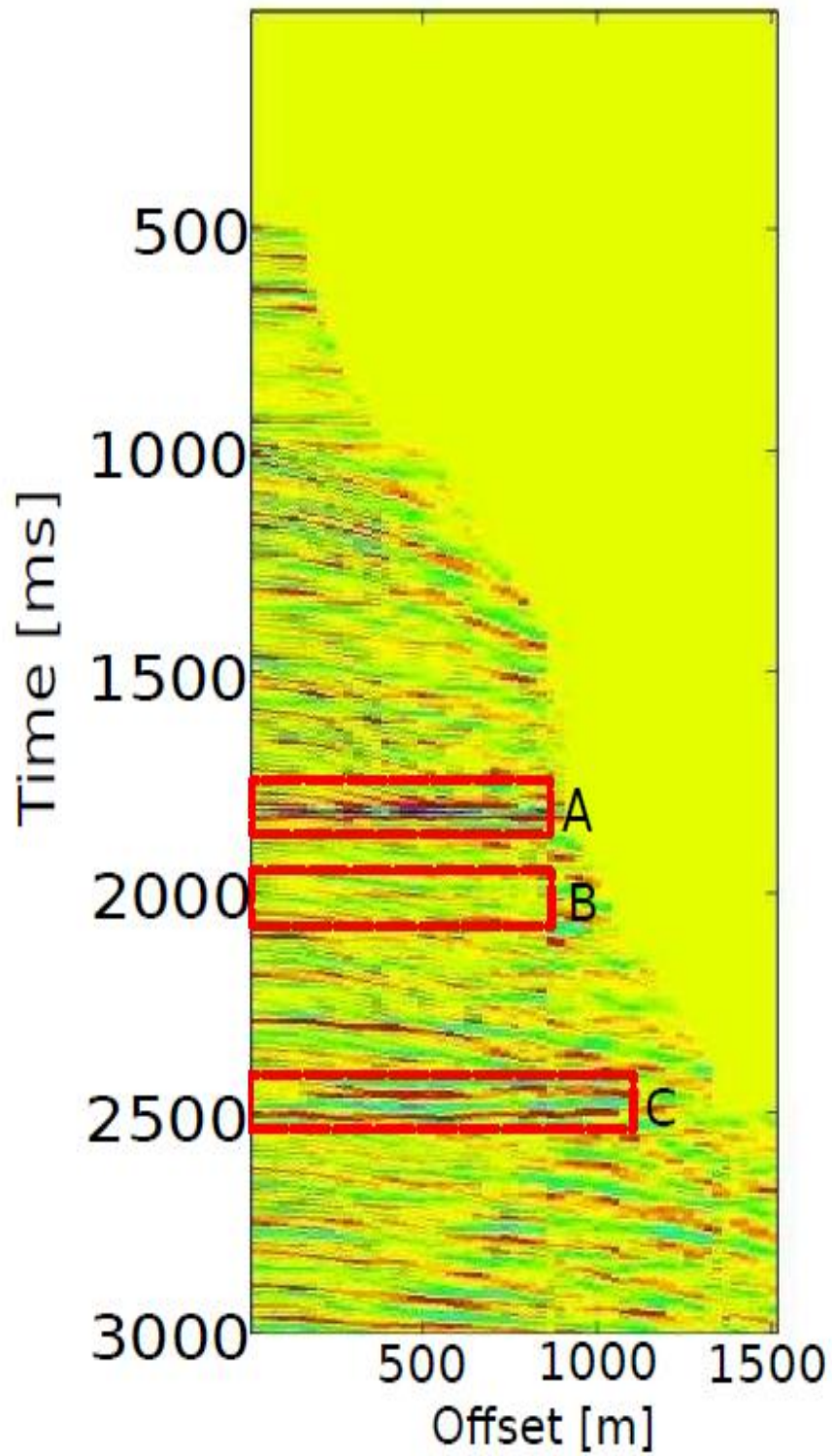
Source: from author

Figure 4.30: CMP 808 in variable density color -graph that displays the anomalies found with the technique of trend angle: (A) anomaly-1, (B) anomaly-2 - seal and (C) anomaly-3.



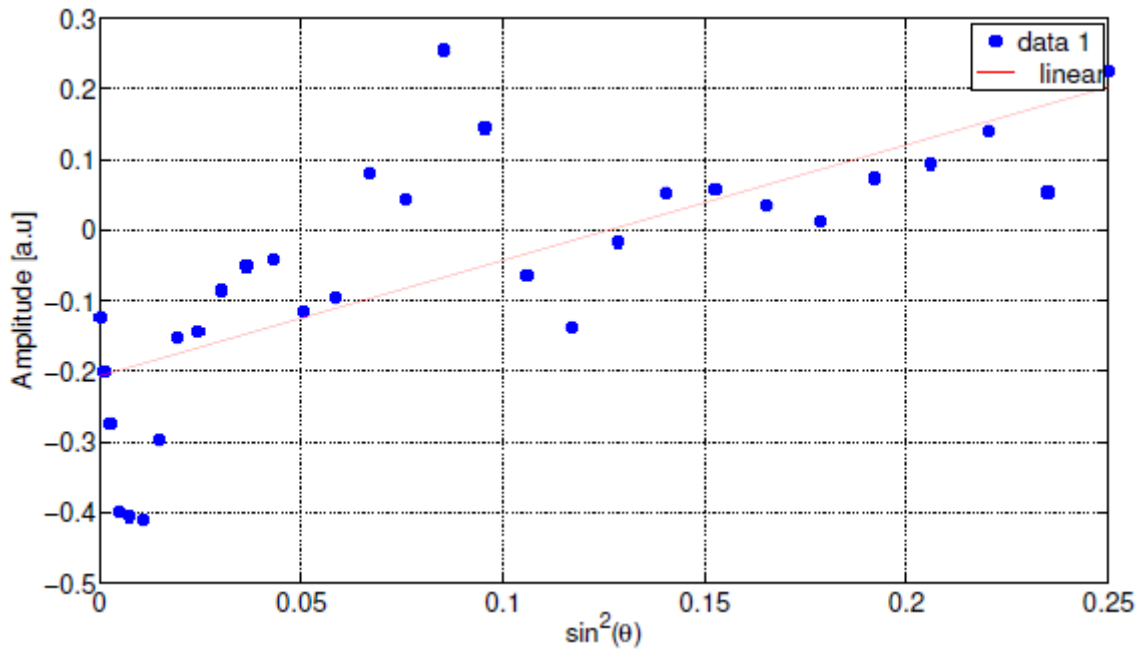
Source: from author

Figure 4.31: CMP 1572 in variable density color - graph that displays the anomalies found with the technique of trend angle (A) anomaly-1, (B) anomaly - 2 - seal and (C) anomaly-3.



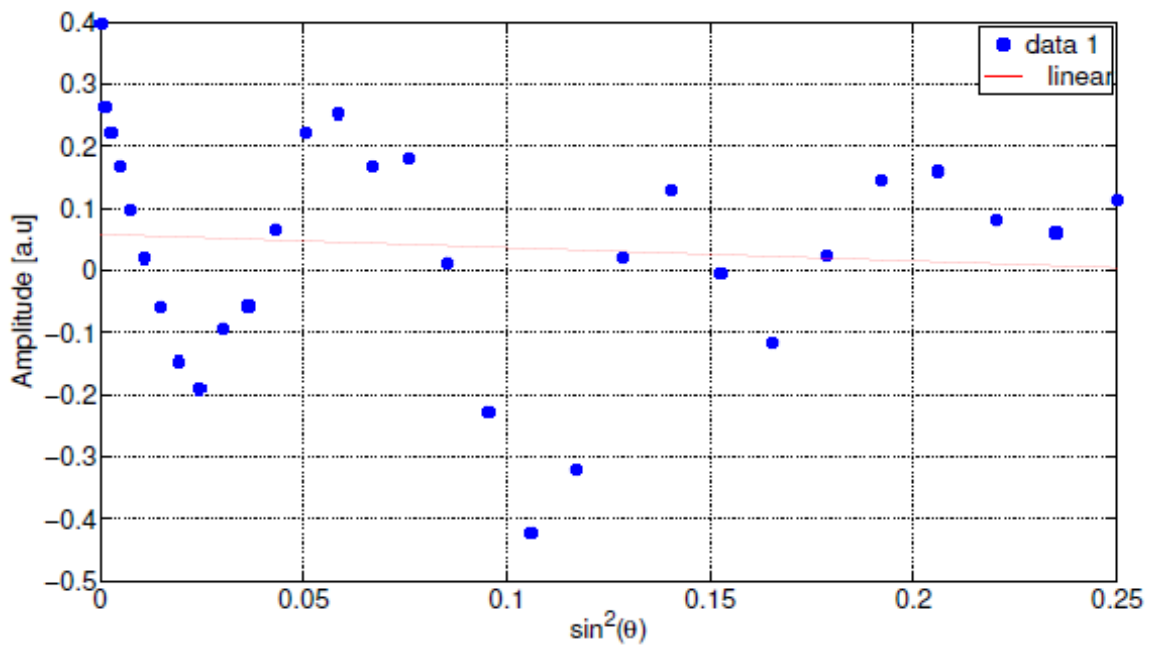
Source: from author

Figure 4.32: Graph that displays the amplitude behavior and their tendency present in the anomaly A - well A.



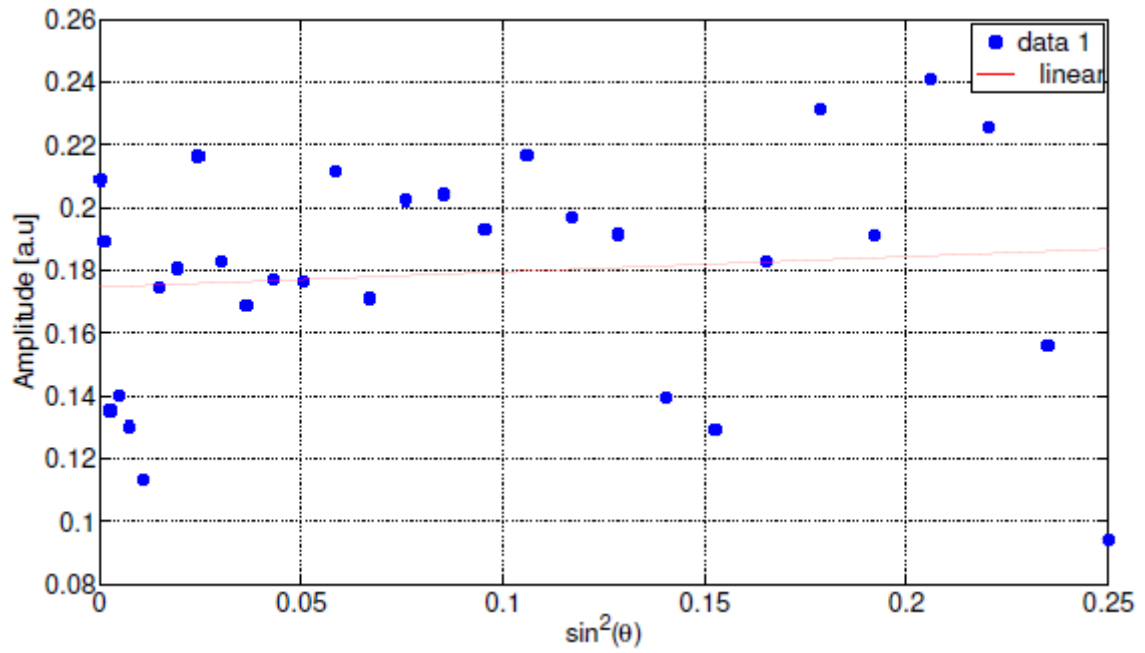
Source: from author

Figure 4.33: Graph showing the trend in amplitude behavior and the presence of a type of seal at the anomaly B - well A.



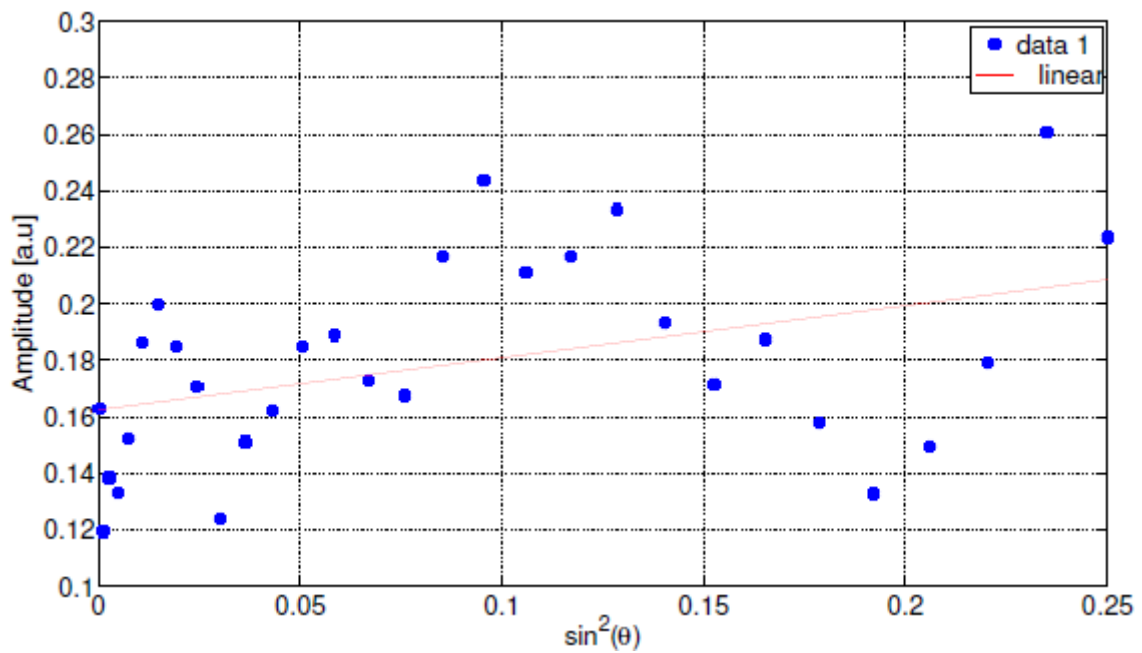
Source: from author

Figure 4.34: Graph showing the trend in amplitude behavior in the anomaly C - well A.



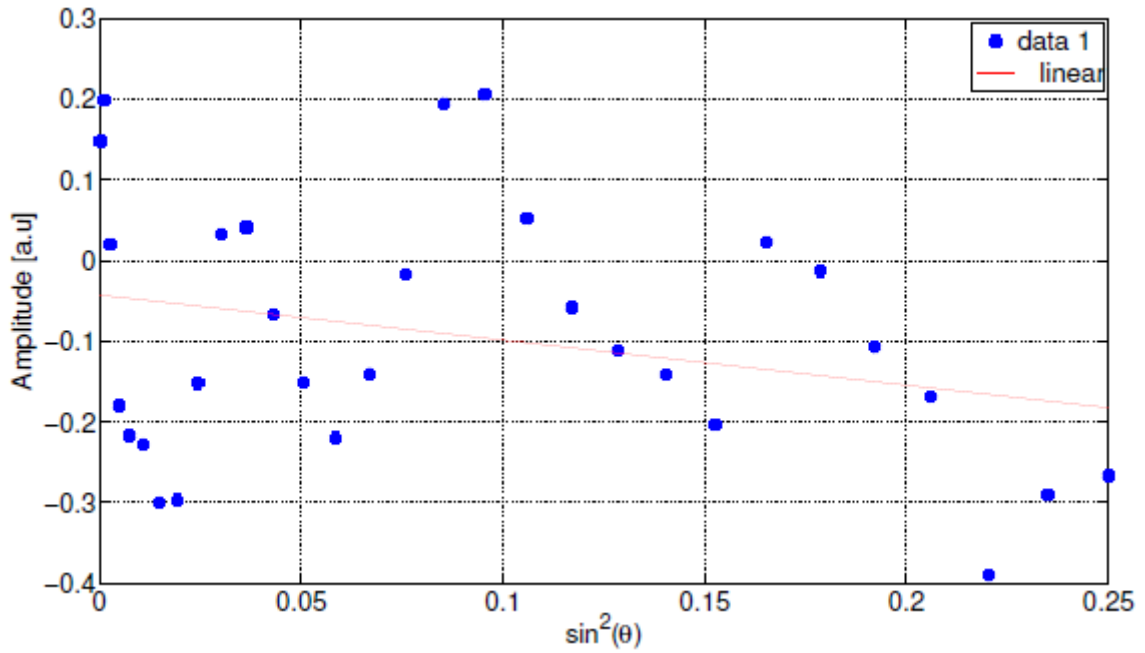
Source: from author

Figure 4.35: Graph that displays the amplitude behavior and their tendency present in the anomaly A - well B.



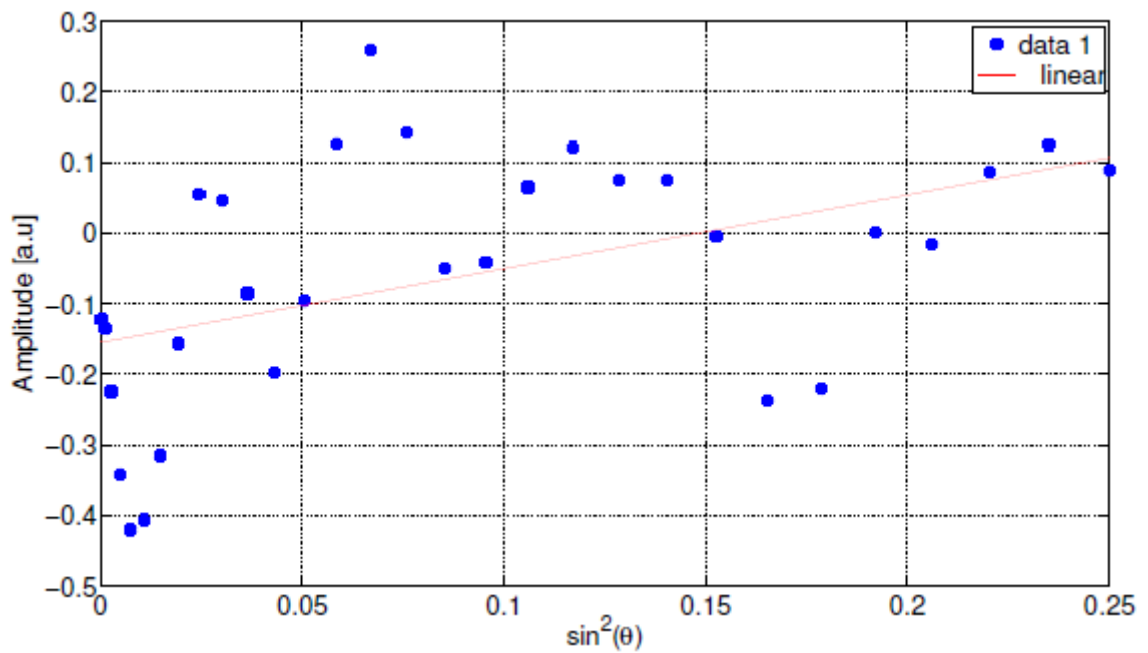
Source: from author

Figure 4.36: Graph showing the trend in amplitude behavior and the presence of a type of seal at the anomaly B - well B.



Source: from author

Figure 4.37: Graph showing the trend in amplitude behavior in the anomaly C - well B.



Source: from author

5 CONCLUSIONS

The main objective of this study was to find the optimal workflow for the identification and classification of anomalous zones present in the seismic data, because of that three different techniques (angle trend, AVO analysis and RPT analysis) were used. The AVO analysis was applied mainly for determining amplitude anomalies present for the results of the re-processing of seismic data. The methodology of the trend angle was the main methodology used to classify anomalies in the results of AVO analysis and was also used for the determination of the origin of anomalies (anomalies generated by the presence of hydrocarbon or generated by fractured environment). At finally the RPT analysis methodology was used to classify the fluid content present in the results of the application of angle trend.

The application of techniques of AVO analysis, RPT analysis and trend angle were performed for the entire seismic section of the Viking Graben area, allowing highlight anomalous zones present, as shown in the CMP 600, which by results this work has a high probability of containing hydrocarbon. The anomalies found between wells A and B which could prove their origin (caused by faults or hydrocarbon content), anomalous zones found in the area near the wells A and B area are confirmed in the forefront in the study of Madiba and McMechan (2003).

In general, from interpretation and results obtained from trend angle and AVO techniques demonstrate that the potential is high for the presence of hydrocarbon in the seismic section from Viking Graben area which has different amplitude anomalies, of which anomalies near the wells A and B and the present in the CMP 600 were tested and classified by application of AVO analysis, and trend analysis angle RPT.

The main technique used to determine the amplitude anomalies on seismic data was the AVO analysis, which could determine variations in the P-wave velocity while passing through different environments (solids, fluids and fractured). The application of AVO analysis allowed us to observe different areas, in the seismic section, contain high hydrocarbon potential, but due to highly fractured environment, most of the bright spots are generated by the presence of fractures which are called

false positives.

In the application of the RPT analysis (Rock-physics template) and trend angle techniques, the results showed a way to discretize, to some degree, the presence of fluid detected in the wells A and B, using templates of rock-physics and attributes analysis (in this case the trend angle), which it have a high probability to contain gas sand. Additionally, it was shown that the methods used: (a) trend angle and (b) rock physics template can be discretized in some degree the type of fluid present in the reservoir. Beyond that, as mentioned before, the results obtained by applying the trend angle methodology in real well-logs data, resulted in three very remarkable anomalies, two of which indicate the presence of areas most likely to contain fluids economically profitable (oil and gas). The remaining anomaly indicate the presence of a material that does the work of seal and due the amplitude behavior suggest a very compact material.

In the application of the AVO and RPT analysis techniques and methodology of trend angle, we can see the need to have an environment with high s/n ratio in order to try to eliminate the ambiguity of the results is also necessary to make good seismic data processing, which preserve and keep the amplitudes as close to the field amplitudes acquired.

How suggestions for future work, we highlight the implementation of the technique of inversion of seismic data combining rock physics (MAVKO et al., 2008), to calculate the data matrix implemented in the methodology trend angle, which would be an advantage for the characterization of the area.

With this study was possible to better understand the characteristics of the data and techniques to apply for reservoir characterization, identifying key steps to get the best possible results. The present study is the first step in developing an inversion of seismic data for improved reservoir characterization, which would be closest to the geological environment model. Because the methodologies used have a high sensitivity to the data, any optimization performed in later works this will be of great importance, as it will help in improving the method which is the main objective.

REFERENCES

- ABBOTTS, I., *United Kingdom oil and gas fields 25 years*. The Geological Society, v.14, p.21-207. (*Memoir*, v.14), 1991.
- AKI, K.; RICHARDS, P., *Quantitative seismology - Theory and methods*, v. I y II, W. H. Freeman and Co, 1980.
- ANDREW, R.; BEZDAN, S., Shear-wave velocity estimation techniques: a comparison, SEG convention, *Geophysics*, 2001.
- ARVID, N.; LARSEN, B., Cenozoic tectonic subsidence, dynamics of the Norwegian margin. *Geological Society*, v. 276, 2000.
- AVSETH; VEGGELAND, Seismic screening for hydrocarbon prospects using rock-physics attributes, *SEG*, v. 33, p. 266-274, 2014.
- AVSETH, P., MUKERJI, T., MAVKO, G., Quantitative Seismic Interpretation Applying Rock Physics Tools to Reduce Interpretation Risk. *SEG*, v. 25, p. 106-110, 2005.
- BATZLE, M., HAN, D.; HOFMANN, R., Fluid mobility and frequency-dependent seismic velocity and direct measurements. *Geophysics*, v. 73, n. 1, p.N1-N9, 2006.
- BOLT, H., Wireline depth determination, Society of Professional Well Log Analysts, rev. 3.3 Apr., available in www.spwla.org, 2012.
- BORTFELD, R., Approximations to the reflection and transmission coefficients of plane longitudinal and transverse waves. *Geophysical Prospecting*, v. 9, n. 4, p. 485-503, 1961.
- BORUAH, N., Rock physics template (RPT) analysis of well logs for lithology and fluid classification, 8vo International Conference and Exposition on Petroleum Geophysics, p. 55-62, 2010.
- BROWN, R.; KORRINGA, J., On the dependence of the elastic properties of a porous rock on the compressibility of the pore-fluid. *Geophysics*, v. 40, n. 2, p. 608-616, 2005.
- BROWN, S., Introduction to the petroleum geology of the North Sea. Special Publication, *Geological Society*, v. 61, p. 219-254, 1990.
- CASTAGNA; J., BATZLE; M.; EASTWOOD, R., Relationships between compressional-wave and shear-wave velocities in clastics silicate rocks. *Geophysics*, v. 50, n 4, p. 571-581, 1985.
- CASTAGNA, J., BATZLE, M.; EASTWOOD, R., Framework for AVO gradient and intercept interpretation. *Geophysics*, n° 63, v. 3, p. 948-956, 1998.
- CASTAGNA, J., SWANZ, H.; FOSTER D., Framework for AVO gradient and intercept interpretation. *Geophysics*, n° 63, v. 3, p. 948-956, 1998.

CHACKO, S., Porosity identification using amplitude variations with offset: examples from south Sumatra, *Geological Society*, v. 54, p. 942-951, 1989.

CIZ, R.; SHAPIRO, S., Stress-dependent anisotropy in transversely isotropic rocks: Comparison between theory and laboratory experiment on shale. *Geophysics*, v. 74, p. D7-D12, 2007.

DVORKIN, J.; BREVIK, I., Diagnosing high-porosity sandstones: Strength and permeability from porosity and velocity. *Geophysics*, v. 64, n. 3, p. 795-799, 1999.

DVORKIN, J.; MAVKO, G., Implications of the rock pore micro-geometry for the movement and chemical reactivity of CO₂ in carbonates, *Geophysics*, p L69-L86, 2013.

FOURIER, J., Remarques generales sur les temperatures du globe terrestre et des espaces planetaires. *Annales de Chimie et de Physique*, v. 27, p. 136-167, 1824.

GARDNER, G., GARDNER, L.; GREGORY, A., Formation velocity and density the diagnostic basis for stratigraphic traps. *Geophysics*, v. 39, p. 770-780, 1974.

GASSMANN, F., Elastic waves through a packing of spheres, American Geological Institute, SEG, n° 13, v. 10, 1951.

GLENNIE, K.; UNDERHILL, J., Origin, development and evolution of structural styles, outline of the structural framework of the North Sea. *Petroleum geology of the North Sea basic concepts and recent advances*. *Blackwell*, v. 19, n. 4, 1998.

GLENNIE, K., W., Introduction to the petroleum geology of the North Sea, *Petroleum geology of the North Sea basic concepts and recent advances*. *Blackwell*, Fourth Edition, 1982.

GREGORY, A., Aspects of rock physics from laboratory and log data that are important to seismic interpretation. *AAPG*, n. 26, p. 15-46, 1977.

GREGORY, A., GARDNER, L.; WYLLIE, M., An experimental investigation of factors affecting elastic wave velocities in porous media. *Geophysics*, v. 23, p. 459-493, 1958.

HILTERMAN, F., Seismic amplitude interpretation, *Seismic Amplitude Interpretation*: SEG, p. 235, 2001.

KALLIVOKAS, L., et al., Site characterization using full waveform inversion. *Soil Dynamics and Earthquake Engineering*, v. 47, p. 62-82, 2013.

KHAN, S.; JACOBSON, S., Remote sensing and geochemistry for detecting hydrocarbon microseepages. *Geological Society of America Bulletin*, n. 120, p. 96-105, 2008.

KNOTT, C., Reflection and refraction of elastic waves with seismological applications. *Phil. Mag.*, n. 48, p. 64-97, 1899.

- KOEFOED, O., On the effect of Poisson's ratios of rock strata on the reflection coefficients of plane waves. *Geophysical Prospecting*, n. 3, p. 381-387, 1955.
- LEE, M.; COLLETT, T., Integrated analysis of well logs and seismic data at the Keathley canyon, Gulf of Mexico, for estimation of gas hydrate concentrations marine and petroleum geology. n. 25, p. 924-931, 2008.
- MADIBA, G.; MCMECHAN, G., Processing, inversion, and interpretation of a 2D seismic data set from the north Viking Graben, North Sea. *Geophysics*, v. 68, n. 3, p. 837-848, 2003.
- MAVKO, G., CHAN, C.; MUKERJI, T., Fluid substitution: Estimating changes in V_p , without knowing V_s , *Geophysics*, v. 60, n. 6, p. 1775-1755, 1995.
- MAVKO, G., EZEQUIEL, F.; TAPAN, M., Seismic inversion combining rock physics and multiple-point geostatistics, *Geophysics*, v. 73, n. 1, p. R11-R21, 2008.
- MCGREGOR, A., A brief review of AVO anomaly classification. *Geohorizons*, n° 34, 2007.
- MUSKAT, M.; MERES, M., Reflection and transmission coefficients for plane waves in elastic media. *Geophysics*, n. 5, p. 115-148, 1940.
- OSTRANDER, W., Plane-wave reflection coefficients for gas sands at non-normal angles of incidence. *Geophysics*, n. 49, p. 1637-1648, 1984.
- PEGRUM, R.; SPENCER, A., Hydrocarbon plays in the northern North Sea, *Special Publication*, n. 50, p. 441-470, 1990.
- RAYMER, L.; HUNT, E.; GARDNER, J., An improved sonic transit time-to-porosity transform, *Geophysics*, n. 60, p. 220-250, 1980.
- REGUEIRO, J.; GONZALEZ, E., A different seismic AVO attribute for fluid-lithology identification. *SBGf*, 1995.
- RITSEMA, REINIER, A.; GÜRPINAR, A., Seismicity and seismic risk in the offshore North Sea area, *Geophysics*, n. 56. p. 1-4, 1982.
- ROBERT G. KEYS AND DOUGLAS J. FOSTER, Comparison of Seismic Inversion Methods on a Single Real Data Set. *SEG*, n. 4, 1992.
- RUTHERFORD, S.; WILLIAMS, R., Amplitude-versus-offset variations in gas sands. *Geophysics*, v. 54, n. 6, p. 680-688, 1989.
- SHUEY, R., A simplification of the Zoeppritz equations. *Geophysics*, n. 50, p. 609-614, 1985.
- SMITH, G.; GIDLOW, P., Weighted stacking for rock property estimation and detection of gas *Geophysics. Prospection*, n. 35, p. 993-1014, 1987.
- SMITH, T., SONDERGELD, C.; RAI, C., Gassmann fluid substitutions a tutorial. *Geophysics*, v. 68, n. 2, 2003.

SPENCER, A., BIRKELAND, O.; KOCH, J., Petroleum geology of the proven hydrocarbon basins, offshore. *First Break*, v. 5, n. 11, p. 161-176, 1993.

TREWIN, N., Regional development. The Geology of Scotland, *Geological Society of London*, p. 301-303, 2002.

TYSON; S., An Introduction to Reservoir Modeling. 2 ed. Philadelphia, *W.B. Saunders, Pipers' Ash*, p. 238, v. 1, 2007.

WANG, Z., Fundamentals of seismic rock physics. *Geophysics*, v. 6, n° 2, p. 398-412 (MARCH-APRIL 2001), 2001.

WEIWEI, L., Seismic wave propagation in fractured anisotropic carbonate rock: Experiments and theory. *Geophysics*, n. 8, 2011.

WYLLIE, M., GREGORY, A.; GARDNER, L., Elastic wave velocities in heterogeneous and porous media. *Geophysics*, n. 21, p. 41-70, 1956.

YILMAZ, Ö, *Seismic data processing*, Society of Exploration geophysicists, Tulsa, USA, v. 2, 1987.

ZOEPPRITZ, K., Über reflection und durchgang seismischer wellen durch unstetigkeits achen. nachrichten von der königlichen gesellschaft der wissenschaften zu göttingen. *Mathematisch-physikalische Klasse*, n. VII-VIIb, p. 66-84, 1919.

APPENDIX

A GEOLOGY

The geology of the North Sea describes the geological features such as channels, trenches, and ridges today and the geological history, plate tectonics, and geological events that created them.

The basement of the North Sea was formed in an intraplate setting during the Pre-Cambrian. Rigid blocks were overlaid with various depositions, sands and salts. These rigid blocks were transformed to a metamorphic base due to tectonic processes such as continental collisions which cause horizontal pressure, friction and distortion in the Caledonian plate cycle as well as the Variscan plate cycle. The blocks were also subjected to metamorphic evolution during the Triassic and Jurassic periods when the rock was heated up by the intrusion of hot molten rock called magma from the Earth's interior (GLENNIE; UNDERHILL, 1998). The total petroleum system and corresponding assessment unit coincide with the extent of oil and gas accumulations and thermally mature, organic matter-rich marine shales of late Jurassic and earliest Cretaceous age in and adjacent to the Viking Graben of the northern North Sea.

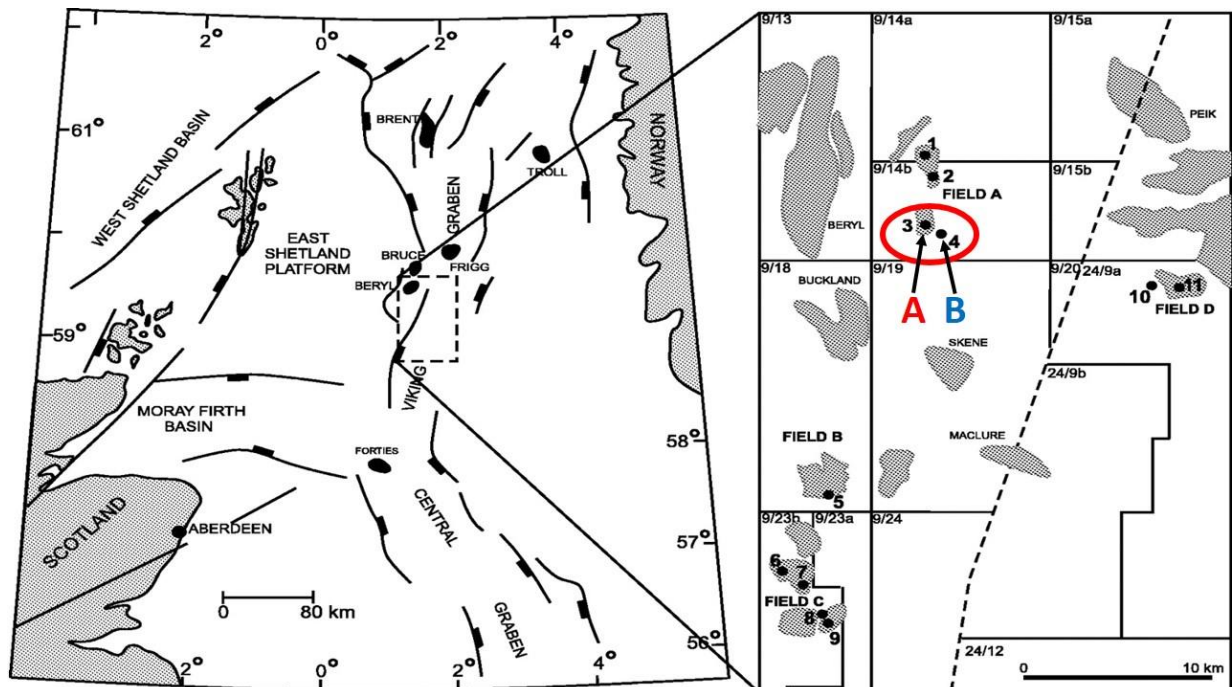
The Caledonian (Iapetus) plate cycle saw the formation of the Iapetus suture during the Caledonian orogeny. The Iapetus suture was a major weakness creating a volcanic fault in the central North Sea during the later Jurassic period. The Iapetus Ocean was replaced with a suture line and mountain range when Laurentia, Baltica and Avalonia continents collided. This collision formed Laurussia (GLENNIE; UNDERHILL, 1998). Triassic and Jurassic volcanic rifting and graben fault systems created highs and lows in the North Sea area. This was followed by late Mesozoic and Cenozoic subsidence creating the intracratonic sedimentary basin of the North Sea. This era experienced higher sea levels because of sea floor spreading, cooler lithosphere temperatures. Plate tectonics and continental orogenies combined to create the continents and the North Sea as we know them today. The final events affecting the North Sea coastline features and submarine topography occurred in the Cenozoic era.

The subsurface of the North Sea area is dominated by grabens: the north-west south east oriented Lower Rhine Graben under the southern North Sea and the Netherlands, RITSEMA et al. (1982) the north-south oriented North Sea Central

Graben that begins north of the Dutch coast and ends in the region east of Scotland, and the “VIKING GRABEN” along the south-east Norwegian coast (RITSEMA et al., 1982).

The Horn Graben is a smaller graben east of the Central Graben and in front of the Danish coast (ARVID; LARSEN, 2000; RITSEMA et al., 1982). Another smaller structure is known as the Terschelling Graben which borders the Central Graben in the West, just north of the Netherlands. A larger graben is found in the subsurface below the Skagerrak, this north-south structure is called the Bamble-Oslo Graben. TREWIN (2002) speak that the Viking Graben is separated from the Faeroe Shetland Basin below the Atlantic by the Shetland Platform, the two structures join in the area north-east of the Shetland Islands (see Figure A.1).

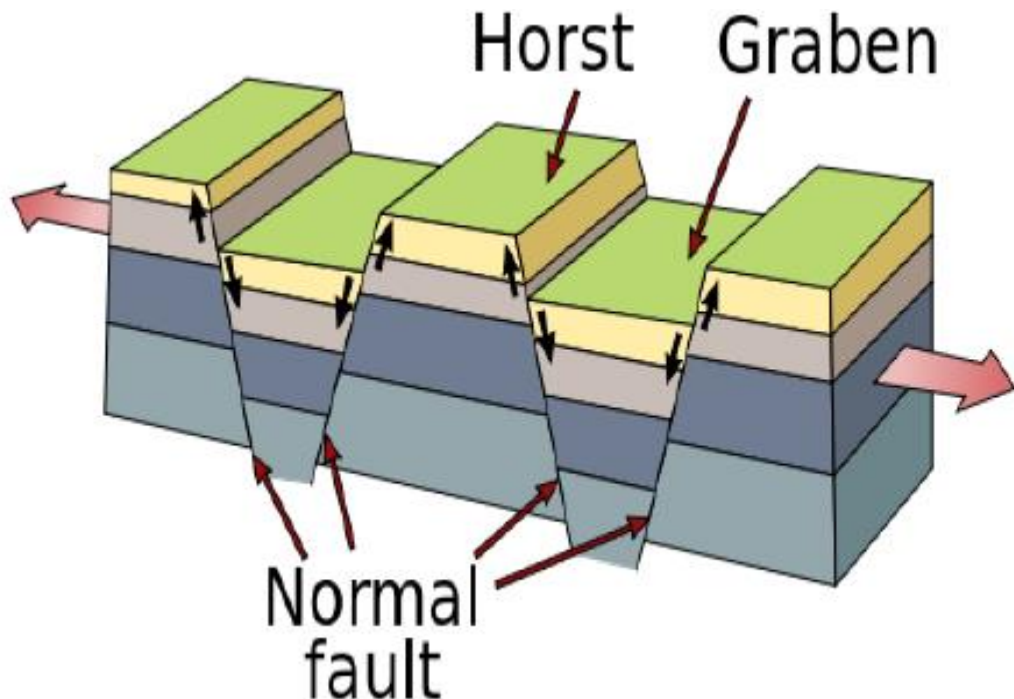
Figure A.1: Map of the Viking Graben area.



Source: Jonk; Hurst; Duranti; Parnell; Mazzini and Fallick (2005), modified from (Brown, 1990)

Virtually all significant oil and gas accumulations in the northern North Sea are believed to have been generated within certain fine grained, organic-carbon-rich marine strata of late Jurassic and earliest Cretaceous age (SPENCER et al., 1993). These Kimmeridgian shales accumulated in oxygen-starved rift basins and may locally attain thickness of 3000 m.

Figure A.2: Schematic representation of a horst and grabens succession.

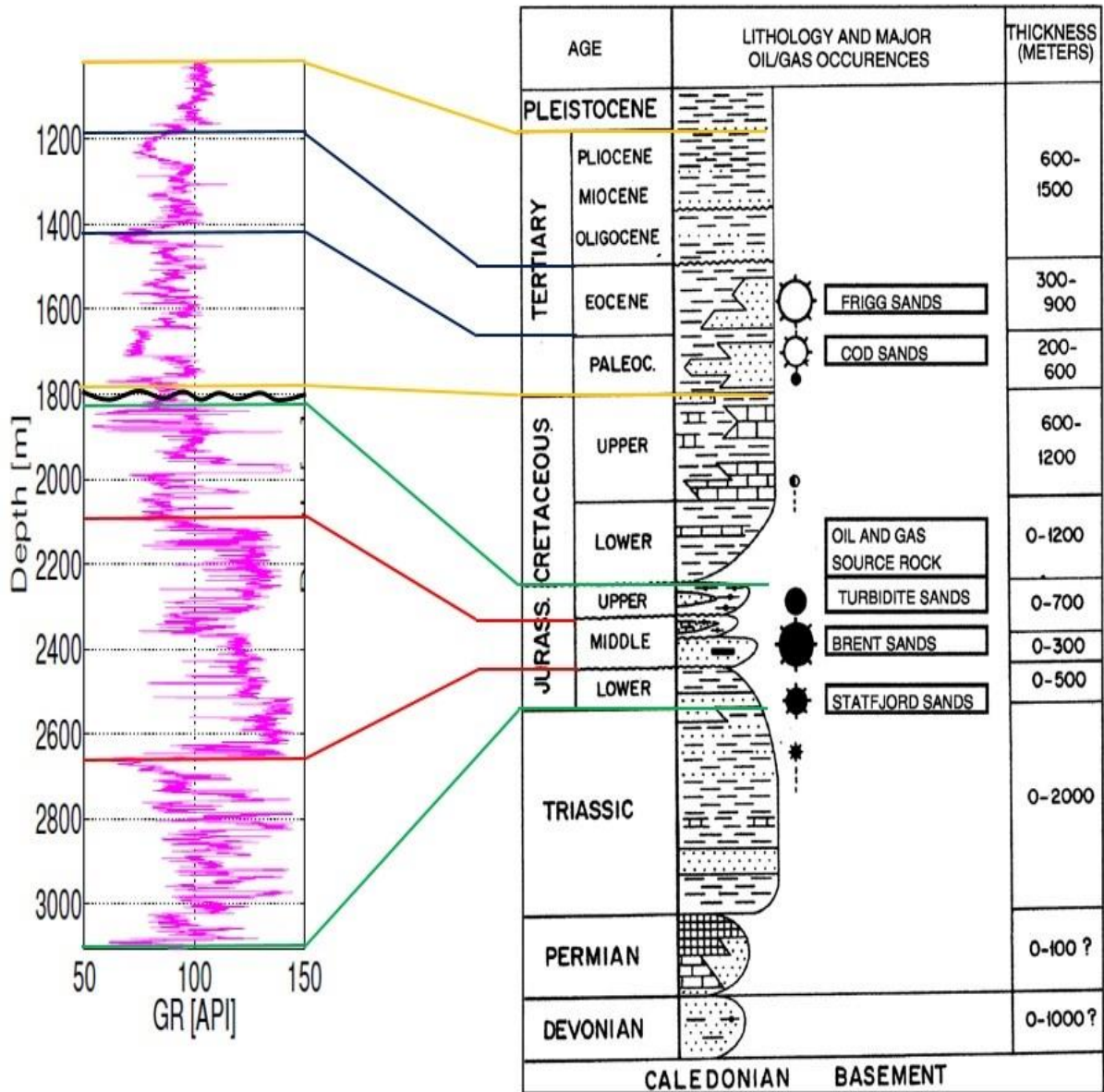


Source: R. Jonk, A. Hurst, D. Duranti, J. Parnell, A. Mazzini, and A. E. Fallick (2005)

The actual source rocks are black shales that display high radioactivity and have total organic carbon (TOC) contents of 2 to 15 percent or more and average about 5 percent TOC. The typical kerogen types within the hot shales are mixtures of organic matter commonly described as type II kerogen reflecting a mixture of planktonic marine algae and degraded terrigenous humic organic matter (ABBOTTS, 1991).

Burial of Viking Graben source rocks has been more or less continuous from the time of deposition until the present day. Some source rocks achieved thermal maturity with respect to oil and gas generation as early as late Cretaceous time and continuing to the present day in some areas. Thus newly generated oil and gas has been available to traps almost continuously during post-early Cretaceous Viking Graben history (PEGRUM; SPENCER, 1991). At various places within the Viking Graben, oil and gas migration has occurred laterally, stratigraphically downward, and vertically upward into and through permeable rocks and fractures of pre-rift, syn-rift, and post-rift age.

Figure A.3: Comparison between stratigraphic column for northern North Sea reservoir rocks (after Parsley, 1990) and gamma ray log from the well A in the Viking Graben field.



Source: Jonk; Hurst; Duranti; Parnell; Mazzini and Fallick (2005).

Significant reservoir rocks include Triassic rocks and outstanding lower to middle Jurassic sandstone reservoirs, including those of the Brent Group, deposited prior to latest Jurassic rifting (BROWN, 1990). Submarine fan complexes containing excellent sandstone reservoirs formed contemporaneously with Late Jurassic rifting. Also, upper Jurassic sandstone reservoirs of the Troll Field reservoir are hundreds of meters thick, with porosity in excess of 30 percent. Submarine fan and channel

sandstones of Paleocene age also constitute significant reservoirs in the Viking Graben.

Largest accumulations occur within fault blocks formed during rifting. Stratigraphically entrapped hydrocarbons occur abundantly in submarine channel and fan complex sandstones deposited during and subsequent to rifting (PEGRUM; SPENCER, 1991). Extra-rift sandstones of the Troll Delta also stratigraphically entrap hydrocarbons. Fine-grained marine mudstones of Tertiary age generally blanket and deeply bury most traps in the Viking Graben and provide a generally effective regional seal in addition to that provided by stratigraphic lithology heterogeneities Spencer et al. (1993).

B GASSMANN'S THEORY

There are several theories that compare the elastic properties of dry and saturated rocks. These models have mainly been explained by pore-elastic theories or effective medium theories. The Gassmann's model which is commonly used in petroleum rock physics is suitable for rocks with spherical and interconnected pores at low frequencies.

To extract fluid types or saturations from seismic, crosswell, or borehole sonic data, we need a procedure to model fluid effects on rock velocity and density. Numerous techniques have been developed. However, Gassmann's equations are by far the most widely used relations to calculate seismic velocity changes because of different fluid saturations in reservoirs. The importance of this grows as seismic data are increasingly used for reservoir monitoring.

According to Smith et al. (2003) the fluids substitutions are an important part of any seismic attribute work, because provided to the interpreter with a valuable tool for modeling various scenarios of fluid, which could explain the anomaly amplitude variation with offset (AVO). Gregory et al. (1958) and Wyllie et al. (1956) proposed an empirical relation-ship to model the velocity and porosity, which was subsequently extended by Raymer et al. (1980). However, the work of Gassmann (1951) are the most used as these relate the bulk modulus of a rock and pore, structure and the properties of fluids.

Gassmann's formulation is straightforward, and the simple input parameters typically can be directly measured from logs or assumed based on rock type. This is a prime reason for its importance in geophysical techniques such as time-lapse reservoir monitoring and direct hydrocarbon indicators (DHI) such as amplitude bright spots" and amplitude vs. offset (AVO).

The Gassmann equation is the most common way of performing a fluid substitution model from one known parameter.

B.1 Gassmann's Equations

$$K_{fl} = \left[\frac{S_w}{K_w} + \frac{1-S_w}{K_{gas}} \right]^{-1}, \quad (\text{B.1})$$

$$K_{dry} = \rho_b \left[V_p^2 - \frac{4}{3} V_s^2 \right], \quad (\text{B.2})$$

$$K_{sat} = K_{dry} + \frac{\left[\left(1 - \frac{K_{dry}}{K_{min}} \right)^2 \right]}{\left[\frac{\phi}{K_{fl}} + \frac{(1-\phi)}{K_{min}} \right]} - \frac{K_{dry}}{K_{min}^2}, \quad (\text{B.3})$$

$$V_p = \sqrt{\frac{K_{sat} + \frac{4}{3}G}{\rho_p}}, \quad (\text{B.4})$$

$$V_s = \sqrt{\frac{G}{\rho_b}}, \quad (\text{B.5})$$

where K_{fl} is the bulk modulus of the fluid, S_w is the saturation of the fluid, K_w is the bulk modulus of the fluid, K_{gas} is the bulk modulus of the gas, K_{dry} is the bulk modulus of the dry rock, ρ is the density, V_p and V_s are the P-wave and S-wave velocities, K_{sat} is the bulk modulus of saturation, K_{min} is the bulk modulus of the matrix, Φ is the fraction of the porosity and the G is the shear modulus.

Numerous assumptions are involved in the derivation of Gassmann's equation:

- Porous material is isotropic, elastic, monomineralic, and homogeneous,
- Pore space is well connected and in pressure equilibrium (zero frequency limit),
- Medium is a closed system with no pore fluid movement across boundaries;
- No chemical interaction between fluids and rock frame (shear modulus remains constant).

Many of these assumptions may not be valid for hydrocarbon reservoirs, and they depend on rock and fluid properties and in-situ conditions. For example, most rocks are anisotropic to some degree. The work of Brown and Korrington (2005) provides an explicit form for an anisotropic fluid substitution. In seismic applications, it is normally assumed that Gassmann's equation works best for seismic data at frequencies less than 100 Hz (MAVKO et al., 1995). Recently published laboratory data (BATZLE et al., 2006) show that acoustic waves may be dispersive in rocks

within the typical seismic band, invalidating assumption 2. In such cases, seismic frequencies may still be too high for application of Gassmann's equation. Pore pressures may not have enough time to reach equilibrium. The rock remains unrelaxed or only partially relaxed.

B.2 Gassmann's Procedure

Given an initial set of velocities and densities (V_{p1} , V_{s1} , ρ_1) corresponding to a rock with an initial set of fluids, you can compute the velocities and densities of the rock with another set of fluid. Often these velocities are measured from well logs, but might also come from a theoretical model.

1. Step 1: extract the dynamic bulk and shear moduli from V_{p1} , V_{s1} and ρ_1 ,

$$K_{sat}^1 = \rho \left((V_{p1})^2 - \frac{4}{3} (V_{s1})^2 \right), \quad (B.6)$$

$$\mu_{sat}^1 = \rho (V_{s1})^2. \quad (B.7)$$

2. Step 2: apply Gassmann's relation, of the following form, to transform the saturated bulk modulus,

$$\frac{K_{sat}^2}{K_{min} - K_{sat}^2} - \frac{K_{fluid}^2}{\phi(K_{min} - K_{fluid}^2)} = \frac{K_{sat}^1}{K_{min} - K_{sat}^1} - \frac{K_{fluid}^1}{\phi(K_{min} - K_{fluid}^1)}, \quad (B.8)$$

Rearranging for K_{sat}

$$K_{sat}^2 = \frac{K_{min}}{\left[\frac{K_{sat}^1}{K_{min} - K_{sat}^1} - \frac{K_{fluid}^1}{\phi(K_{min} - K_{fluid}^1)} + \frac{K_{fluid}^2}{\phi(K_{min} - K_{fluid}^2)} \right]^{-1} + 1}, \quad (B.9)$$

where K_{sat}^1 and K_{sat}^2 are the rock bulk moduli saturated with fluid 1 and fluid 2, and K_{fluid}^1 and K_{fluid}^2 are the bulk moduli of the fluids themselves.

3. Step 3: leave the shear modulus unchanged (rigidity is independent of fluid type),

$$\mu_{sat}^2 = \mu_{sat}^1. \quad (B.10)$$

4. Step 4: correct the bulk density for the change in fluid,

$$\rho_2 = \rho_1 + \phi (\rho_{\text{fluid}}^2 - \rho_{\text{fluid}}^1). \quad (\text{B.11})$$

5. Step 5: recomputed the fluid substituted velocities,

$$V_{p2} = \sqrt{\frac{K_{sat}^2 + \frac{4}{3}\mu_{sat}^2}{\rho_2}}, \quad (\text{B.12})$$

$$V_{s2} = \sqrt{\frac{\mu_{sat}^2}{\rho_2}}. \quad (\text{B.13})$$

No model can be recommended as the best model for a given rock or reservoir formation in advance. Microstructure is one of the main factors that control the elastic properties of the rocks, so before any choice of model, the rock microstructure must be studied in detail. Gassmann's model has several underlying assumptions that restrict the model's universal use.